Understanding Biomass Pyrolysis Kinetics: Improved Modeling Based on Comprehensive Thermokinetic Analysis

5.2.2 The effect of pretreatments

We compare the evolution profiles between the untreated and pretreated samples. The largest differences observed in the thistle sample after the pre-treatments, anticipated by previous analysis in Chapters 3 and 4, are also shown by the evolution profiles of volatile products. Some representative fragment ions in the devolatilization of thistle are shown in Figure 5.3. The formaldehyde (m/z 30) evolution profile suggests that its formation results from the decomposition of all polymeric wood constituents. M/z 31 corresponds to methanol, although it can also be a fragment of hydroxyacetaldehyde. This latter compound is one of the characteristic products of the main cellulose decomposition pathways (Evans and Milne, 1987). The m/z 60 ion can be either acetic acid formed mostly from hemicellulose decomposition or hydroxyacetaldehyde released mainly from cellulose (Faix et al., 1991a; Mészáros et al., 2004a). The peak of $C_3H_5^+$ (m/z 41) is a representative of aliphatic fragments.

The formations of H_2 and CO from about 500 °C are expected to be affected by the pretreatments, as these compounds are typical products of the charring processes from this temperature. The evolution profile of H_2 decreased in the water-washed sample of thistle (compare panels A and B in Figure 5.3), though this result is not clear in the case of CO. The peak heights of these products from thistle are still considerably large even after the pretreatments. This may be a result of the relatively high lignin content of the herbaceous crop. The large amount of CO_2 evolved from all thistle samples can be attributed to the specific structural feature of the lignin present in this biomass. From a lignin with high γ-COOH and γ-CO-O-R group content, carboxyl groups are preferably eliminated by the release of carbon dioxide in the low temperature range (Jakab et al., 1997). As a remarkable result of the pretreatments, higher peaks of the characteristic organic volatile fragments are observed when comparing with those from the untreated thistle sample (compare panels D-F in Figure 5.3).

The decomposition of cellulose is influenced by the removal of mineral matter in such a way that the peak profiles of the organic volatiles released from this carbohydrate are displaced toward higher temperatures, leading to decomposition temperatures (T_{peak}) for thistle similar to those of the wood samples (compare Figures 5.2 and 5.3). The well-known effect of the water-washing to reduce the overlap of hemicellulose and cellulose decomposition (Várhegyi et al., 1989b, 1994) is also observed in the evolution profiles of some ions related to the polysaccharide devolatilization.

The effect of the extraction is also reflected on the evolution of some of the pyrolysis products. The displacement of the MS evolution peaks toward higher temperatures is less evident than from the water-washing, nonetheless, extraction seems to contribute to the better separation between the hemicellulose and cellulose decomposition, as well. The extractives undergo thermal evaporation and decomposition during heating and the labile functional groups are cleaved (DeGroot et al., 1988; Di Blasi et al., 2001a,b). The yields of aliphatic fragments are also diminished by extraction at around 500 °C, although some peaks are still observed even after the pretreatment (See e.g. the evolution of C_3H_5 in Figure 5.3), suggesting that the sample retains part of its extractive content.

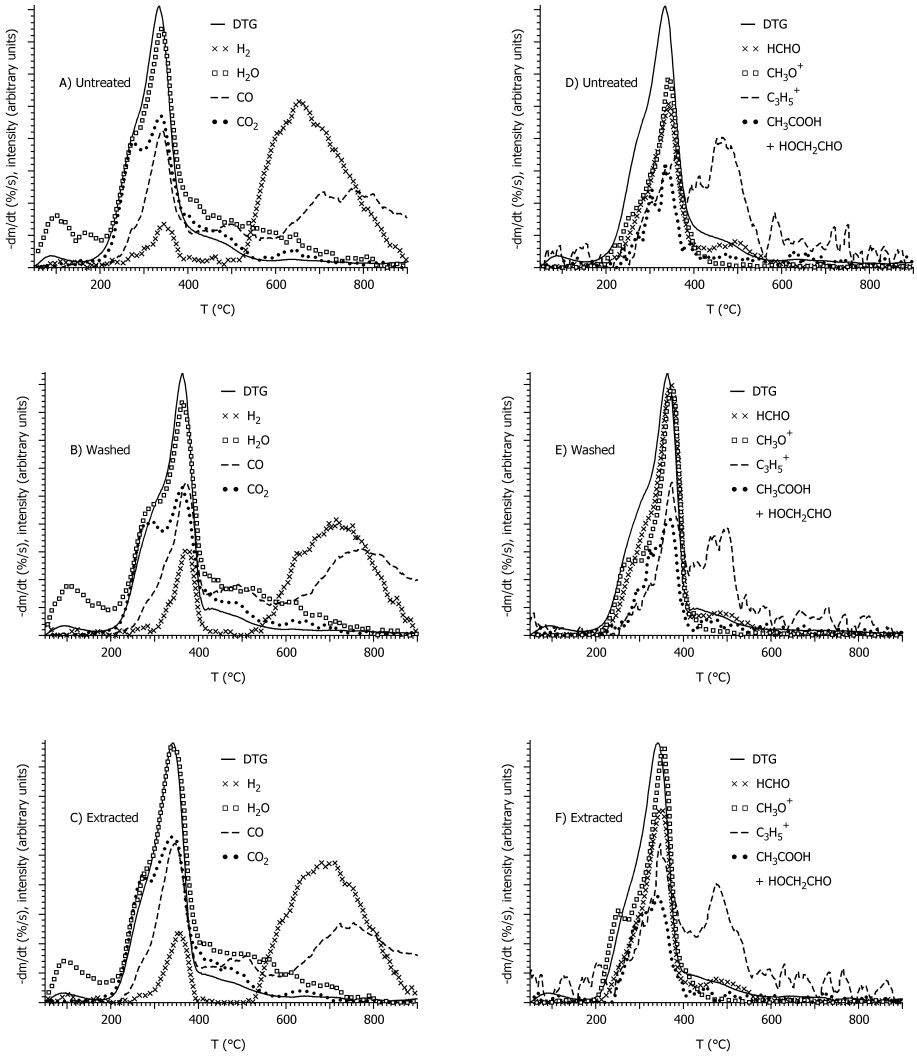

Figure 5.3: The DTG curves and the evolution profiles of some volatiles released from the untreated (A,D), washed (B,E) and extracted (C,F) thistle samples.

Table 5.2: Selected processes in the PCA calculation based on the integrated intensities of the main evolved products from pyrolysis

ion, m/z	Name	Description
2	2	Hydrogen formed in the charring processes (500 - 900 °C).
18	$18_{adsorptive}$	Adsorptive water.
	$18_{reacted}$	Water produced by decomposition of natural polymers.
28	$28_{below600}$	CO produced by decomposition of natural polymers.
	$28_{above600}$	CO formed in the charring processes (600 - 900 °C).
44	44	CO_2 produced by decomposition of natural polymers and charring processes (200 - 750 °C).

5.3 PCA analysis of the MS results

5.3.1 Main characteristics products

The integrated MS intensities of the four main characteristic products from pyrolysis, H_2 (m/z 2), H_2O (m/z 18), CO (m/z 28), and CO_2 (m/z 44), were included in a first PCA calculation. The different processes in which the amounts of the evolved products have been determined are listed in Table 5.2. We considered somewhat different temperature ranges for a given product depending on the sample, since the entire decomposition domain varied between the thistle and the wood species.

The resulting score plot is shown in Figure 5.4A. In the case of the wood species, the untreated and the extracted samples exhibit great similarities, whereas the water-washed samples are farther away from the untreated samples implying that water-washing has a significant effect on the formation of volatiles, as well. This is in accordance with the preliminary PCA results performed on the thermogravimetric data (see Section 3.4.2), although in the latter PCA calculation the different wood species cannot be separated into well-defined clusters. This suggests that the reaction pathways for the release of the main pyrolysis products are the same for pine and beech samples. The points corresponding to thistle lie clearly far away from the wood sample even after the pretreatments. The effect of the extraction was not evident from the PCA calculation based on the DTG characteristics. The present results allow us to conclude that extraction has a clearly different effect on the thermal behavior of the herbaceous crop than on the wood species, as the larger distance between the extracted (ET) and the untreated sample (UT) implies.

The loading plot in Figure 5.4B shows the original variables (the selected integrated MS intensities) in the field of the two first principal components. All the variables play a significant role in determining the first principal component, account-

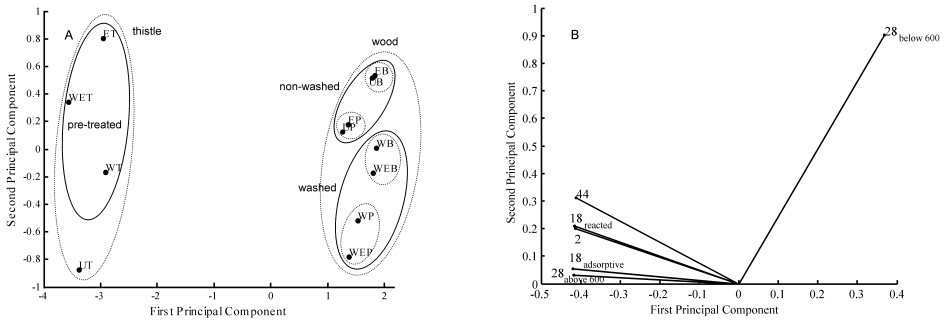

Figure 5.4: Principal Component Analysis from the Integrated Intensities of the four main pyrolysis products (H_2, H_2O, CO, and CO_2): (A) score plot, and (B) Loadings (see table 5.2 for the description of the selected processes in this calculation). The first principal component describes 95% of the total variance and the second is responsible for 5%.

ing for the differences in the type of species. Note that the evolution of both CO (m/z 28) below 600 °C and CO_2 (m/z 44) have the biggest influence on determining the second principal component, which accounted for the differences between untreated and pretreated samples in the case of the thistle (see the clusters in Figure 5.4A). The present result implies that not only water-washing but also extraction affected the evolution of the major gas species from the thistle biomass, given the distances observed between the untreated (UT) and the pretreated samples in the score plot, Figure 5.4A.

5.3.2 Other volatile products

In the attempt to get a deeper knowledge about the differences outlined above, we selected the MS integrals of the 17 most significant products, with good signal/noise ratios, for a further PCA calculation. Given the particular behavior of the herbaceous thistle sample, as well as the distinct effect of the pretreatments observed on the different species, the samples were analyzed independently in two groups, i.e. the herbaceous crop and the wood species. Figure 5.5 shows the PCA results for the wood samples. For this analysis 3 principal components were taken into account since more than 90% of the total variance could not be explained with only two components.

This sort of arrangement allowed a better distinction of the differences between the two wood species. In the three-dimensional score plot (panel A) the non-washed samples of pine (UP and EP samples) appear as a separate group. It can be connected to the higher extractive and mineral matter content of the pine sample. The two wood species can be distinguished from each other on the first principal component domain (see panel B). It is interesting to note how the samples of different species lie closer as a result of the water-washing pretreatment, indicating that the difference

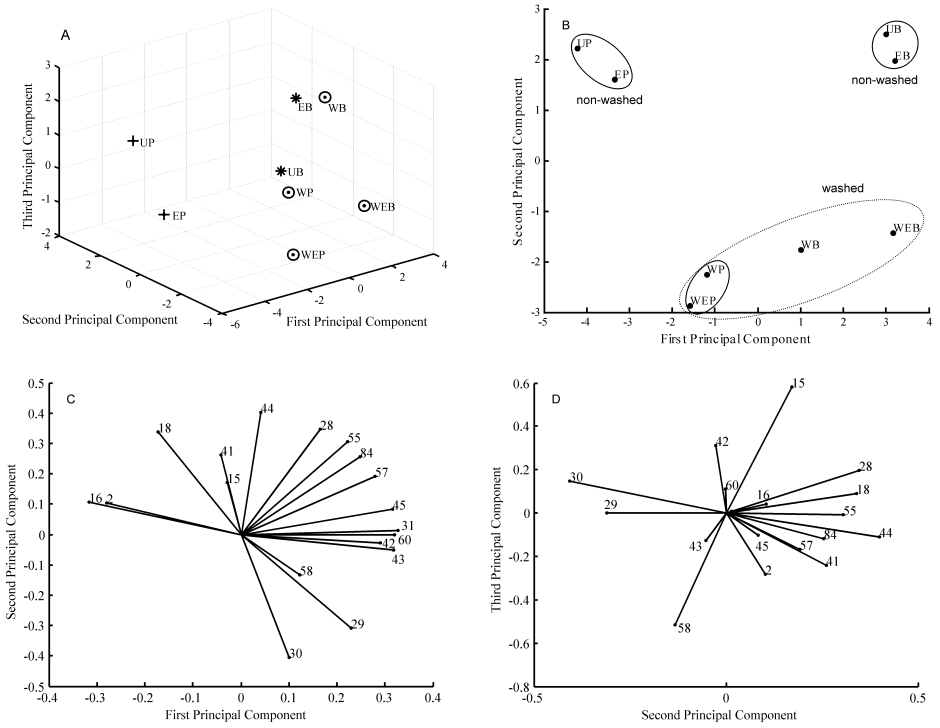

Figure 5.5: Principal Component Analysis from the integrated intensities of 17 selected ions for the woody samples: (A - B) score plots, and (C - D) loadings. The first principal component describes 50 % of the total variance, the second is responsible for 29 % and the third for 12 %.

between the different pretreated samples is smaller than that between the original beech and pine samples. The same observation was obtained from the features of DTG curves, as well. The intensities of the m/z 31, 60, 43, 42, 16 and 2 ions seem to have major influence on the first principal component (see panel C), related to the differences between pine and beech species. Note that these ions are associated to distinctive products of polysaccharides and lignin decomposition. In the case of the second principal component, which accounts for the differences occurring as a result of pretreatments (observe panels B and D), the m/z 30, 28, 41, 15, 29 and 44 ions provide the biggest contribution. These ions are representative of the major vapor and gas-phase pyrolysis products, for which water-washing appears to have considerably affected the evolution.

Although the amount of most of the organic volatiles released from pine increased after the two pretreatments, the peak heights of the fragment ions corresponding to the evolution of some carbonyl compounds (e.g. acetone and hydroxyacetaldehyde) slightly decreased from the water-washed beech sample (see Figure 5.6). On the other hand, water (m/z 18) diminished for both wood samples after water-washing (See panels C and E). As outlined by other authors, the inorganic ions catalyze the scission of functional groups and char formation which leads to the increased intensity of water from the original samples in comparison with the washed samples. By the same reaction pathway, the scission of the side-groups and end-groups of the polymeric cell wall constituents leads to the release of methanol, hydroxyacetaldehyde (m/z 31) and low molecular weight carbonyl compounds represented by the m/z 43 ion (CH_3CO^+) (Evans and Milne, 1987; Antal and Várhegyi, 1995). Observe that the latter ions were identified as variables with major influence on the differences between the given species in the PCA results. The m/z 18 ion intensity appeared related to the similar effect of the pretreatments on both pine and beech, observed in the PCA analysis of their product evolution profiles (see Figure 5.5D).

Figure 5.7 shows the score plots and the loading plot of the results corresponding to the single evaluation of thistle. Two principal components have been applied for the evaluation of the data. The most evident distinction occurs on the domain of the first principal component, where the extracted thistle (ET) approaches the rest of the pre-treated samples (WET and WT) (see panel B). This is in accordance with the results of the PCA calculation shown in Figure 5.4. The integrated intensities of the m/z 60 and 43 ions contributed mostly to the first principal component (see Figure 5.7C), however, the contribution of other ions (e.g. m/z 28, 31, 18, 84, 55, 15, 29) is not negligible. All these results offer much evidence to confirm the more significant influence of both pretreatments on the thermal decomposition of the herbaceous crop.

5.4 Determination of the volatile composition

We were also interested in determining the total amounts of the main volatile products evolved during the process. The MS integrals of hydrogen, water, carbon dioxide and carbon monoxide were related to corresponding factors from calibration procedures (see the experimental section of this chapter and detail presented in the Appendix

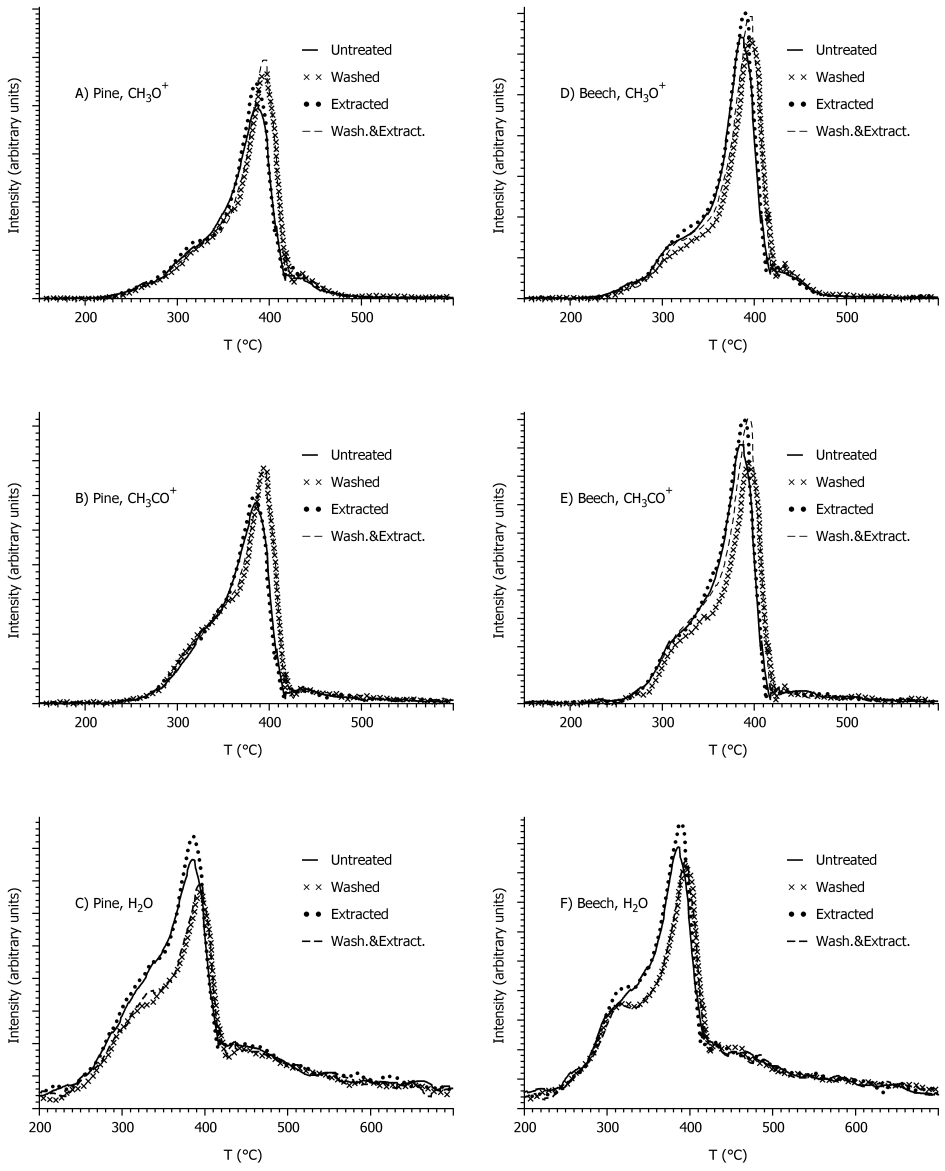

Figure 5.6: Evolution profiles of some volatiles released from the pine (A-C) and beech (D-F) samples.

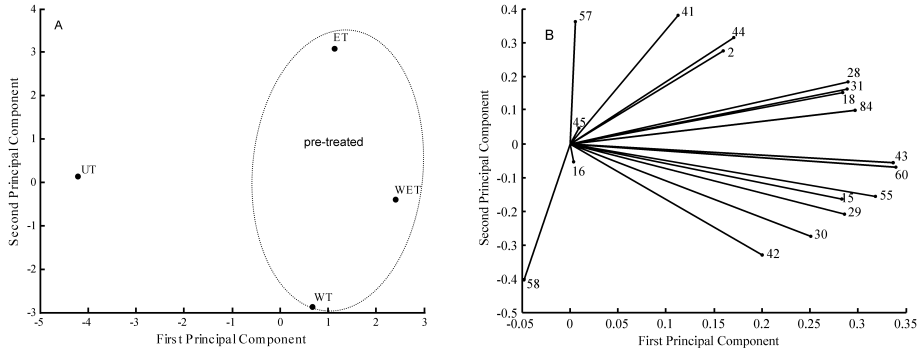

Figure 5.7: Principal Component Analysis from the integrated intensities of 17 selected ions for the thistle sample: (A) score plot, and (B) loadings. The first principal component describes 47 % of the total variance and the second is responsible for 33 %.

D). Special care was needed to properly handle baseline uncertainties and get reliable comparisons between the different types of samples and pretreatments. The global mass loss in the 50 - 200 °C temperature range, which corresponds to the release of adsorptive water, served as the reference value for a proper evaluation of m/z 18 intensity. According to this reference, an appropriate baseline correction was chosen to correct the corresponding intensity curves by their baseline shift during the experiments. The different processes in which the amounts of the evolved products were determined are the same considered in the PCA analysis (see Table 5.2). The total amounts over the entire temperature range of decomposition are listed in Table 5.3.

Table 5.3 supports the discussion in Sections 5.2 and 5.3. Higher amounts of H_2O, CO, CO_2 and H_2 are obtained from the non-washed (untreated and extracted) samples of the given biomasses. Similarly, higher yields of carbon dioxide and hydrogen are observed for thistle compared to those from the wood samples. The amounts of other organic volatile products from pyrolysis are represented by the VM fractions in Table 5.3. The higher organic evolution from wood compared with thistle is evidenced by these values.

The amounts of individual volatile products from slow pyrolysis are not frequently reported in the literature. Most of the studies quantifying yields of vapor and gas pyrolysis products have been carried out at higher heating rates, or under fast pyrolysis regime (Piskorz et al., 1988; Scott et al., 1999; Nunn et al., 1985; Banyasz et al., 2001). Results in the present work are closer to those reported by Radmanesh et al. (2006) in the GC analysis of individual gases from two types of woods (Canadian beech and saw dust) at heating rates from 5 to 50 °C/min. Similar carbon dioxide and carbon monoxide evolutions from beech wood were reported by Branca et al. (2003) under conditions of continuous updraft gasification (heating rates from 30 to 90 °C/min) or slow-conventional pyrolysis. Higher yields of individual gases from biomass have been

Table 5.3: Total amounts (% m/m) of pyrolysis decomposition products. Temperature range, 200 - 900 °C

	Sample	H_2O (%)[c]	CO (%)	CO_2 (%)	H_2 (%)	Char[a] (%)	VM[b] (%)
Thistle	*Untreated*	11.03	5.10	10.79	0.42	26	46
	Washed	9.03	5.49	8.73	0.38	21	56
	Extracted	12.05	5.81	9.75	0.48	26	46
	Washed and extracted	11.33	5.70	9.53	0.50	23	50
Pine	*Untreated*	12.35	5.23	6.44	0.25	16	60
	Washed	10.08	4.91	5.04	0.24	14	66
	Extracted	12.23	5.31	6.44	0.26	17	59
	Washed and extracted	10.34	4.96	5.66	0.24	15	64
Beech	*Untreated*	11.74	5.68	6.57	0.23	14	62
	Washed	9.15	5.19	5.74	0.17	11	69
	Extracted	11.47	5.84	6.91	0.23	14	61
	Washed and extracted	10.87	5.00	5.83	0.20	12	66

[a] At 900 °C.
[b] Other volatiles by difference.
[c] All % on dry basis.

commonly observed under higher thermal severity, which favors secondary cracking of tar to gas species (Nunn et al., 1985; Di Blasi et al., 1999; Branca et al., 2003). On the other hand, the present amounts of reactive water, CO and CO_2 released from thistle are roughly similar to the quantities reported by Piskorz et al. (1988) in their analysis of herbaceous species (sweet sorghum and sweet sorghum bagasse) under fast pyrolysis conditions.

5.5 Product distribution. kinetic study

In the chapter before, we succeeded in a satisfactory kinetic description of the primary thermal decomposition of the samples, by assuming a linear combination of partial reactions related to fractions of the main biomass components. In the attempt to provide the kinetic approach with much insight into the real chemical phenomena, we observed the connection between the product evolution profiles and the partial processes assumed. At the same time, we were interested in kinetically elucidating the evolution of the major volatile products from slow pyrolysis.

As figures 5.2 and 5.3 imply, the evolution profiles of H_2, H_2O, CO, and CO_2, as well as some other representative fragment ions (e.g. formaldehyde), result from the decomposition of all polymeric wood constituents. It suggests that all the assumed partial reactions contribute to their production. The peaks of CO and hydrogen in the 500 - 900 °C temperature range, in addition to the release of CO_2, CO, methane and some aliphatic fragment ions from thistle at around 500 °C, should be then counted by the last, high temperature partial process described in Chapter 4. It is interesting to note that the CH_4 maxima at around 440 °C, observed in the pine and beech devolatilizations, match with the temperature peaks of the last partial reactions in the decomposition of the untreated wood samples (compare mean values in Table 4.7 with the corresponding T peaks in Figures 5.2A-B). The evolution profiles of the organic volatiles from thistle imply that part of the cellulose decomposes in an unusually low temperature range, merging into the hemicellulose domain (see Figure 5.2). Note that this results was also evidenced by the kinetic analysis.

Following the previous exposition, we tried to kinetically describe the individual production of the four volatile species for which we had available calibration data. We assumed the formation of every species as the same linear combination of partial reactions previously discussed:

$$dm_{v_s}/dt = \sum_{j=1}^{M} c_{sj} d\alpha_j/dt \tag{5.4}$$

where, m_{v_s} is the normalized mass of a given volatile species s calculated at every time, and c_{sj} is the fraction of volatile s released from the jth pseudocomponent. Each partial reaction is approximated by the same Equation 4.2.

Employing the last set of accepted E and log A parameters (mean values in Tables 4.6 and 4.7), we calculated c_ij coefficients by the nonlinear least-squares evaluation (described in Section 4.1.2) of the intensity data of a given volatile species. Resulting

values were then related to the corresponding calibration data. In other words, the total amounts of reacted H_2O, CO, and CO_2 are the sum of fractions of the volatiles released from every simulated pseudocomponent. The adsorbed water was not included in this analysis. Furthermore, we did not consider the release of H_2 within the 200 - 550 °C temperature range, since the m/z 2 intensity corresponds to a fragment ion of other organic molecules in this temperature domain.

Some examples of this procedure, in the description of the CO_2 evolution from different type of samples, are illustrated in Figure 5.8. In the case of thistle, we plotted the range of highest temperatures, too, so as to emphasize the extent of the last partial reaction accounting for the products of the further charring processes.

An acceptable simulation of the CO evolution in thistle required special attention. Given the noticeable evolution of this product at around 500 °C, and above 600 °C, we assumed a different course of the last partial process of this biomass. Instead of the third order partial reaction, three independent first order reactions were considered. They represent the CO evolution from lignin at around 415 °C, the corresponding production from char formation reactions and oxalate decomposition at around 500 °C, and the further charring contribution above 600 °C (see Figure 5.9). More favorable results were obtained by assuming the same energy of activation for the two first processes (same E_4 for thistle in Table 4.5) and estimating a new E value for the later one. Corresponding log A parameters for the three processes were calculated. The same procedure, employing the activation energies of the water-washed experiments for all type of samples, as in Section 4.2.5, was applied in these latter calculations. The hydrogen evolution at the highest temperature range was simulated by a first order reaction. The later CO evolution, above 600 °C, was considered in the case of the wood samples, as well.

The new results are shown in Tables 5.4 and 5.5. c_j coefficients are presented there as % of the moisture free initial sample mass. Total evolution (total c) is calculated as the sum of the individual contributions from the partial reactions. These values can be compared to the results in Table 5.3. Acceptable agreement is observed, although some of the simulated values resulted slightly smaller than those directly calculated from the integration of the experimental MS curves (remember that the adsorbed water was not counted in the simulation). Differences can be due to baseline uncertanties and the probable mathematical ill-definition of the last partial processes.

Kinetic models for the description of individual volatile evolutions from pyrolysis are unusually found in the literature. More works have been devoted to the global prediction of the three fractions, char, tar and gas (see, for example, the review of Di Blasi (1998)). A simple one step reaction has been used for the kinetic description of a given gas evolution, e.g. H_2, CH_4, CO, and CO_2 (Radmanesh et al., 2006; Nunn et al., 1985; Bilbao et al., 1995). The largely sparse experimental data presented by Radmanesh et al. (2006) did not allow to identify the multiple sources of these gases, normally indicated by broader profiles, in addition to shoulders on the evolution curves. Multiple peaks for individual evolutions of 21 volatile species were considered by Wójtowicz et al. (2003) in their kinetic analysis of tobacco pyrolysis from TG-FTIR experiments. Common mean E (in a Gaussian distribution) and log A parameters were used to describe individual peaks belonging to the given volatiles. In other

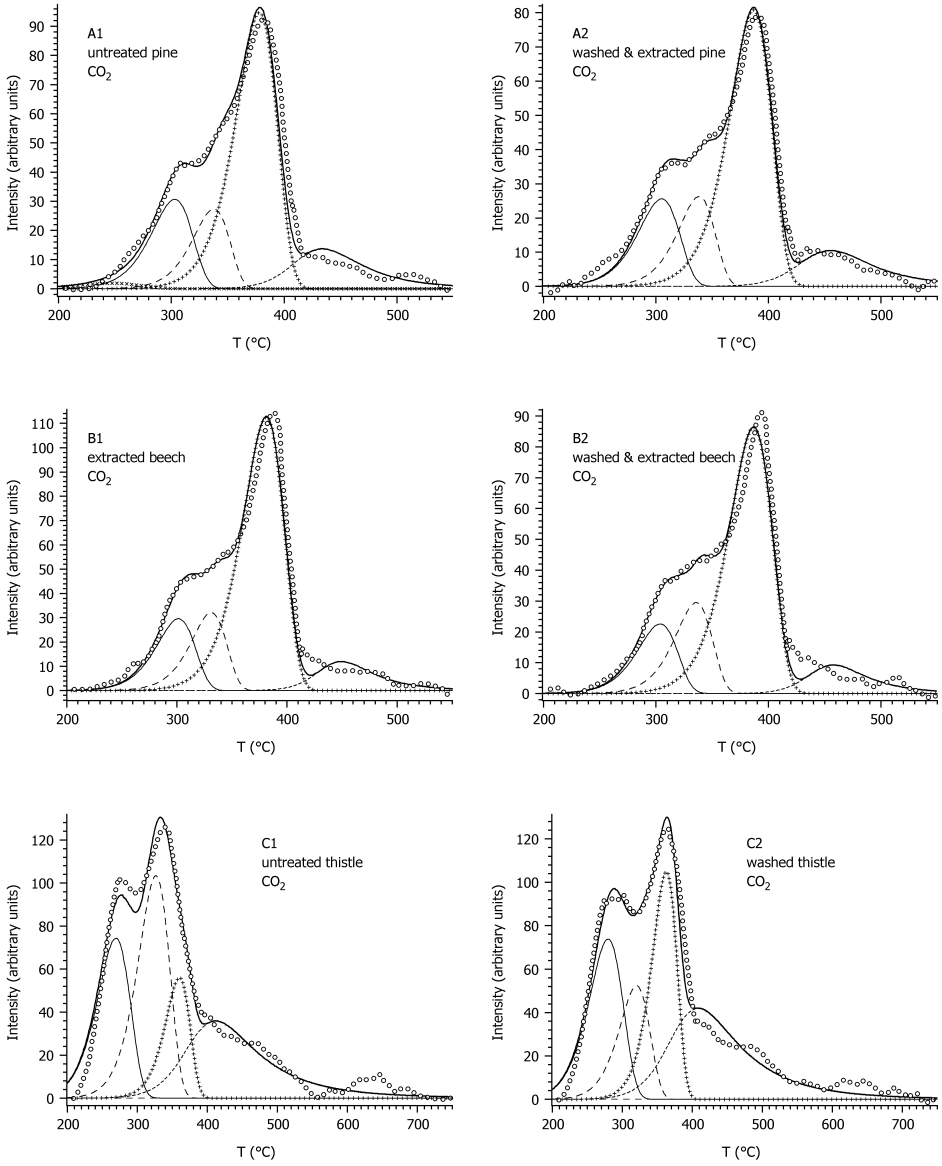

Figure 5.8: Observed (o o o) and simulated (—) intensity curves of CO_2 released from untreated and pretreated samples of wood (A - B) and thistle (C) biomasses (see Table 4.3 for the description of the simulated partial reactions).

Table 5.4: Kinetic parameters for the description of some volatile product evolutions (H_2, H_2O, CO, and CO_2) from the slow pyrolysis of thistle biomass. The rest of E, log A and n parameters were already presented in Tables 4.5 and 4.6

pseudocomp.			**UT**[a]	**WT**	**ET**	**WET**
1st	H_2O	c (%)	1.70	2.10	2.26	3.03
	CO	c (%)	0.13	0.20	0.38	0.38
	CO_2	c (%)	2.34	2.44	2.76	3.10
2nd	H_2O	c (%)	4.69	1.63	2.93	1.84
	CO	c (%)	1.41	0.37	0.88	0.33
	CO_2	c (%)	3.26	1.61	2.37	1.55
3rd	H_2O	c (%)	2.76	4.79	4.40	5.51
	CO	c (%)	0.84	1.69	1.59	1.63
	CO_2	c (%)	1.44	2.75	2.07	3.08
4th	H_2O	c (%)	0.56	1.58	1.60	2.38
	CO [b]	**log**A (s^{-1})		8.03		
		E (**kJ/mol**)		130		
		n		1		
		c (%)	0.37	0.40	0.40	0.47
	CO [c]	**log**A (s^{-1})		6.84		
		E (**kJ/mol**)		130		
		n		1		
		c (%)	0.58	0.66	0.64	0.75
	CO [d]	**log**A (s^{-1})		4.56 ± 0.14		
		E (**kJ/mol**)		136		
		n		1		
		c (%)	1.82	1.87	1.73	1.95
	CO_2	**c** (%)	2.95	3.42	3.50	3.45
	H_2[d]	**log**A (s^{-1})		2.31 ± 0.16		
		E (**kJ/mol**)		89		
		n		1		
		c (%)	0.41	0.39	0.49	0.51
total c	H_2	c (%)	0.41	0.39	0.49	0.51
	H_2O	c (%)	9.71	10.10	11.19	12.76
	CO	c (%)	5.14	5.19	5.61	5.52
	CO_2	c (%)	10.00	10.21	10.70	11.18

[a] See Table 3.10 for the notation of the samples.
[b] Evolution at around 415 °C.
[c] Evolution at around 500 °C.
[d] Evolution above 600 °C.

Table 5.5: Kinetic parameters for the description of some volatile product evolutions (H_2, H_2O, CO, and CO_2) from the slow pyrolysis of pine and beech biomasses. The rest of E , log A and n parameters were already presented in Tables 4.5 and 4.7

pseudocomp.			**UP**[a]	**WP**	**EP**	**WEP**	**UB**	**WB**	**EB**	**WEB**
i	H_2O	c (%)	0.03							
	CO	c (%)	– [b]							
	CO_2	c (%)	0.07							
1st	H_2O	c (%)	1.19	0.97	1.24	0.99	0.81	1.05	1.05	1.12
	CO	c (%)	0.15	0.11	0.18	0.09	0.11	0.12	0.14	0.14
	CO_2	c (%)	0.78	0.61	0.80	0.66	0.58	0.52	0.73	0.56
2nd	H_2O	c (%)	1.19	1.02	1.22	1.11	0.98	0.80	1.09	0.90
	CO	c (%)	0.26	0.23	0.34	0.29	0.17	0.23	0.26	0.27
	CO_2	c (%)	0.64	0.55	0.67	0.62	0.70	0.46	0.74	0.70
3rd	H_2O	c (%)	5.11	4.19	5.54	4.41	5.20	4.54	5.93	4.91
	CO	c (%)	2.44	2.62	2.74	2.61	2.87	2.90	3.13	2.90
	CO_2	c (%)	2.57	2.10	2.82	2.25	2.92	2.14	3.14	2.47
4th	H_2O	c (%)	0.78	0.88	0.50	0.41	0.76	0.51	0.29	0.32
	CO[c]	c (%)	0.73	0.60	0.68	0.42	0.69	0.61	0.52	0.48
	CO[d]	**log**A (s^{-1})		1.97 ± 0.18			12.44			
		E **(kJ/mol)**		93			311			
		n		1			1			
		c (%)	0.62	0.18	0.46	0.39	0.11	0.28	–	–
	CO_2	c (%)	0.65	0.58	0.48	0.50	0.62	0.22	0.47	0.37
	H_2[d]	**log**A (s^{-1})		5.37 ± 0.08				5.87 ± 0.13		
		E **(kJ/mol)**		154				165		
		n		1				1		
		c (%)	0.17	0.16	0.17	0.18	0.13	0.10	0.12	0.11
total c	H_2	c (%)	0.17	0.16	0.17	0.18	0.13	0.10	0.12	0.11
	H_2O	c (%)	8.28	7.06	8.50	6.91	7.75	6.91	8.37	7.25
	CO	c (%)	4.21	3.73	4.40	3.80	3.95	4.15	4.06	3.80
	CO_2	c (%)	4.63	3.85	4.77	4.02	4.81	3.33	5.08	4.10

[a] See Table 3.10 for the notation of the samples.
[b] Sign – denotes neglegible values.
[c] Evolution in the temperature range of the third order partial reaction.
[d] Evolution above 600 °C.

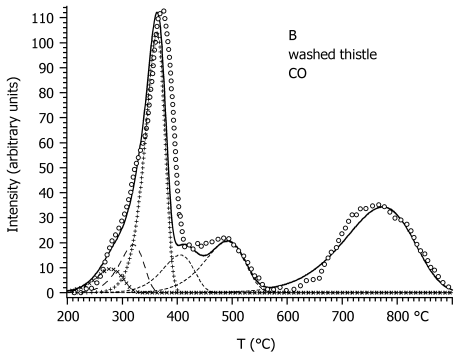

Figure 5.9: Observed (o o o) and simulated (—) intensity curves of CO released from washed thistle.

words, they used the idea of "pools" of precursor material that contribute to different volatiles by the same kinetics. This is in a similar way as in the present work, though neither they clearly defined the physical meaning of those pools nor associated them to the global mass loss kinetics of the samples.

Figure 5.10 shows some examples of the evolution profiles simulated by the current approach. For comparative purposes, we applied the kinetic model presented by Radmanesh et al. (2006) for the description of the H_2, CO, and CO_2 evolutions from beech biomass at 20 °C/min (see Figure 5.11)[3]. Given the appreciable difference between the experimental data and the Radmanesh et al.'s simulation, we calculated new kinetic parameters for their approach (one single reaction for a given species) by evaluating our experimental curves. The log A values resulted appreciably different of those published by them (e.g. 4.0 min^{-1} compared to 8.9 min^{-1} for the prediction of CO evolution from beech biomass). This simulation is also included in Figure 5.10 for additional comparison.

MS signals have rarely been used in the least squares evaluation of the thermoanalytical behavior of biomass materials. A simple example was given by Szabó et al. (1990) for the evolution of benzene released from subbituminous coals. Later, they presented a detailed kinetic evaluation of mass spectrometric intensities of biomass charcoal devolatilization, describing overlapped peaks by a distributed activation energy model (Várhegyi et al., 2002). We are aware of the uncertainty associated to MS data. Contamination of the instrument due to tar deposit is likely to occur. This results in electrostatic problems on the TG signal and adds uncertainty of the actual sample temperature. Moreover, intensity profiles enclose background signals that could not be completely removed by baseline corrections. The type of procedure

[3]In order to synchronize the time scale of our experiments with that of the Radmanesh et al.'s work, we applied a delay of 11 min on their simulated results, following the author's instruction in a personal communication.

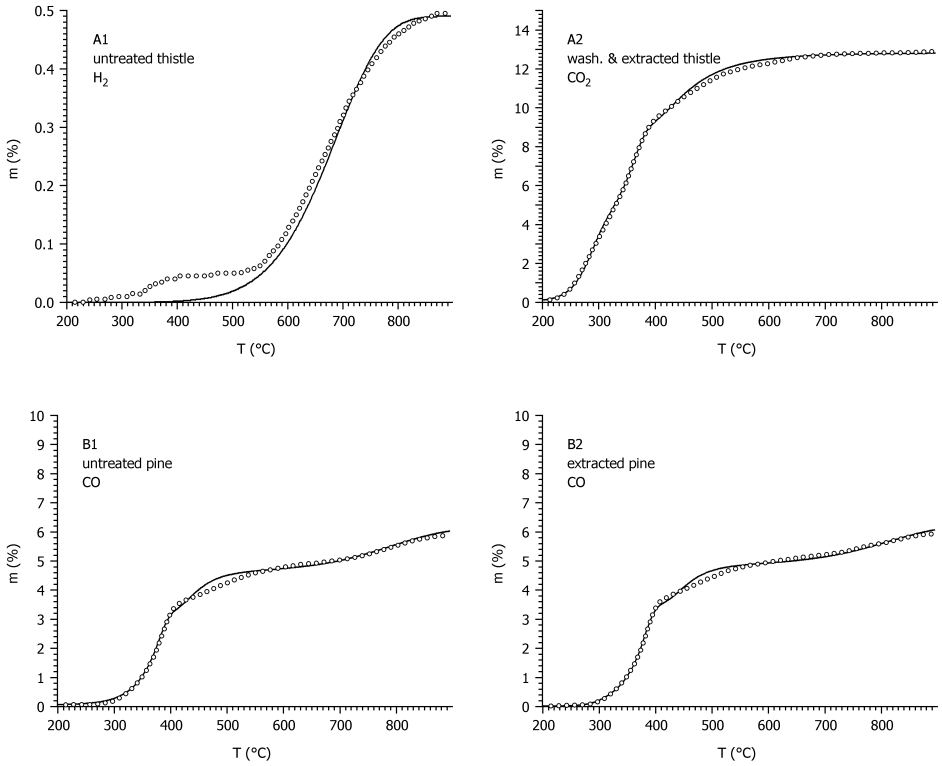

Figure 5.10: Observed (o o o) and simulated (—) yield curves of selected volatile species released from untreated and pretreated biomass samples.

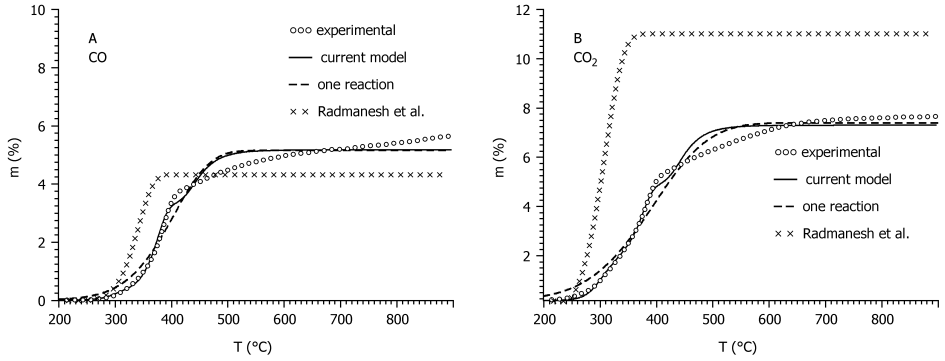

Figure 5.11: Comparison between the observed (o o o) and differently simulated yield curves of CO and CO_2 released from the untreated beech sample at 20 °C/min. An approximation by a simple one step reaction (- -), with parameters calculated from the current experiments, has been also included.

for these corrections can also introduce even more uncertainty. In addition, there is no way to calibrate the apparatus for some other gas signals, since it is not possible to mimic the experimental conditions of a TG-MS experiment by introducing calibrating gases into the instruments.

As we observed in the chapter before, it is necessary to increase the information content of the experiments for a reliable resolution of overlapping peaks. From a mathematical point of view, an infinite number of good solutions exist in the evaluation of single experiments. That is why we involved isothermal sections (stepwise experiments) in our kinetic evaluation of the global mass loss of the samples. However, we did not have available the analysis of evolution profiles in the experiments subjected to a stepwise heating program. Remember that the set of E and $\log A$ parameters used in this part of the work were obtained from the simultaneous evaluation of the stepwise and the linear heating rate experiments. In this way can partially deal with the lack of information exposed before.

More than expecting an accurate kinetic description of the volatile evolution, the purpose of presenting the values in Tables 5.4 and 5.5 is helping the quantification of species that could be interesting for several applications. We wanted this approach to be consistent with the type of kinetic model we have been supporting along this thesis. So far, we were able to predict the global mass loss and temperature-time history of the devolatilization only. The kinetic description of some volatiles compounds somehow allow us to step up to models or scale-up attempts of residues conversion process, even though many important considerations are still remaining.

Figure 5.12 summarize the kinetic scheme heretofore applied in this thesis for the description of the primary biomass pyrolysis. In short, a global mechanism consisting of several parallel reactions is assumed. Employing Equations 4.1 and 4.2, with para-

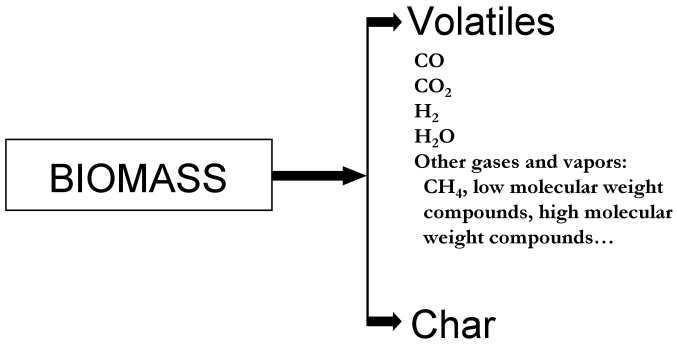

Figure 5.12: Kinetic scheme applied in this thesis for the primary pyrolysis of biomass.

meters in Tables 4.6 and 4.7, we can obtain the total fractions of volatiles and solid residue as functions of time and/or temperature. Individual profiles of H_2, H_2O, CO, and CO_2 can be obtained by using the same type of equations, with parameters in Tables 5.4 and 5.5. The fraction corresponding to other gases and vapors (see Figures 5.12 and 5.13) is calculated as the difference between the global volatile production and the sum of contributions of the four species obtained individually. We included all the aforementioned equations and parameters in another simulation framework, Aspen Custom Modeler (ACM)[4]. Figure 5.13 is an example of the type of results that can be obtained from this simulation.

5.6 Conclusions of this chapter

The devolatilization behavior of the three biomass materials studied in this thesis (pine, beech and thistle), including their pretreated versions, was investigated by thermogravimetry/mass spectrometry. The evolution profiles of the low molecular mass products give further evidence to explain the particular thermal behavior of the herbaceous crop sample compared to that of a regular wood biomass. The experimental results corroborated the catalytic effect of the inorganic matter and the influence of the lignin and extractive degradation characteristics on the evolution of the different volatile compounds, as well. Accordingly, the charring reactions played a more significant role in the decomposition of the thistle sample. In this case, higher

[4]The purpose of this simulation will be presented in Chapter 7.

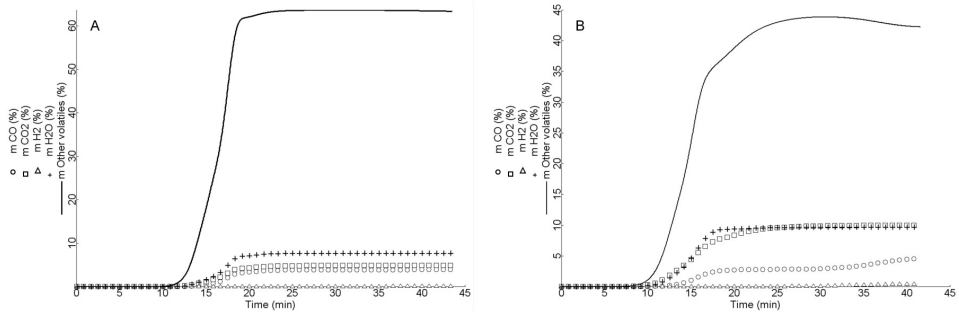

Figure 5.13: Simulated yield curves of volatiles released from the untreated beech (A) and thistle (B) samples at 20 °C/min. Selected results from the pyrolysis Aspen custom model.

overlapping in the thermal decomposition of hemicellulose and cellulose was also evidenced. The wood samples evolved more organic products (aldehydes, acids, ketones, furan derivatives, etc.) due to their higher polysaccharide content.

Chemometric evaluation (PCA calculations) of the mass spectrometric intensities of the major volatile products revealed some other specific differences due to the type of sample and pretreatment. As in the analysis of the DTG characteristics, the thistle sample exhibited the largest changes upon the pretreatments. The chemometric studies showed that the thermal behavior of wood and thistle is still considerably different after the elimination of some of the inorganic ions and extractive compounds. It reflects the different macromolecular composition of these materials. Furthermore, the different effect of the extraction on the herbaceous crop than on the wood species was evidenced. While water-washing largely affected the evolution of the pyrolysis products for all the samples, only in the case of thistle extraction had a non-negligible effect on the production the major gas species and other distinctive products of polysaccharides decomposition.

We observed the connection between the characteristic vapor and gas-phase product evolutions and the partial reactions assumed for the description of the global thermal decomposition. Thus, the same kinetic approach of multiple peaks was applied to elucidate the evolution of the quantified volatile species. The very last set of accepted E and log A parameters were employed in the evaluations. In this way, the total amounts of reacted H_2O, CO, and CO_2 were predicted as the sum of fractions of the volatiles released from every simulated pseudocomponent. The CO evolution from thistle required a different consideration of the last partial process. It was assumed as the sum of independent contributions from lignin decomposition and further charring processes. The release of H_2 and CO above 600 °C from all the sample was simulated by first order reactions.

Chapter

SIX

Thermal study by DSC and FTIR. Secondary decomposition

So far, we have only dealt with primary decomposition reactions. In this chapter we are interested in the information traced by the heat of pyrolysis on the primary and secondary biomass decomposition. DSC is the technique used with this purpose. Additionally, we analyze the results from a FTIR device coupled with the TG/DSC equipment. Finally, we test the ability of our best kinetic approach, from the chapters before, to describe the global mass loss under conditions that also favored secondary vapor-solid interactions. Sections 6.1 - 6.5 are part of paper A.1.1[1].

6.1 Introductory view

Heat of reaction has an important influence on the course of the thermal conversion. As the pyrolysis reactions are exothermic and/or endothermic in the different operating conditions, the understanding of the effect of reaction heat is important for modeling of the thermochemical processes[2].

Differential scanning calorimetry is a technique used to determine the variation of thermal flows emitted or received by a sample when subjected to a temperature program in a controlled atmosphere. When heating or cooling, any change occurring in the material is accompanied by an exchange of heat: the DSC permits determining the temperature of this transformation and quantifying the heat. DSC has been proved to be an effective technique for the obtainment of reliable values of the elementary heat of pyrolysis in the absence of complicating phenomena, as heat or mass transfer limitations (Rath et al., 2003).

In the chapters before, we succeeded in a satisfactory kinetic description of the primary decomposition of the samples, in spite of the different heating programs, pretreatments and thermogravimetric analyzers used in this work. We identified low heat transfer intrusions in our experiments, in part attributed to a low heat demand

[1] Gómez, C. J., Barontini, F., Cozzani, V., Velo, E., Puigjaner, L., 2006.

[2] The literature on the role of secondary decomposition in both the exothermicity of the process and the further formation of char was already exposed in chapter 2.

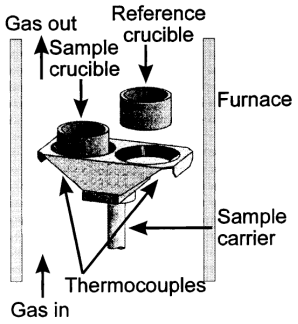

Figure 6.1: The DSC 25 system of two crucibles, one reference and one sample crucible (source: Stenseng et al. (2001)).

of our samples. In the first part of this chapter, we shed some light on the real heat demand of the materials used in this thesis, from the results of a DSC study. The influence of the pretreatments is also analyzed. We are unaware of calorimetric studies evidencing the effect of chemical pretreatments on the endothermic and/or exothermic character of the reactions.

With the goal of gaining insight into the entire pyrolytic phenomena, the TG/DSC results under conditions that favor vapor-solid secondary interactions are considered as well. These correspond to experiments using covered crucibles. Series of experiments with different initial sample masses are also analyzed. In a further part of the chapter, we present the on-line analysis of volatile compounds formed during TG runs, obtained with an FTIR analyzer under conditions of both primary and secondary pyrolysis. This analysis allows us to make some quantification of the extent of secondary reactions on the volatiles evolution, too. The final proposal of kinetic approach for biomass pyrolysis of this thesis, including primary and secondary stages, is then presented.

6.2 Experimental Section

DSC experimental data were obtained using a Mettler DSC 25 calorimeter (see figure 6.1 for the sample holder configuration). Experimental runs were performed using pure nitrogen as the purge gas (gas velocity around 0.005 m/s). Typical total sample weights of about 2 to 10 mg were used. The DSC runs were performed using aluminum crucibles. Depending on the experimental conditions desired, the crucible was used without a lid (thus resulting in a 5.3 mm diameter surface available for mass transfer to the gas flow), or using a pierced lid (thus limiting the surface available for mass transfer to a 1 mm diameter hole). A preliminary calibration of the DSC was performed using the heat of fusion of a known quantity of indium.

Simultaneous thermogravimetric (TG) and DSC data were obtained using two

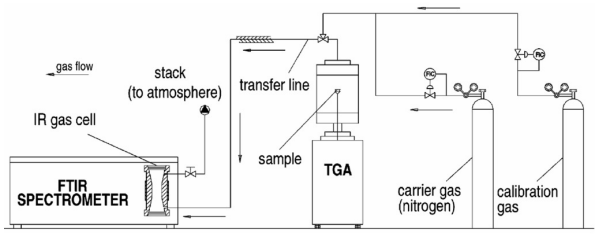

Figure 6.2: Configuration of the TG-FTIR coupling (source: Marsanich et al. (2002)).

equipments: the Netzsch STA 409/C thermoanalyzer and the Setaram thermobalance (see Section 3.2.4 for the technical specifications of these instruments and the experimental conditions applied). Samples in both holders with and without a lid were considered. The DTG characteristics of the resulting experiments were already exposed in Tables 3.7, 3.8 and 3.9.

FTIR measurements were carried out using a Bruker Equinox 55 spectrometer equipped with MCT detectors. TG-FTIR simultaneous measurements were carried out coupling the FTIR spectrometer to the Netzsch TG using a 2mm internal diameter teflon tube. The 800mm long transfer line and the head of the TG balance were heated at a constant temperature of 200 °C to limit the condensation of volatile decomposition products. FTIR measurements were carried out with a MCT detector in a specifically developed low volume gas cell (8.7 ml) with a 123mm pathlength, heated at a constant temperature of 250 °C. The gas flow from the TG outlet to the IR gas cell was of 60ml and a residence time of 30s in the transfer line could be evaluated for the evolved gases. This value was assumed as the time delay correction to be used for the comparison of TG and IR results. During TG-FTIR runs, spectra were collected at $4cm^{-1}$ resolution, co-adding 16 scans per spectrum. This resulted in a temporal resolution of 9.5s, more than sufficient to follow the gas evolution rates characteristic of TG runs at heating rates of 20 °C/min (Barontini et al., 2001).

Runs in all these equipments were performed using the constant heating rate of 20 °C/min. At the end of each run, the furnace was cooled to ambient temperature still providing a nitrogen purge gas flow. The char formed was weighted and a second run was performed on the char sample using the same experimental conditions. All the DSC results reported in this study were corrected by baselines obtained from runs with empty crucibles. The resulting experimental heat flows from the biomass samples will be denoted as Q_{run}, while the heat traces from the residual char will be identified as Q_{char}.

6.3 Calculation of the heat of pyrolysis

In order to achieve quantitative data on the heat of reaction from the DSC curves, it was necessary to obtain reasonable reference lines. We made the same assumption as Rath et al. (2003), for which the heat flow curves obtained from DSC measurements are the sum of two components: the heat flow necessary to heat the sample and the heat of reaction. To separate the first effect from the second one, a theoretical heat flow curve for sample heating was calculated from available specific heat and conversion data.

Table 6.1: Specific heat of wood and char (source: Rath et al. (2003))

Substance	**Specific heat c_p ($\mathbf{Jkg^{-1}K^{-1}}$)**
wood	$c_{p,wood} = 1113.68 + 4.8567(T - 273.15)$
char	$c_{p,char} = \frac{8314}{5.75}\left[e^{\frac{380}{T}}\left(\frac{e^{\frac{380}{T}}-1}{\frac{380}{T}}\right)^{-2} + 2e^{\frac{1800}{T}}\left(\frac{e^{\frac{1800}{T}}-1}{\frac{1800}{T}}\right)^{-2}\right]$

For these calculations, a dimensionless sample conversion was defined as:

$$X(T) = \left(\frac{W_0 - W_{(t)}}{W_0 - W_f}\right) \tag{6.1}$$

W_f is the final sample weight, $W_f = W_{char}$, the mass of char produced in the run (See the "Nomenclature" Chapter for symbols and subscripts). This is used to estimate the heat flow curve Q_s

$$Q_s = (1 - X(T))Q_{bio,s} + X(T)Q_{char,s} \tag{6.2}$$

where

$$Q_{bio,s} = W_0 c_{p,bio}\frac{dT}{dt} \tag{6.3}$$

and

$$Q_{char,s} = W_{char} c_{p,char}\frac{dT}{dt} \tag{6.4}$$

dT/dt is the heating rate (20 °C/min) and c_p is the specific heat calculated according to formulas given in literature and reported in Table 6.1. Q_s represents the heat flow necessary to heat the sample without considering any heat of reaction. Thus, in the absence of other complicating phenomena, the heat flow due to thermal effects of the reaction, Q_r, may be estimated subtracting Q_s from the baseline corrected experimental DSC heat flow curve, Q_{run}.

It is known that the absence of a lid has an important effect on both the shape and the apparent baseline of the heat flow curve. The effect on the baseline was recognized to be the effect of radiative heat exchange, due to the different emissivity of the sample with respect to the empty crucible in runs without a lid (Rath et al., 2003). If crucibles without a lid are used, the influence of heat radiation effects

must be also considered. In this work, the radiative heat, Q_{rad}, is calculated as the difference between the calculated $Q_{char,s}$ (equation 6.4) and the experimental heat flow from the residual char, Q_{char}.

The same procedure described above is used to obtain the reaction heat curve from the DSC results in the presence of a pierced lid. However, in these runs, radiation heat flow effects need not to be considered. Thus, only Q_s is subtracted from the experimental Q_{run} curve.

The total heat of pyrolysis, H_{total}, is then calculated from a numerical integration

$$H_{total} = \frac{1}{W_0} \int_{T_1}^{T_2} Q_r dt \tag{6.5}$$

where T_1 and T_2 denote the temperatures of starting and ending of decomposition, respectively, varying for each sample depending on the characteristics of the DTG curves.

6.4 Thermal analysis by DSC

6.4.1 Results of DSC runs without a lid

Firstly, we were interested in determining the heat of primary decomposition of the whole series of untreated and pretreated samples. With this purpose, we considered the results of the DSC runs in uncovered pans, as the absence of the lid promotes evaporation and diffusion of primary volatiles, reducing secondary interactions. Figure 6.3 compares the DTG and DSC resulting traces for 6 mg of untreated beech and thistle. The characteristics of the DTG curves, were already discussed in earlier chapters. The two peaks corresponding to heat demand and differential weight loss match in the woody sample (see panel A in Figure 6.3), exhibiting curves with similar shapes and clearly endothermic behavior. On the other hand, the herbaceous crop reveals its very special character by a heat demand with undefined local minimums.

The calculation procedure explained in the previous section is based on results of the type displayed in Figure 6.4. The figure shows the heat flow curves obtained for runs performed with the biomass sample and its corresponding residual char. The figure also gives the calculated heat flow Q_s and the difference Q_{rad} between the calculated and measured heat flow for char heating. This difference can be explained by heat radiation effects in the DSC measurement cell when a lid is not used.

Figure 6.5 shows the heat flow curves due to reaction thermal effects, Q_r, obtained subtracting the sum of Q_{rad} and Q_s from the baseline-corrected heat flow curve, Q_{run}. This procedure helped in the clarification of the thermal effects. A final exothermic stage in the untreated woody sample can be now observed, at temperatures between 407 and 475 °C. This behavior was also identified by Rath et al. (2003) in the thermal decomposition of spruce and beech wood. It can be explained by the domain of lignin decomposition, which is largely associated to the char-forming exothermic reactions. The water-washed sample exhibits higher endothermic flow. The latter

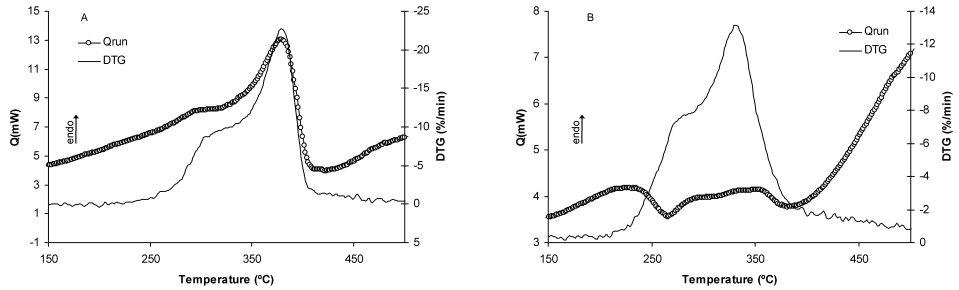

Figure 6.3: DTG and DSC experimental results with 6 mg initial sample mass of untreated beech (A) and untreated thistle (B) samples at 20 °C/min, in crucibles without a lid.

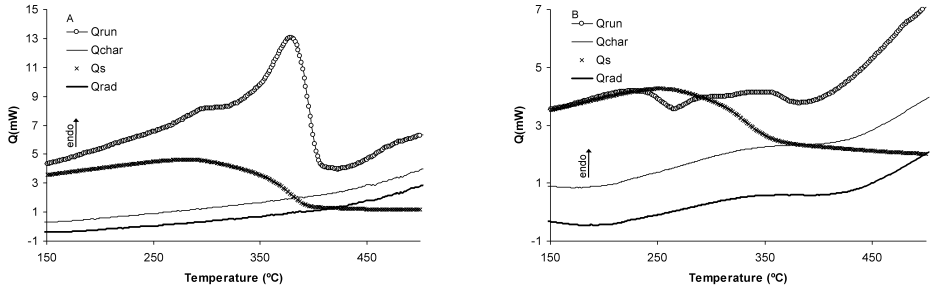

Figure 6.4: DSC results for biomass and char from untreated beech (A) and untreated thistle (B) at 20 °C/min, in crucibles without a lid.

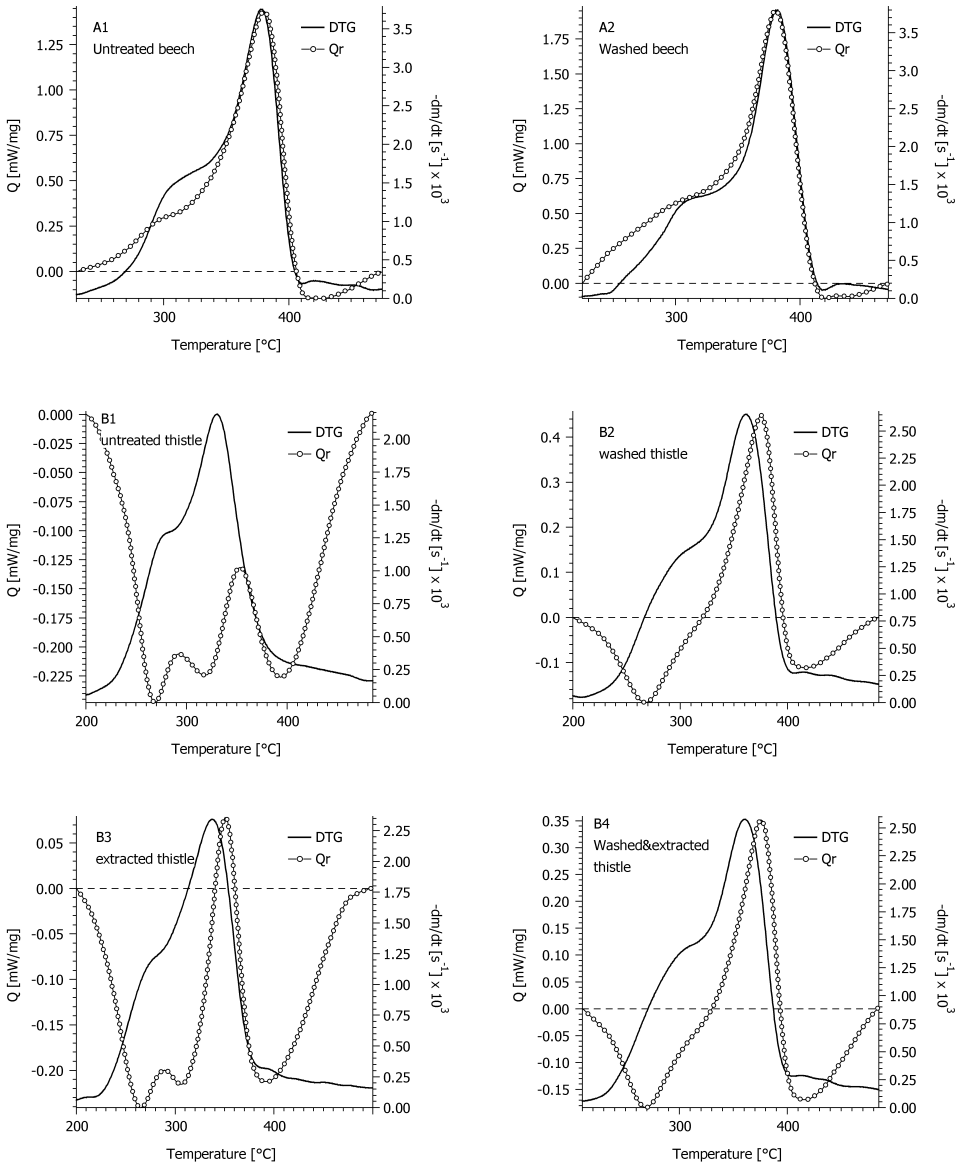

Figure 6.5: DTG and heat flow of pyrolysis for untreated and pretreated biomass samples at 20 °C/min, in crucibles without a lid. Negative values of Q correspond to exothermic behavior.

result is connected to the lower mineral matter content, and consequently, to the minor promotion of char yield in this sample.

In the case of the herbaceous crop, the heat flow of the untreated sample totally falls in the exothermic side. Local shoulders can be now observed between 270 and 400 °C (see panel B1 in Figure 6.5). At the same time, the heat answer of the water-washed sample noticeably approaches to the shape of the DTG curve, becoming similar to that of a regular biomass (compares panels A and B), as expected. The extraction also leads to a heat flow touching the endothermic side, although at a minor extent (see panel B3). In any case, the thermal decomposition of thistle starts and ends with exothermic stages, coinciding with the wide temperature range of lignin decomposition. The endothermic behavior becomes increasingly important between 270 and 395 °C, which is within the main range of devolatilization of the holocellulose content. Note that the temperature peak of the heat flow is slightly above the occurrence of the maximum DTG in the herbaceous crop. The endothermic maxima (around 350 °C in the untreated thistle and 370 °C for the pretreated samples) coincide with the DTG peaks of the partial reaction that characterized the cellulose decomposition (compare panel B of Figure 6.5 with Figure 4.7).

The values of heat of pyrolysis are given in Table 6.2. Since we are also interested in the relationship between char production and heat of reaction, the final solid residue is reported[3]. Pretreatments increase the endothermic character of the process, as anticipated. It coincides with a decreasing on the char production. While the thermal decomposition of the herbaceous crop is dominated by exothermic phenomena, the woody samples evidence a high endothermic character. However, they do not achieve as high endothermicity as a sample of pure cellulose under conditions of primary decomposition (reported between 560 and 710 J/g by Stenseng et al. (2001)). The present results are well in the range of previous studies with wood biomass (Rath et al., 2003) and confirm the observations exposed by Stenseng et al. (2001) in their work on straw biomass, related to the much lower heat demand of this sample compared to that of a pure cellulose. Values of heat of pyrolysis for herbaceous crop are not commonly reported in the literature.

6.4.2 Results of DSC runs with a lid

With the purpose of observing the influence of the secondary decomposition on the pyrolytic phenomena, we prolonged the vapor-phase residence times by hermetic sealing of the aluminum DSC crucibles containing the samples. The surface available for mass transfer was limited to a 1 mm diameter hole punctured in the top. The corresponding procedure described in Section 6.3 was applied to obtain the reaction heat curves. Selection of the resulting Q_r flows in crucibles with a lid are presented in Figure 6.6. For the woody sample, an exothermic effect appears to prevail at the beginning of the decomposition. It suggest that the resistance to the flow of primary volatiles from their vicinity, created by the presence of a lid, enhances secondary char forming reactions even from low temperatures. The last exothermic stage (between

[3]The reader should be addressed to Chapter3 for a revision of the equivalent experimental conditions between the different equipments.

Table 6.2: Heats of pyrolysis in crucibles without a lid. Values correspond to arithmetic averages from repeated experiments

Type of wood	**Char yield** $(-)^a$	**Total heat** (Jg^{-1})
untreated thistle^b	0.34	-132.7
extracted thistle^b	0.31	-122.2
washed thistle^b	0.26	-37.5
washed&ext. thistle^b	0.26	-23.8
untreated pine^c	0.25	143.4
extracted pine^c	0.24	178.4
washed&ext. pine^c	0.22	305.1
untreated beech^b	0.17	222.2

^{a}At 550 °C.
^{b}From the Mettler calorimeter.
^{c}From the TG/DSC Setaram thermobalance.

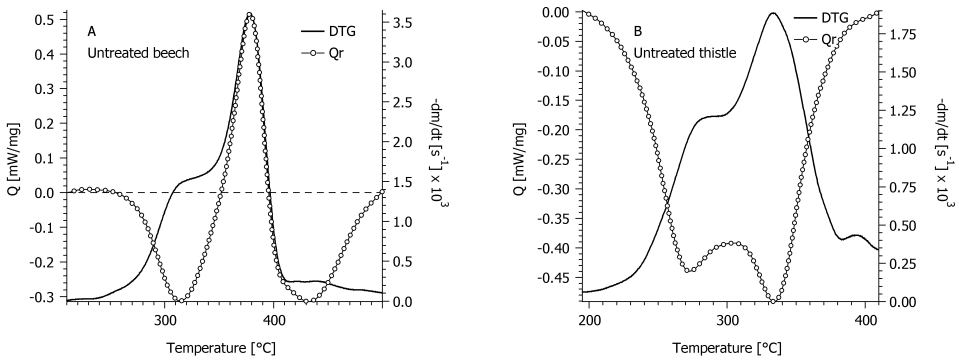

Figure 6.6: DTG and heat flow of pyrolysis for untreated samples of beech (A) and thistle (B) at 20 °C/min, in crucibles with a lid. Negative values of Q correspond to exothermic behavior.

407 and 475 °C) appears more pronounced than for the uncovered sample (compare Figures 6.5 and 6.6, panels A). In the case of thistle, the exothermic character of the thermal decomposition is emphasized. Numerical values in table 6.3 remark these observations.

In figure 6.7 we compare results of both type, with and without a lid, for the thistle sample, as a function of the char yield. The values correspond to repeated experiments with all the untreated and pretreated samples. We found linear trends for every type of sample (straight dotted lines), with correlation coefficients above 0.94. The known relationship between char production and heat of pyrolysis is then

Table 6.3: Heats of pyrolysis in crucibles with a lid

Type of wood	**Char yield** $(-)$	**Total heat**[a] (Jg^{-1})
untreated thistle	0.36	-178.5
extracted thistle	0.34	-170.1
washed thistle	0.29	-142.6
washed&ext. thistle	0.30	-111.8
untreated beech	0.22	-67.6

[a]Values correspond to arithmetic averages from repeated experiments in the Mettler calorimeter.

evidenced. The heat values appear displaced to the left on the figure, as long as the effectiveness of the pretreatments increases. The slopes of the tendency lines are very similar between the two washed samples. Furthermore, they are higher than those corresponding to the untreated and the extracted thistle sample, suggesting that the washed samples are more affected by the enhancing of exothermic answer with the presence of a lid. There is another interesting observation from tables 6.2 and 6.3, also evidenced in Figure 6.7: for a given initial sample weight of thistle, wider alterations in char yield and heat of pyrolysis are observed by the effect of the water-washing than by using a sealed crucibles with the untreated sample. I.e. increase of the exothermic behavior of the untreated thistle by the lid does not exceed 50 J/g.

6.4.3 Influence of initial mass

Another source of resistance to the flow of the volatile pyrolysis products is the use of relative high initial sample masses. Rath et al. (2003) reported variations of total heat of pyrolysis up to 150 J/g when initial sample masses of beech varied around 3.3 mg. We were also interested in these effects and evaluated the heat of pyrolysis for series of untreated and washed samples with different initial sample masses, in pans with and without a lid.

Slow pyrolysis with initial masses in the range between 2 and 10 mg produced slightly different char yields. Figure 6.8 represents the variation of the solid fraction with the initial sample mass. We have calculated linear correlations in the attempt to express the resulting variations in quantitative form. Washed samples appear slightly more affected, with variations in the char yield up to 1.5% of the initial sample mass (see the slopes in the table included in Figure 6.8). As observed before, less char is produced when the sample is washed than if the lid is avoided. E.g., in the case of the washed sample, the solid production decrease up to 11% of the initial mass, whereas only a maximum of 4% char yield increases with the use of a lid (from the differences between the intercepts of the straight lines). Employing 0.5mg of pure cellulose in a sealed DSC crucible, Várhegyi et al. (1988a) observed char yields whithin the range obtained by the addition of some inorganic salts. The heat of pyrolysis appears highly affected by the variations in the initial sample mass (see Figure 6.9). For char yields

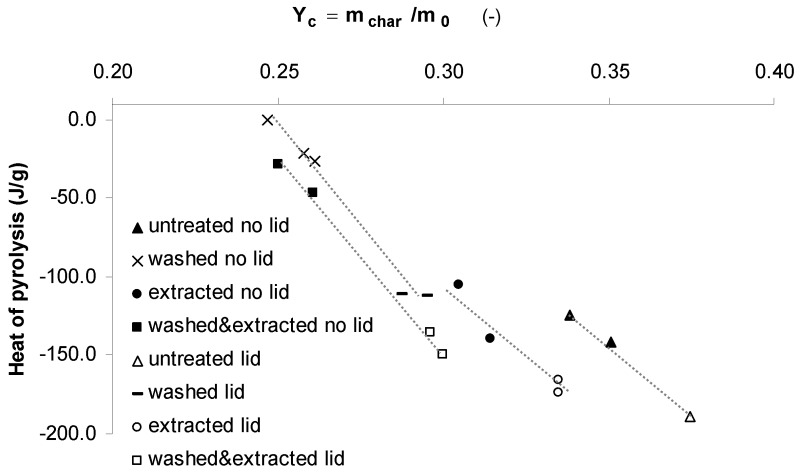

Figure 6.7: Heat of pyrolysis as function of the char yield for all untreated and pretreated 6 mg thistle samples, in crucibles with and without a lid.

varying around 20% of the initial mass, the heat values range from 10 to -200 J/g. Linear trends with similar slopes can be clearly observed in most of the cases. Again, the presence of the lid does not provide the highest variations.

6.5 Product analysis by FTIR

We aim at adding new insight into the understanding of the different chemical processes occurring during the thermal decomposition. In a second part of this study, we coupled an available FTIR equipment to the Netzsch TG/DSC analyzer, and considered series of untreated and washed samples with different initial sample masses, in crucibles with and without a lid. Since discussion on the extent of secondary vapor-solid reactions has been traditionally focused on the observation of the final mass, we wanted to assess the phenomena by considering the evolution profiles of the volatile pyrolysis products, as well. The resistance to the flow of the vapor phase from its vicinity affects both the decomposing sample and the evolving vapors: the decomposition occurs in the presence of the vapors, and these vapors spend a longer time at a higher partial pressure in the hot zone above the sample (Várhegyi et al., 1988a). Thus, the traces of the product gases releasing from the sample should be affected at some level.

The simultaneous observation of the volatile pyrolysis products under conditions

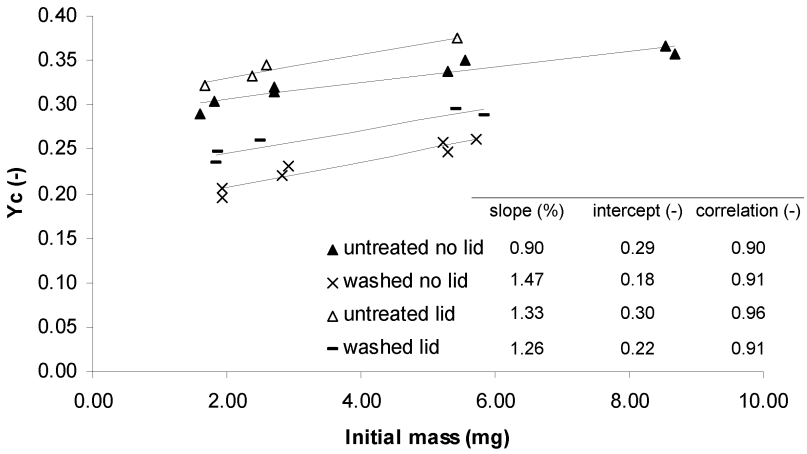

Figure 6.8: Char yield as function of the initial mass of untreated and washed thistle, in crucibles with and without a lid. Data in the table correspond to the linear correlations. % respect to the initial mass.

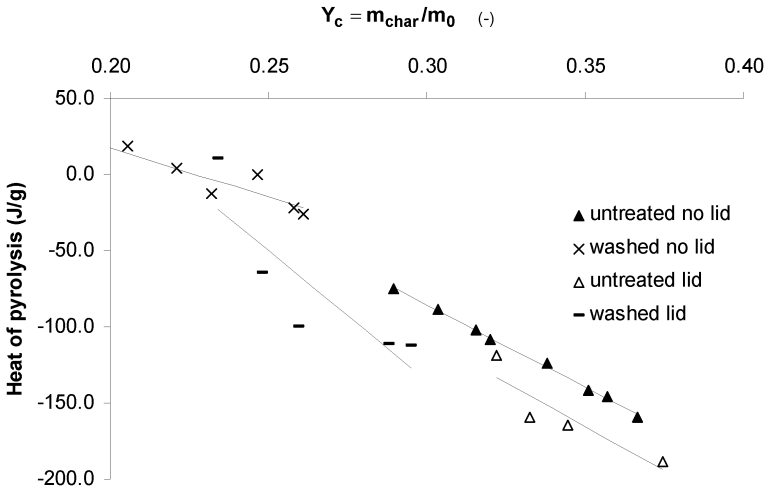

Figure 6.9: Heat of pyrolysis as function of the char yield for different initial sample masses of untreated and washed thistle, in crucibles with and without a lid.

that clearly favor secondary vapor-solid interactions has been rarely reported in the literature. In their TG/MS analysis of small samples of cellulose, Várhegyi et al. (1988a) observed changes in the mass spectrometric intensities belonging to the main pyrolysis products, when the sample was sealed in a DSC crucible with a pinhole.

The coupling of thermogravimetric analyzers with FTIR spectrometers for the on-line monitoring of evolved volatile compounds has provided useful input to the analysis of volatile products relevant to biomass pyrolysis, in the regime of slow primary decomposition (Wójtowicz et al., 2003). The main use of the TG-FTIR data has been the qualitative identification of reaction products formed during the TG run. Besides, FTIR is frequently used to characterize biomass chars (Mok et al., 1992; Várhegyi et al., 1998)

From infrared spectroscopy, the chemical composition is analyzed by identifying bands or signals characteristic of specific functionalities. In the process of characterizing volatile products of biomass pyrolysis, a variety of effects complicate the determination. Such effects include possible condensation of vapors, partial oxidative conditions and uncontrolled secondary cracking of the pyrolysis vapors. Moreover, the number of evolving products can be enormous, and they may emerge at the same time. Convenient techniques to separate the signatures and expose various components are required. In the present work, we swept the volatile products by a transfer line heated at a constant temperature of 200 °C to minimize the condensation of volatile decomposition products. We limited the observation to the largest conspicu-

ous peaks corresponding to simple species (CO and CO_2) and characteristic bands of organic pyrolysis products (C=O and C-H stretching vibrations).

A linear relation exists between spectral absorbance at a given wavenumber and concentration of a gaseous compound (Lambert-Beer law). Even in the absence of a experimental calibration, TG-FTIR measurements can be used to generate a specific gas profile to monitor qualitatively the evolution of a gas as a function of the time or the temperature of the TG furnace (Barontini et al., 2001). This requires that the compound of interest has a wavenumber absorption interval that is free of additional contributions from other substances. The contemporary formation of a wide number of volatile compounds complicates the selection of such intervals. In this work, the correct selection of those band positions, at low-noise portions of the spectrum, was based on the instrument's library enriched by the experience of the Department of Chemical Engineering at the University of Pisa in applying the TG-FTIR technique to analyze different feed stocks[4]. It allowed us to compare the release of the producing functionalities for the different type of experiments.

The assignment of the wavenumber ranges used for the determination of the emission profiles is presented in Table 6.4. These correspond to signals characteristic of volatile products from pyrolysis. The tarry volatile fraction contains a complex soup of organic compounds mixed with noncondensable gases (as detailed in the chapter before). Absorptions due to C-H stretching vibrations are associated to alkyl and aromatic functionalities. Signals due to C=O stretching vibrations come mainly from ketones, carbonyl and ester groups.

Table 6.4: Wavenumber ranges used for the determination of emission profiles

Wavenumber (cm^{-1})	**Assignment**
2400 - 2240	CO_2
2236 - 2143	CO
1820 - 1660	C=O stretching
3150 - 2600	C-H bond stretching

6.5.1 Analysis of the spectra stack plots

Typical spectral outputs (stack plots) from the FTIR analysis are shown in Figures 6.10 and 6.11. Infrared spectrums provide information as a function of both wavenumber and temperature. In Figure 6.10 we compare the absorptions at the temperature peak (T_{peak}) in the decomposition of 6 mg the given samples (see tables 3.8 and 3.9 in Chapter 3). In Figure 6.11 we plot the absorptions at the temperature of the shoulder (around 330 °C), in the decomposition of untreated beech.

At the temperature of maximum devolatilization (Figure 6.10), the untreated thistle sample evidences the lowest spectral absorbances associated to C=O and C-H

[4]Cozzani et al. Personal communication.

stretching vibrations, and the highest contribution to the CO_2 release. This may be a result of the higher lignin content of the herbaceous crop, since the evolution of organic groups is expected to be considerably higher from polysaccharides than from lignin (Evans and Milne, 1987; Mészáros et al., 2004a). This result is coincident with the TG/MS qualitative and quantitative analysis of the samples in the chapter before. On the other hand, beech, the sample which evidenced the maximum rate of decomposition, shows correspondingly the biggest C=O and C-H traces. The volatile organic production from the thistle sample becomes closer to that from beech as a result of the water-washing pre-treatment. At the same time, the CO_2 production is still considerably higher from the washed thistle sample (observe the corresponding band in Figure 6.10 panel A). The larger CO_2 evolved from the thistle samples can be attributed to the specific structural feature of the lignin present in this biomass (see the explanation in Section 5.2.2).

The use of covered pans appears to modify the release of some of the volatile products (compare panels A and B in Figure 6.10). Absorptions due to C=O and C-H bands decrease for all the samples, while the CO_2 production from beech increases, becoming roughly equal to those from the thistle samples. The closed vessel prevents the quick escape of the products from the hot zone. Thus, these vapors may undergo further decomposition and form additional quantities of CO_2 and CO (Várhegyi et al., 1988a).

In the case of the untreated beech sample at the temperature of the shoulder corresponding to hemicellulose decomposition (Figure 6.11), higher absorptions on the C=O vibration zone is observed when covered pans are used. It is even intensified by employing higher initial sample masses (compare panels A and B). It seems as if the resistance to the flow of primary volatiles from their vicinity could somehow promote the releasing of carbonyl functionalities at the temperature domain of hemicellulose decomposition.

6.5.2 Analysis of the product evolution profiles

We produced the emission profiles of the volatile functionalities studied in the given samples, normalized by the initial sample mass. Figures 6.12 and 6.13 compare the evolution using different sample masses in crucibles with and without a lid, at the temperature ranges with the lowest noise on the main decomposition domain. Both increase in the initial sample mass and use of covered pans entail some decrease in the production of hydrocarbons and organic compounds, represented by C=O and C-H bond stretching. Secondary char formation reactions compromise the evolution of the organic vapors, as evidenced by the stack plots. Using lids, the decrease in the evolution of carbonyl functionalities by employing higher initial masses, from the temperature shoulder associated to hemicellulose, is highly remarkable in the case of beech (observe panel A2 in Figure 6.12).

The carbon monoxide production is affected by several factors. On the one hand, CO evolves owing to the large number of hydroxyl groups and oxygen atoms present in the natural polymers that make up the cell walls. Thus, its pattern evolution fits the release of hydrocarbons and organic compounds. On the other hand, carbon monoxide

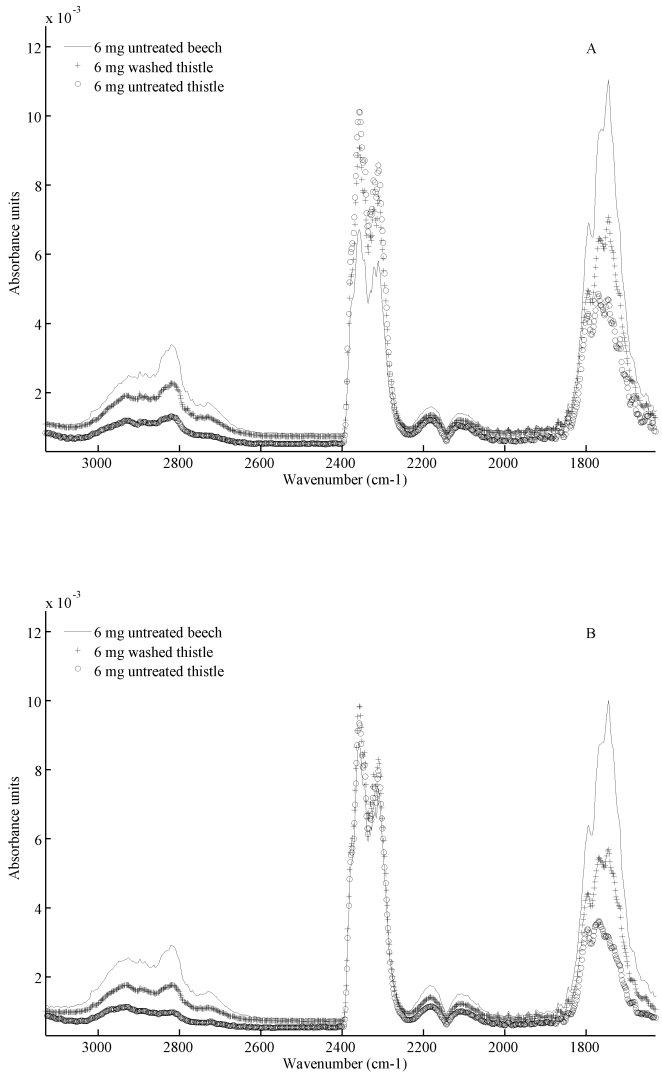

Figure 6.10: Comparison between the FTIR spectrums in the pyrolysis of 6 mg untreated beech, untreated thistle, and washed thistle, at the temperature of maximum devolatilization, using uncovered (A) and covered pans (B). Intensities have been normalized by the initial sample mass.

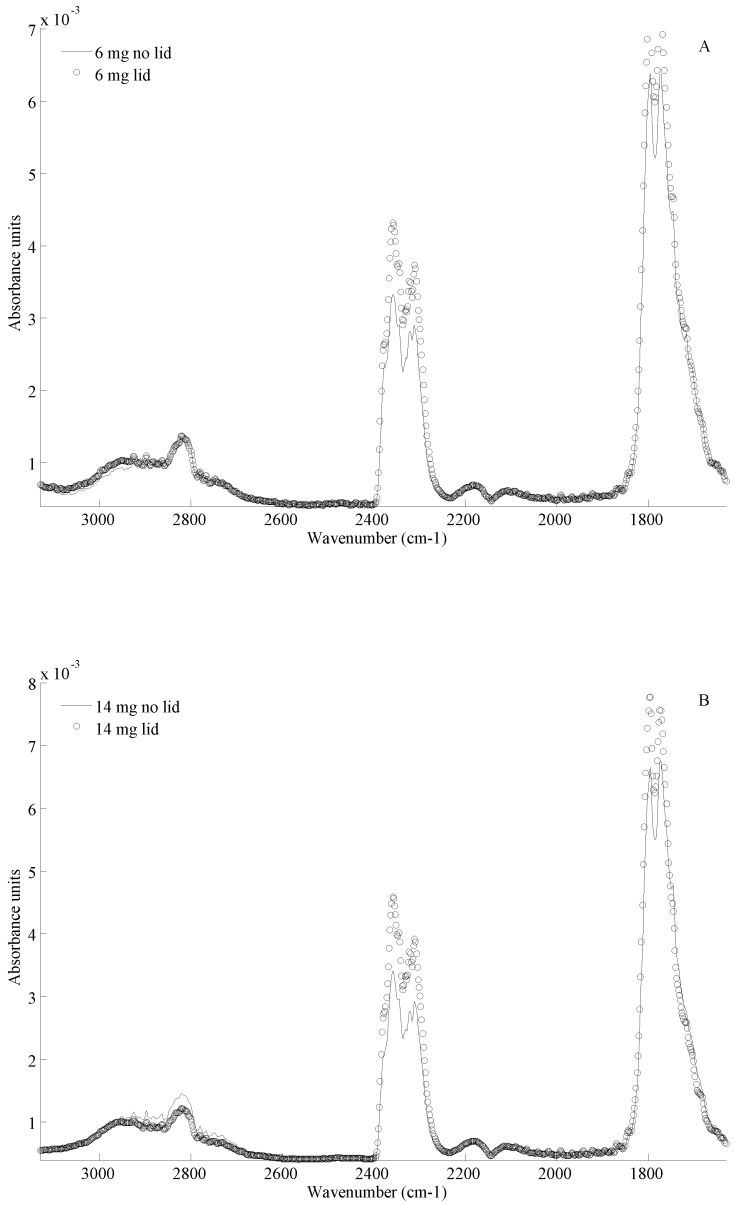

Figure 6.11: Comparison between the FTIR spectrums in the pyrolysis of 6 mg (A) and 14 mg (B) of untreated beech, at the temperature of the shoulder of the hemicellulose decomposition, using uncovered and covered pans. Intensities have been normalized by the initial sample mass.

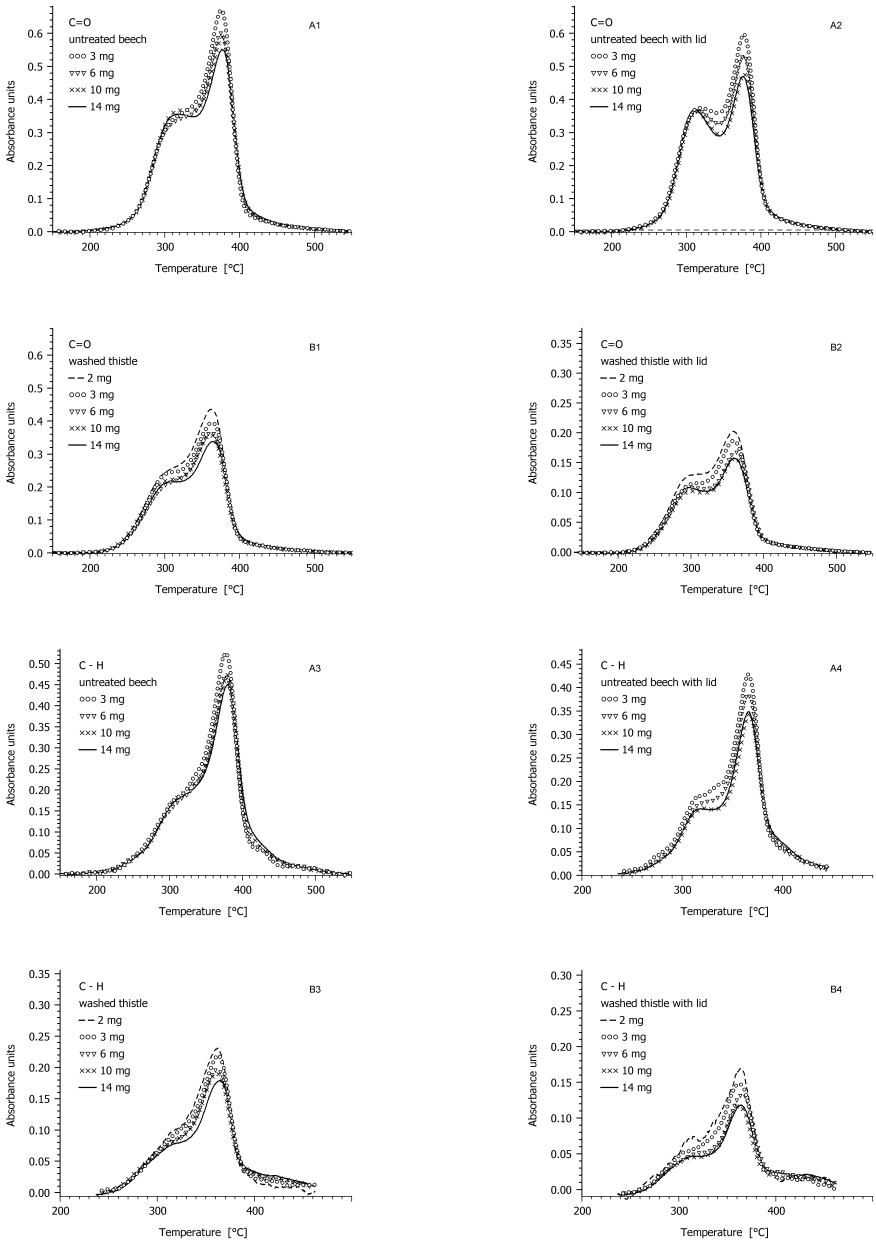

Figure 6.12: Organic product evolution profiles from several initial sample masses of untreated beech (A) and washed thistle (B) at 20 °C/min, using uncovered (1 and 3) and covered pans (2 and 4). The scaling factors for the individual functionalities evolved from wood and thistle are the same.

is one of the cracking products from the char formation reactions. Consequently, additional quantities of CO can be expected from enhanced secondary interactions. These multiple sources can explain the different behaviors observed in Figure 6.13. CO_2 is the highest evolved product from thistle as discussed before, and the most clear evidence of the further char formation reactions by prolonging the vapor-phase residence times.

6.6 Secondary decomposition. Kinetic study

6.6.1 Global kinetic approach

In order to achieve the global kinetic description of all the types of experiments considered in this thesis, we observed how the best kinetic approach applied in the latter chapters can predict the behavior of the samples employing different initial sample masses and covered crucibles. Firstly, we simulated the DTG curves using the same E, log A and c_j parameters in Tables 4.6 and 4.7 (reference values). Figures 6.14 and 6.15 show selections of these results. Experiments without lids resulted quite well-fitted, in spite of the diverse initial sample masses . The experiments with lids evidenced slightly higher deviations. From the analysis of the DTG characteristics in Chapter 3, we had observed shifting in the temperature onset, as well as slightly wider DTG curves, shifted in T_{peak} by maximum 6 °C, by the presence of a pierced lid (see Section 3.4.1). Lower DTG peaks compared with the simulated curves are also observed in some cases. Both increase in sample size and presence of a lid resulted in an increase of char yield. Besides, the FTIR experiments gave us evidence of alterations in the volatile product distribution. Secondary vapor-solid interactions could affect the decomposition in that way, as discussed previously.

Bearing in mind the latter observations, we considered the presence of the secondary vapor-solid interactions in our kinetic approach. We assumed these interactions as the contribution of an additional reaction, for which part of the reactive organic vapors produced during pyrolysis form extra char and produce different types of vapors and gases, when held in the presence of the reacting solid sample. The generic reaction scheme is represented in Figure 6.16. This is complementary to Figure 5.12. We have added some letters and symbols (K_2, γ, β) to represent the specific secondary reaction rate and the corresponding volatiles and char formation ratios produced by this interaction.

The kinetic equations for the mechanism shown are as follows:

$$dm_b/dt = -\sum_{j=1}^{M} c_j d\alpha_j/dt \tag{6.6}$$

$$dm_{c_1}/dt = dm_b/dt \tag{6.7}$$

$$dm_{v_1}/dt = -dm_b/dt - K_2 m_{v_1} \tag{6.8}$$

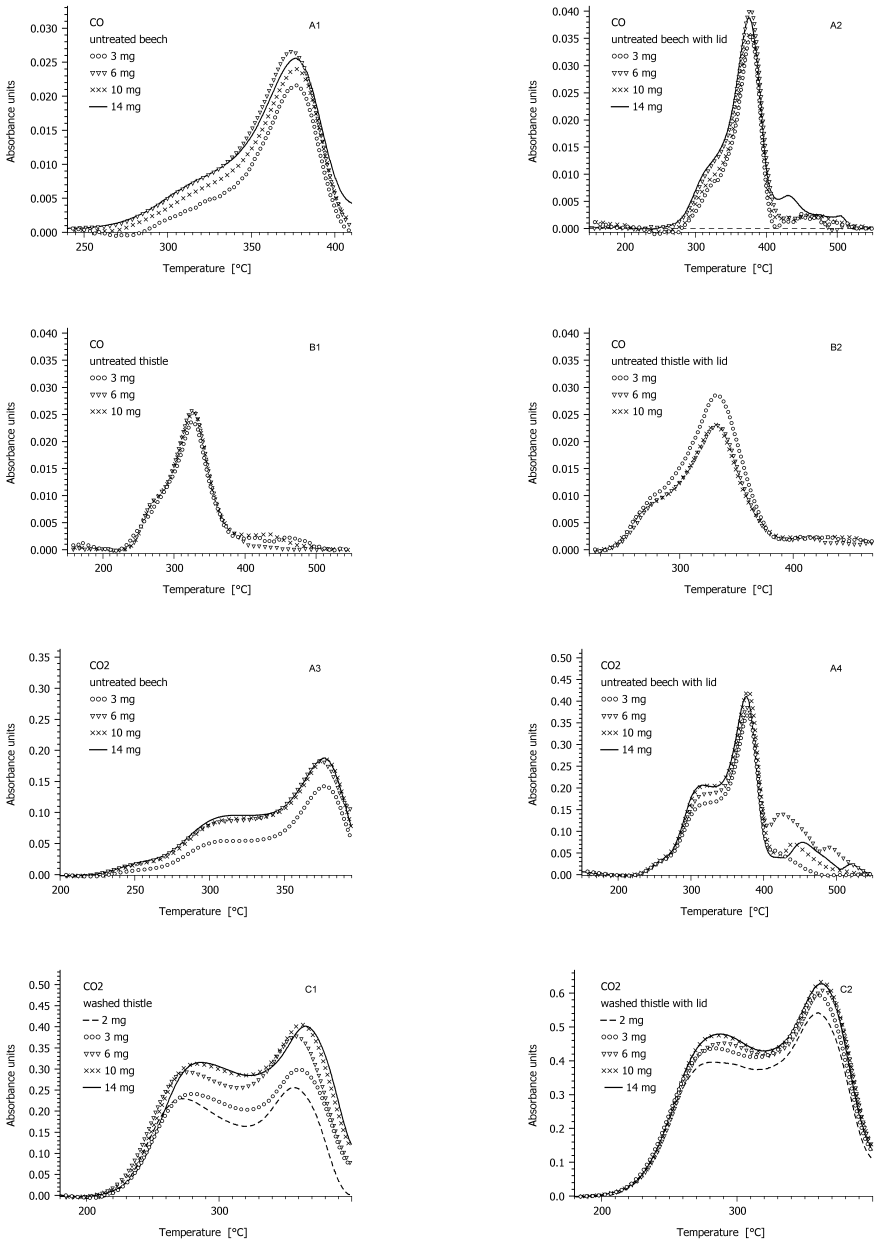

Figure 6.13: CO and CO_2 evolution profiles from several initial sample masses of untreated beech (A), untreated thistle (B) and washed thistle (C) at 20 °C/min, using uncovered (1 and 3) and covered pans (2 and 4). The scaling factors for the individual species evolved from wood and thistle are the same.

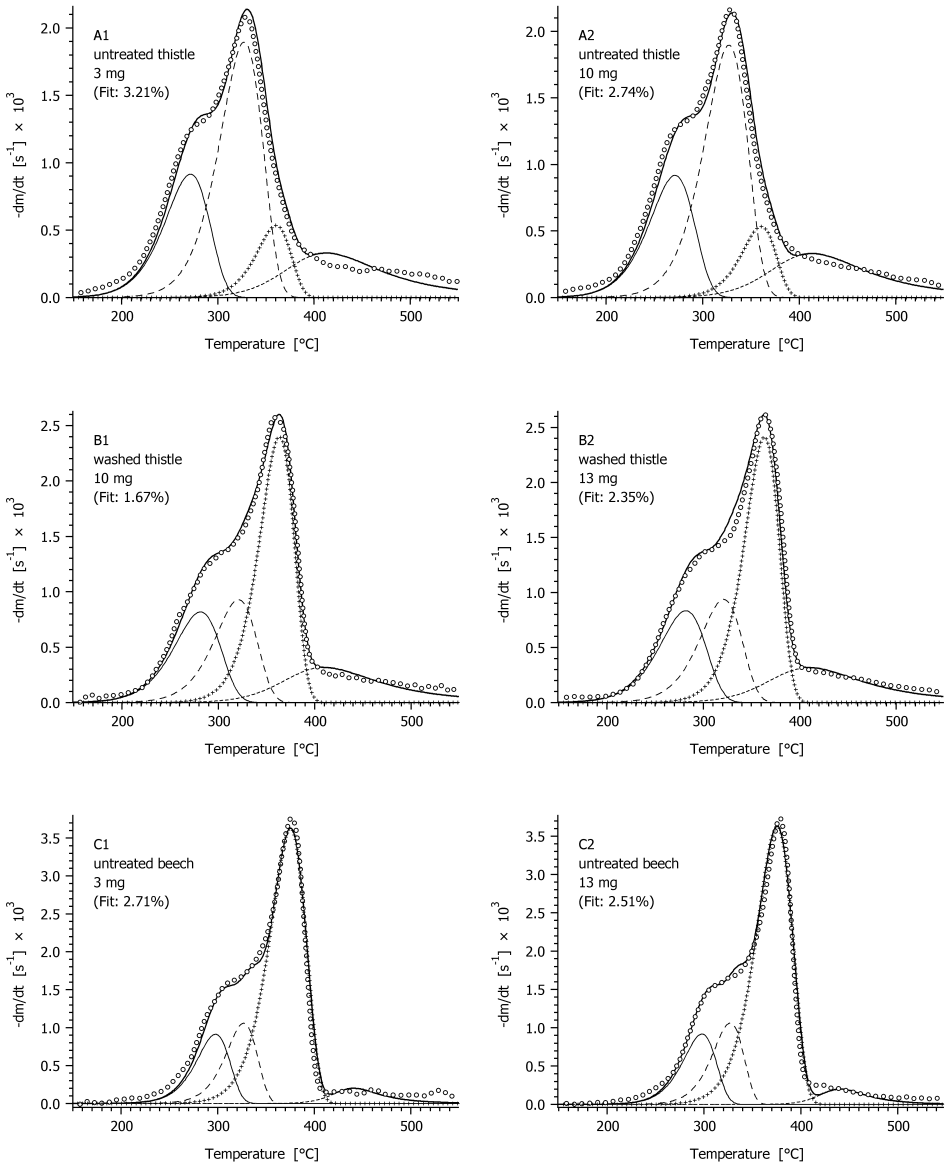

Figure 6.14: Comparison between the observed (o o o) and simulated (—) DTG curves for different biomass samples at 20 °C/min in the Netzsch thermobalance, with different initial sample masses in crucibles without a lid. The kinetic model is the same described in Section 4.2.5, with kinetic parameters from mean values in Tables 4.6 and 4.7.

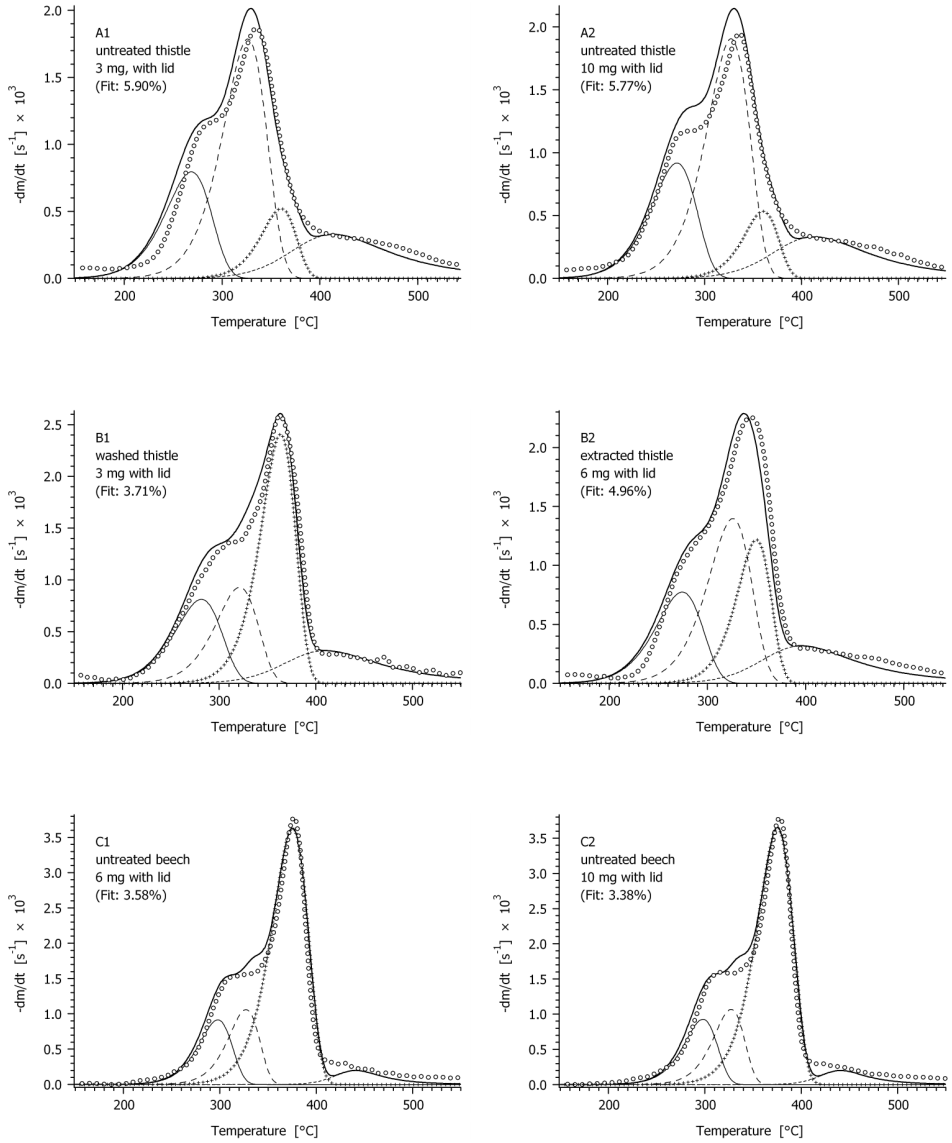

Figure 6.15: Comparison between the observed (o o o) and simulated (—) DTG curves for different biomass samples at 20 °C/min in the Netzsch thermobalance, with different initial sample masses in crucibles with a lid. The kinetic model is the same described in Section 4.2.5, with kinetic parameters from mean values in Tables 4.6 and 4.7.

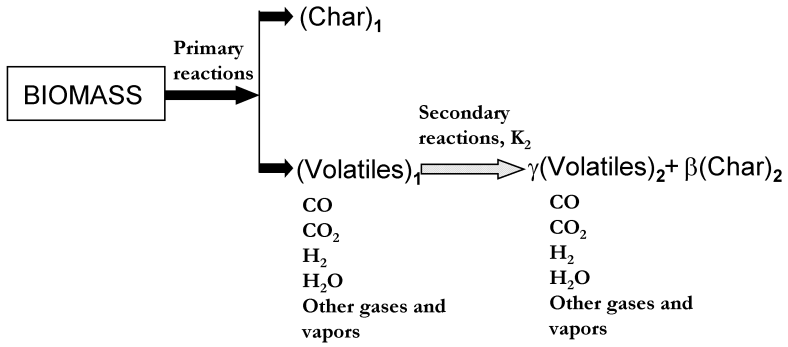

Figure 6.16: Kinetic scheme applied in this thesis for the global, primary and secondary biomass pyrolysis.

$$dm_{c_2}/dt = \beta K_2 m_{v_1} \tag{6.9}$$

$$dm_{v_2}/dt = \gamma K_2 m_{v_1} \tag{6.10}$$

where m_b, m_{c_1}, m_{c_2}, m_{v_1}, m_{v_2} are the normalized masses (divided by the initial sample mass) of virgin biomass, solid from the primary devolatilization, char produced by the secondary decomposition, total volatiles produced by the primary reactions and total volatiles produced by the secondary decomposition, respectively. The solid product from the primary decomposition, m_{c_1}, is assumed as a catalyst of the tarry organic vapors decomposition, not as a reactant in the secondary reaction. Thus, the rate of primary solid formation (Equation 6.7) is the same overall reaction rate for primary decomposition, calculated by Equation 4.1. Note that the reaction order for the secondary process has been assumed as $n = 1$. The specific secondary reaction rate, K_2, is approximated by an Arrhenius equation:

$$K_2 = A_{sec} exp(-E_{sec}/RT) \tag{6.11}$$

Here A_{sec} and E_{sec} are correspondingly the preexponential factor and the apparent activation energy for the secondary vapor-solid interactions.

From the global mass balance, the normalized sample mass calculated from the model, m^{calc}, is the sum of the solid fractions produced by both primary and sec-

Table 6.5: Summarized kinetic parameters for the secondary decomposition of biomass materials

			$\log A_{sec}$ (s^{-1})	E_{sec} (kJ/mol)	β
thistle	**parameters**	**washed**	**3.09**	**58**	**0.05**
	differences[a]	**extracted**	0.37		-0.01
		washed&extracted	0.52		0.00
		untreated	0.13		0.01
beech	**Parameters**	**untreated**	**5.06**	**84**	**0.05**

[a]Alterations from the parameters of the washed sample.

ondary decomposition. Thus, the variation of sample mass with time is made by the addition of Equations 6.7 and 6.9:

$$dm^{calc}/dt = -\sum_{j=1}^{M} c_j d\alpha_j/dt + \beta K_2 m_{v_1} \tag{6.12}$$

where β is the overall fraction of volatiles that repolymerize to form extra char by the secondary interactions. Note that the secondary stage is assumed as a successive reaction respect to the primary decomposition. Thus, we do not describe the amount of the reactive volatile species by reacted fractions (α), as we did for the description of the primary devolatilization reactions.

In order to calculate β, A_{sec} and E_{sec} and complete the entire set of parameters of the global model, we required the evaluation of the experimental DTG results from crucibles with lids and different initial sample masses, by minimizing the sum defined by Equation 4.4 in Chapter 4, using least squares non-linear methods.

The experimental data was treated in the same way as in Section 4.1.2. A fit quantity was calculated by Equation 4.5. A modified version of the MATLAB program used in Chapter 4 was applied for the determination of the unknown parameters.

6.6.2 Kinetic evaluation of the overall mass loss

The series of experiments with lids and different initial sample masses were evaluated simultaneously for the given samples[5]. Again, the best fit activation energies of the water-washed experiments of thistle were employ to evaluate the rest of untreated and pretreated samples. Figure 6.17 shows some of the curves simulated by the current model. Some improvement is observed in the fit by using the approximation of the secondary decomposition (see Figures 6.15 and 6.17). Table 6.17 summarizes the latter results. The water washed samples provide the reference values in the case of thistle.

[5]The reader should be addressed to Chapter 3, Table 3.4 to remember the type of samples for which covered pans with different initial sample masses were used.

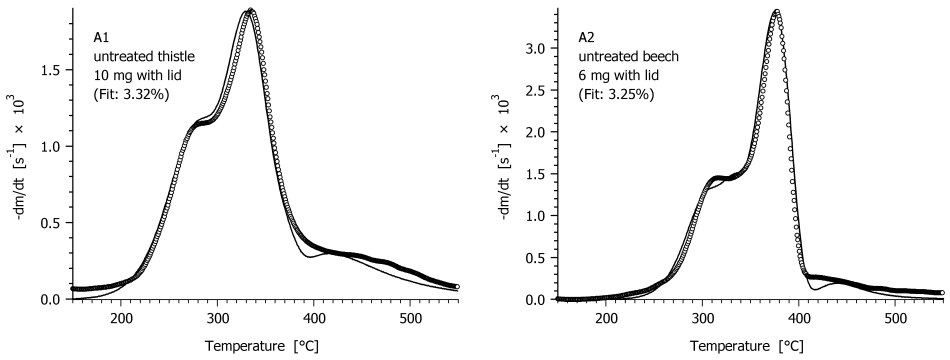

Figure 6.17: Comparison between the observed (o o o) and simulated (—) DTG curves at 20 °C/min for different biomass samples with different initial sample masses in crucibles with a lid. The kinetic model is described in Section 6.6.1.

β value also expresses the additional char formation from the secondary decomposition. From the study of the DTG characteristics in Chapter 3, we observed increase of char yield up to 6% (or 0.06 fraction of the initial sample mass) in the washed sample of thistle by both increase in the initial sample mass and the presence of a lid. Being the current results close to that from the observation of the DTG characteristics, we consider the resulting β value suitable to represent the extra char formation by the secondary vapor-solid interactions.

Several authors have proposed generalized mechanisms to describe biomass pyrolysis that include both primary and secondary reactions. In these models, the primary stage has been described through different kinetics to obtain the three fractions, gas, char and tar (Shafizadeh and Chin, 1977; Thurner and Mann, 1981; Font et al., 1991; Koufopanos et al., 1991; Miller and Bellan, 1997), similar to the extended Broido-Shafizadeh scheme of cellulose pyrolysis (kinetic parameters for the secondary stage found in Liden et al. (1988)). Some of these works have neglected the secondary char formation reaction, only considering the tar cracking to gas species in the second stage (Miller and Bellan, 1997; Di Blasi and Russo, 1994). We are unaware of previous global mechanisms of independent parallel reactions, which do not predict product fractions separately, accounting the secondary char-forming process. The A_{sec} and E_{sec} parameters obtained for the beech sample resulted similar to the values published by Koufopanos et al. (1991) for further secondary interactions of woody material. In their approach, both primary volatiles and char are reactants than produce different types of vapors, gases and char, resulting in a modified final product distribution.

Table 6.6: Comparison between the total amounts (% m/m) of gaseous products obtained from different analytical techniques. Temperature range, 200 - 550 °C

Sample		CO FTIR (%)	CO MS (%)[a]	CO_2 FTIR (%)	CO_2 MS (%)[a]
Thistle	*Untreated*	3.35	3.24	10.80	10.79
	Washed	3.77	3.66	8.29	8.73
Beech	*Untreated*	4.76	5.25	5.49	5.40

[a]Differences between these values and those presented in Table 5.3 obey to the different temperature ranges of the corresponding calculations.

6.6.3 Product distribution from the secondary char-forming process

We observed noticeable changes in the major volatile profiles when samples were covered and different initial sample masses were used (see Section 6.5). Having obtained acceptable kinetic parameters for the entire description of the secondary vapor-solid interactions, we were interested in quantify the changes in the production of given volatiles as a consequence of this process.

As in the determination of specific volatile yields from MS intensities, we required calibration factors to obtain quantitative data on evolved gaseous products (CO and CO_2) from the TG-FTIR application. In order to obtain the amounts of a given gas evolved in the entire range of decomposition, the FTIR intensities were integrated within the temperature ranges with good signal/noise ratios. Then, we applied calibration factors from a pulse calibration technique proposed and presented by Marsanich et al. (2002). They employed the same equipment and experimental conditions as for our current experiments. The correspondence between the values obtained from FTIR signals and the total CO and CO_2 amounts previously calculated from the MS intensities was verified for the equivalent experiments without lids[6]. We got very close values from both sources (see Table 6.6).

From the FTIR analysis, we observed increase in the CO and CO_2 peaks when vapors hold in the presence of the reacting solid sample. In order to quantitatively predict the evolutions of these gas species from the covered samples with different initial sample masses, we consider the production rate of extra CO and CO_2 similar to the secondary volatile formation in Equation 6.10:

$$dm_{CO}/dt = \gamma_{CO} K_2 m_{v_1} \tag{6.13}$$

$$dm_{CO_2}/dt = \gamma_{CO_2} K_2 m_{v_1} \tag{6.14}$$

where m_{CO} and m_{CO_2} are the normalized masses (divided by the initial sample mass) of CO and CO_2 produced by the secondary reactions. γ_{CO} and γ_{CO_2} represent

[6]The reader should be addressed to Chapter 3 for a revision of the equivalent experimental conditions between the Perkin-Elmer and the Netzsch equipments.

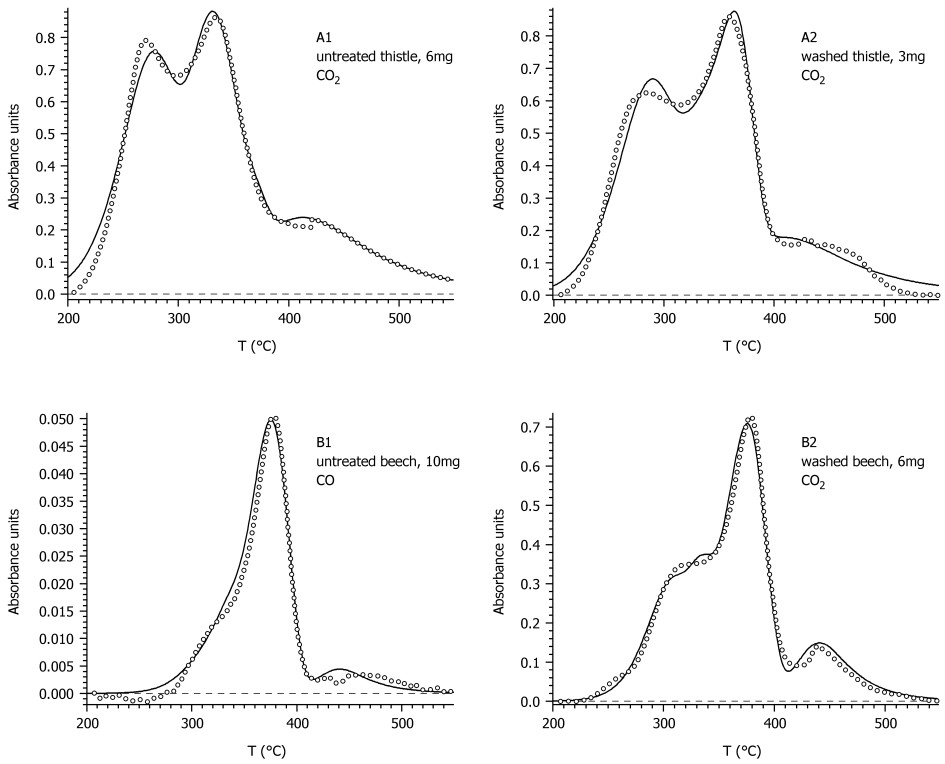

Figure 6.18: Observed (o o o) and simulated (—) FTIR traces of CO_2 released from different initial sample masses of thistle (A) and beech (B) biomasses in crucibles with lids.

the fractions of primary products that react to produce additional gas contributions. The overall production of these gases calculated for the model is then the sum of the contributions from both primary and secondary stages:

$$dm_s^{calc}/dt = dm_{v_s}/dt + dm_s/dt \tag{6.15}$$

with s referred to the given gas species and dm_{v_s}/dt solved by Equation 5.4. To determine the unknown γ parameters we evaluated the FTIR experimental profiles of CO and CO_2, and related the values calculated to the corresponding calibration factors. Least squares non-linear methods and procedures explained before were used. Figure 6.18 show some examples of the simultaneous evaluation of profiles from experiments with different initial sample mass, with γ parameters (converted to mass fractions) in Table 6.7. An acceptable agreement is observed between experimental and simulated curves.

Table 6.7: γ parameters representing the fraction of the overall primary products that react with char to produce extra gas from biomass pyrolysis

		γ_{CO}	γ_{CO_2}
thistle	**untreated**	0.00	0.05
	washed	0.01	0.06
beech	**untreated**	0.04	0.05

γ parameters also represent the extra gas formation from the secondary vapor-solid reactions. From values in Table 6.7, the additional formation of CO in thistle is not evident, as it was previously observed by the qualitative analysis of the FTIR profiles. On the other hand, the current results also imply that a considerable amount of CO_2 is produced as a consequence of secondary interactions for all the samples (compare the present values with the corresponding overall gas yields predicted, total c, in Tables 5.4 and 5.5). We are unaware of previous studies quantifying the extra production of gases from secondary interactions in biomass pyrolysis.

We added the last results, on the kinetic evaluation of the secondary decomposition, to the Aspen custom model introduced in the Chapter before. Employing the equations listed in Section 6.6.1 in addition to Equations 4.1 and 4.2, with parameters in Tables 4.6, 4.7 and 6.5, we can obtain the total fractions of volatiles and solid residue as functions of time and/or temperature, for a biomass that has been subjected to primary and secondary vapor-solid stages. Individual profiles of CO, and CO_2 from the global process can be obtained by using equations of type 6.15, with parameters in Tables 5.4, 5.5 and 6.7. The fraction corresponding to other gases and vapors (see Figures 6.16 and 6.19) is calculated as the difference between the global volatile production and the sum of contributions of the two gas species quantified individually.

6.7 Conclusions of this chapter

The devolatilization behavior of the three biomass materials studied in this thesis (pine, beech and thistle), including their pretreated versions, was investigated by thermogravimetry/differential scanning calorimetry (TG/DSC) and thermogravimetry/fourier transform infrared spectroscopy (TG/FTIR), under conditions for both primary and secondary pyrolysis. From the information traced by the heat of pyrolysis, the exothermic character of the thistle thermal degradation was revealed. Both pretreatments added endothermicity to the process. None of the samples achieved as high endothermicity as a sample of pure cellulose under conditions of primary decomposition. It revealed the low heat demand of our samples and, thus, they would have been less affected by heat transfer intrusions during the experiments. Differences in chemical composition of the samples (characterized by contents of holocellulose, lignin, inorganic ions and extractives) produced wider differences in both the heat of pyrolysis and char production than holding captivate the vapor products in crucibles with lids.

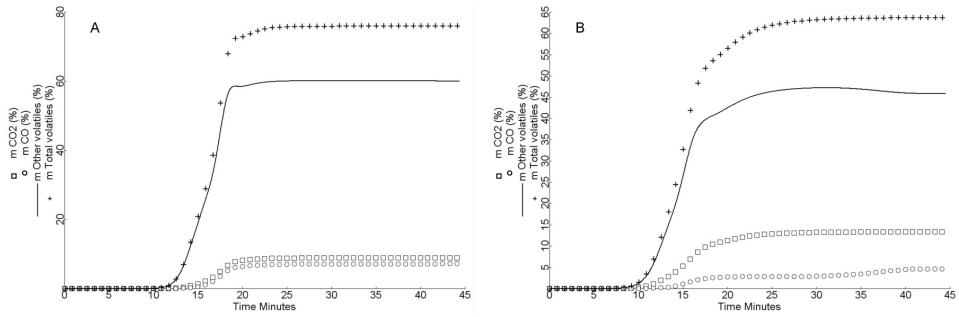

Figure 6.19: Simulated yield curves of volatiles released from the untreated beech (A) and thistle (B) samples at 20 °C/min in a process involving secondary vapor-solid interactions. Selected results from the pyrolysis Aspen custom model.

The role of vapor-solid secondary interactions was evidenced by the evolution profiles of the main gaseous products, too. FTIR profiles of characteristics functionalities revealed the higher formation of CO_2 and CO due to the enhancement of char-forming reactions by prolonging the vapor-phase residence times, at the expense of the tarry organic vapor evolution.

A successive reaction was added to the kinetic model of parallel independent reactions, in order to describe the secondary vapor-solid interactions in our experiments. We assumed these interactions as the repolymerization of part of the reactive organic vapors produced during primary pyrolysis, forming extra char and producing different types of vapors and gases, when held in the presence of the reacting solid sample. The additional formations of CO_2 and CO under these conditions were also counted individually. Then, the global, primary and secondary pyrolysis kinetic model describing the entire set of experiments carried out along the thesis was finally accomplished.

Chapter

SEVEN

Future work. Pyrolysis extension to practical applications.

Along this thesis, we have touched key aspects in the kinetic description of primary and secondary biomass pyrolysis, mainly in the regime of chemical kinetic control, with the analysis of different representative biomass materials. However, much remains to be learned about the fundamental chemical and physical processes governing the pyrolytic decomposition of biomass, on the one hand, and the applicability of the type of kinetic description evaluated in this thesis for engineering purposes, on the other hand. The analysis of conditions commonly applied in commercial thermochemical conversion processes (i.e. more severe heating conditions and/or larger particle and feed sizes) has been out of the scope of this thesis. The applicability of our kinetic approach on the description of the thermal decomposition of other type of materials is still waiting for discussion. In a first part of this chapter, we present the results of applying the present type of kinetic description over the decomposition of scrap tires. Furthermore, we discuss some other important aspects for future work in the field of engineering applications.

7.1 Kinetic study of scrap tires pyrolysis

The disposal of used automotive tires is an increasing economical and environmental problem for most of the developed countries. One common way of disposal is land filling. Scrap tire is bulky and it is not a biodegradable residue and therefore it is not possible to achieve its natural degradation in landfills. As a consequence, open dumping of scrap tire not only occupies a large space, presents an eyesore and could cause potential health and environmental hazards, but also illustrates wastage of valuable energy resource (Aylón et al., 2005). To circumvent these disadvantages, car tires are used for substituting fossil fuels in the cement industry. This thermal recycling strategy can utilize the high energy content of the tires. An alternative to combustion of used tires is upgrading by pyrolysis (Seidelt et al., 2006).

It is well known that tire is made of rubber materials (polybutadiene, styrene-butadiene rubber and polyisoprene or natural rubber), carbon black, some fibrous

materials and many other additives like processing oil, plasticizer or vulcanization accelerators (Seidelt et al., 2006; Aylón et al., 2005). It has high volatile and fixed carbon contents with heating value greater than that of coal. This makes rubber from old tire a good raw material for thermochemical processes. Waste tire pyrolysis has been widely studied for years. It leads to the production of the three fractions, solid carbon residue, a condensable fraction and gases, similarly to the pyrolysis of biomasses (Berrueco et al., 2005). We have applied the kinetic approach of independent partial reactions in the description of the pyrolytic decomposition of a sample of scrap tire. More than adding new insight into the field, the purpose with performing this kinetic analysis is to observe the performance of the approach followed in this thesis, describing the thermal decomposition of a not strictly biogenic material. A summary of the results will be presented.

7.1.1 Experimental part

The tyre samples under study came from "Instituto de Carboquímica" (Zaragoza, Spain). Particles of sizes below 1 mm were subjected to N2 and air atmosphere, at 5 and 20 °C/min linear heating rates, using the Cahn and Setaram thermogravimetric equipments. An initial sample mass of 10 mg was used. The rest of experimental conditions and procedures were the same as in Section 3.2.4. The proximate analysis and elemental composition of the samples are shown in Table 7.1.

Table 7.1: Tire samples analysis

	Proximate (% by weight)			
	moisture	volatile matter	fixed carbon	ash
tyre sample	0.54	62.71	29.64	7.11

	Ultimate (% by weight; dry ash-free samples)		
	C	H	S
tyre sample	88.30	7.69	1.95

7.1.2 Thermokinetic study

A similar procedure to that applied in Chapter 4 for the kinetic evaluation of curves coming from different apparatus and heating rates was employed in this case. Setaram DTG results at 5 °C/min were evaluated by the same model of pseudocomponents described in Section 4.1. Latter, resulting E and c_j parameters were used to estimate the best log A value that fit the Cahn DTG curves. Figure 7.2 and Table 7.2 summarize the results in N_2 atmosphere. The Setaram results provide the reference values in Table 7.2, while the Cahn results are presented as differences from the references. In N_2 atmosphere, three partial reactions, with different nth order, were necessary to

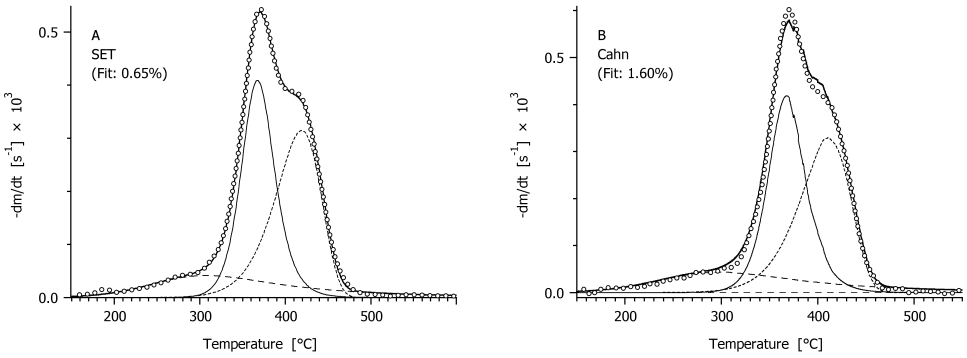

Figure 7.1: Comparison between observed (o o o) and simulated (—) DTG curves of waste tire pyrolysis in nitrogen atmosphere at 5 °C/min employing the nth-order reaction model of pseudocomponents.

Table 7.2: Summarized results of the kinetic evaluation of waste tire pyrolysis in nitrogen atmosphere at 5 °C/min employing the nth-order reaction model of pseudocomponents

partial reaction		$\log A$ (s^{-1})	T_{peak} (°C)	E (kJ/mol)	c	n
1st	**reference value**	**2.28**	**306**	**57**	**0.11**	**3**
	diff. Cahn	0.11	1			
2nd	**reference value**	**18.48**	**368**	**254**	**0.26**	**2**
	diff. Cahn	0.01	1			
3rd	**reference value**	**8.49**	**419**	**146**	**0.27**	**1**
	diff. Cahn	0.13	8			

describe well the characteristics of the observed DTG curves. The peak on the low temperature region (around 300 °C) is dominated by the decomposition of the tire rubber additives. These are a mixture of different products (extender oils, plasticizers and other additives) with different properties and therefore different behavior under pyrolysis conditions (Aylón et al., 2005). The sharp peak between 300 and 450 °C corresponds to the decomposition of natural rubber (Conesa et al., 1998). The last partial reaction can be assigned to the decomposition of styrene-butadiene rubber. Three partial reactions with similar kinetic parameters were also obtained by other authors like Conesa et al. (1998) and Aylón et al. (2005).

The results obtained from the Setaram, 5 °C/min experiments were also used to predict the behavior of the samples at a higher heating rate, 20 °C/min[1]. An excellent fit was also obtained in this case, as shown in Figure 4.5, indicating the strength of

[1]Remember the discussion on the application of actual kinetic approaches to different heating regimes in Chapter 4.

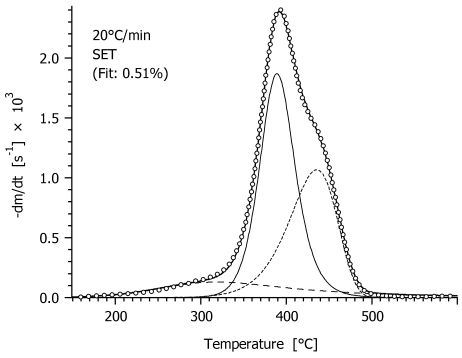

Figure 7.2: Comparison between observed (o o o) and simulated (—) DTG curves of waste tire pyrolysis in nitrogen atmosphere at 20 °C/min employing the nth-order reaction model of pseudocomponents and the same resulting kinetic parameters at 5 °C/min.

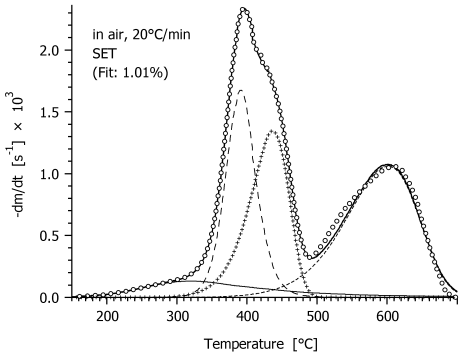

Figure 7.3: Comparison between observed (o o o) and simulated (—) DTG curves of waste tire pyrolysis in air atmosphere at 20 °C/min employing the nth-order reaction model of pseudocomponents.

the approaches used in our work.

For the evaluation of the experiments in air atmosphere, an additional partial reaction was taken into account (see Figure 7.3). From the analysis of the DTG characteristics, we observed similar $T_{hcstart}$ and T_{peak} between the curves in both oxidative and inert atmosphere. Consequently, acceptable results were obtained by keeping E and $\log A$ values for the three first reactions constant an equal to the set of reference values in Table 7.2. The peak arising between 400 and 670 °C is due to the burnoff of the char formed. Resulting kinetic parameters are summarized in Table 7.3

Table 7.3: Summarized results of the kinetic evaluation of waste tire pyrolysis in air atmosphere at 5 °C/min employing the nth-order reaction model of partial reactions

partial reaction	$\log A$ (s^{-1})	E (kJ/mol)	c	n
1st	**2.28**	**57**	**0.09**	**3**
2nd	**18.48**	**254**	**0.27**	**2**
3rd	**8.49**	**146**	**0.27**	**1**
4th	**4.86**	**118**	**0.41**	**1**

7.2 Future research

Several assumptions and considerations in our work still require attention and they are worth mentioning in this subsection so as to encourage future research. The selection of the experimental conditions applied in this thesis highly obeyed to availability of analytical devices and experimental equipments, as well as time limitations. Some interesting conditions for engineering applications were out of the scope of the work.

The heating rates applied in this thesis are within the range of interest for conventional charcoal kilns and retorts, and some technologies of fixed-bed updraft gasification (Antal and Grønli, 2003; Branca et al., 2003). For applications where the volatile fractions (gases and vapors) are the major product of interest, heating rates are expected to be considerably higher (Scott et al., 1999; Nunn et al., 1985; Di Blasi et al., 1999; Branca et al., 2003). This condition of high thermal severity also allows studying the secondary cracking of pyrolysis vapors to light volatile and gas species, normally occurring at temperatures above 600 °C. This process is out of the extent of our work. Experimental work in the area of high thermal severity, joined to a suitable kinetic description of the latter process, are still required in the attempt to elucidate the global phenomena.

In terms of practical applications, the grinding of biomass materials to micro-particle sizes can result economically unfeasible. In many cases, macro-particle models are relevant for the prediction of commercial pyrolysis processes (Miller and Bellan, 1997). The performance of industrial-scale kilns and retorts that carbonize large wood chips and other biomass particles is influenced by the strong exotherm associated with charcoal formation from secondary pyrolysis (Antal and Grønli, 2003). Our study of the secondary decomposition was just limited to feasible sample size conditions in thermogravimetric, small scale experiments. Even for this relatively narrow range, we observed high variations in heat of reaction depending on the initial sample mass. In order to make our kinetic approach suitable for modeling of those industrial applications, transport phenomena should be also accounted for, in addition to the variation of particle properties as chemical reactions take place (see e.g. the works of Di Blasi and Russo (1994), Babu and Chaurasia (2004), Babu and Chaurasia (2003), Miller and Bellan (1997), Pyle and Zaror (1984) and the revision of Kersten et al. (2005) as interesting references).

In the attempt to increase the information content of actual series of experiments, we involved isothermal sections (stepwise heating program) in our work. However, we only had available stepwise experiments for the global mass loss determination. The kinetic evaluation of intensity profiles was based on experiments under linear heating programs. For a more suitable evaluation of these profiles, analysis of the product evolutions at another heating conditions could have been worthy considering. Besides, analysis of the evolution of some other volatile species like methane could have provided even more insight into the study of the chemical phenomena, on the one hand, and facilitate the quantification of total gas and tar fractions, on the other hand. Another thermoanalytical technique has been applied to the samples to increase the information content of the product analysis experiments. The observation of pyrolysis/gas chromatography-mass spectrometry results has been already started.

7.2.1 Modeling and simulation of biomass pyrolysis as a unit or step in engineering applications

In terms of engineering purposes, pyrolysis can be used as an independent process for the production of useful energy (fuels) and/or chemicals. It also occurs as the first step in a gasification or combustion process. The use of consistent data from pyrolysis, valid over wide temperature ranges and for different materials, is particularly important in gasification process because, contrary to coal gasification where the devolatilization stage contributes only for 20-40% of the total volatiles released, in biomass gasification this contribution increases up to 60-80%. On the other hand, the pyrolysis characteristics influence the predictions of both the producer gas quality and activity of gasification reactions, through hydrogen, carbon dioxide, and steam concentrations (Di Blasi et al., 1999; Radmanesh et al., 2006). Besides, for an optimum design of combustion or gasification processes for waste chars, knowledge of the char properties is essential, including the influence of the char production conditions (Henrich et al., 1999).

In the latter Chapters we introduced a pyrolysis simulation program (employing ACM) that contains the kinetic approach accounting for primary and secondary biomass decomposition. The purpose with programming this model is to make kinetics available to couple with some other important issues in process modeling (i.e. gas-phase reactions, transport phenomena, including heat convection, conduction and radiation, volatiles and gas transport by diffusion and convection and momentum transfer), as well as to compare the performance of our current kinetic approach with some others suited for modeling or scale-up attempts. Besides, we will able to study the performance of this type of kinetic description over the decomposition of other type of biomass residues.

We could add now the resulting parameters of the tire sample, as another material of interest within the simulation. Having available the variation of gas product yield with temperature from this material, we could estimate acceptable parameters to predict the evolution profiles of interesting products from tire pyrolysis, comparing different approaches, as we made in Chapter 5.

The next step in the simulation would be coupling pyrolysis kinetics with trans-

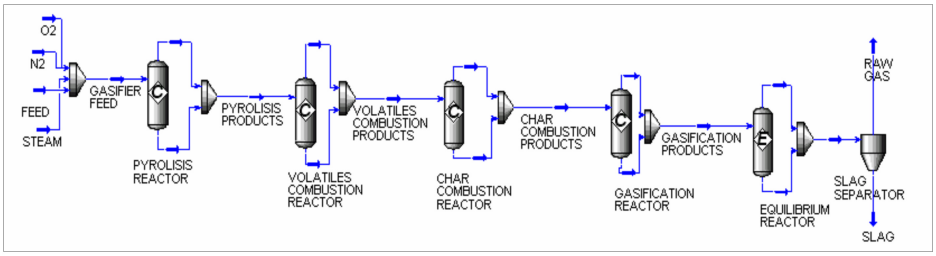

Figure 7.4: Gasifier modeling mass-flow diagram. [A.4.1]

port equations, considering intra and extra-particle phenomena and the operating conditions prevailing in practical pyrolysis reactors. We also need to add a kinetic expression to represent the secondary tar cracking to gas at elevate temperatures, when residence times are relevant.

Our research group is currently interested in modeling a gasification process for different types of feedstock, targeted to clean power produced from gas and steam turbine-generator sets and fuel cells[2]. The model considers gasification as a staged process divided into five different steps: pyrolysis, volatiles combustion, char combustion, char gasification and equilibrium reactions. In the development of the pyrolysis stage, we are contemplating comparison of kinetic approach performances. Apart from the description presented in this thesis we will consider some other approaches from the literature, which range from empirical correlations (e.g. the work of Petersen and Werther (2005)) to description of the intrinsic chemical kinetics of the single particle (e.g the works of Pyle and Zaror (1984), Babu and Chaurasia (2003) and Nunn et al. (1985)). Most of these models do not describe individual volatile evolutions, which is necessary to model consecutive stages. Thus, combination of published approaches will be considered. The pyrolysis custom model, accomplished with the additional considerations discussed before, will be added to an AspenPlus flowsheet of the gasification process.

Future research work should also justify the replacement of the single gasification unit by a pyrolysis plus a combustion or gasification reactor. This replacement should imply the use of simpler equipment, operation and control in each individual reactor and improved environmental compatibility (Henrich et al., 1999). On the other hand, the development of models of whole biomass pyrolysis and gasification could facilitate the analysis of the optimal conditions to minimize the current drawbacks of the gasification process (e.g. tar elimination and product fuel storage and transport). This analysis will be also matter of a further work.

[2]See Section A.4.

Chapter

EIGHT

Global conclusions

On doing a retrospective analysis of the work accomplished in this thesis, a number of issues come forth. Concluding remarks have been discussed throughout the document for the particular issues addressed. The overall conclusions are outlined in this chapter. The contributions of the approach followed in this thesis will be highlighted as a summary list.

8.1 Research contributions

The present thesis adds insight into the field of biomass pyrolysis kinetics. Along this work, the thermal behavior of biomass materials representative of carpentry residues (pine and beech), and an energy plantation (thistle) was studied by different thermoanalytical techniques, within the range of slow pyrolysis, including various pretreatments to eliminate inorganic matter and extractives.

One of the most important contributions of this work lies in the rigorous and thorough analysis of thermogravimetric results. The main criticism of the thermogravimetric studies, associated to the intrusion of varied systematic errors due to the configuration of the thermoanalyzer and the experimental procedures, was studied by statistically analyzing (PCA calculations) the thermal behavior of the same feedstock in different original equipments. We analyzed experimental conditions that can be considered roughly equivalent between different instruments, from results in previous studies. Resulting shifting in characteristic temperatures and final masses did not exceed reported scattering on the pyrolysis of pure cellulose. The scattering in the current results were influenced not only by the well-known transport phenomena limitations in the sample crucible, but also by some other physical aspects related to the geometry and configuration of the furnace. Some differences in the experimental procedures, like temperature calibrations and scarcity in data collection, are also key factors. Different initial sample masses in an apparatus did not imply higher influence on the scattering than that from the use of a different thermobalance.

From these results, we can infer part of the reasons for the widely different kinetic parameters published in the literature on biomass pyrolysis. This finding can encourage future researchers to be more careful at the moment to draw conclusions from studies based on a single apparatus. On the whole, we consider this part of the work as a reference to offer to the thermogravimetric studies. Apart from the Round-Robin study of Gronli and coworkers, establishing a reference on the kinetic studies with Avicel cellulose, no other similar work with whole biomass has been presented before.

We observed that the evaluation of the highly overlapped peaks in thermogravimetric analysis is an ill-conditioned task from single experiments. The simultaneous evaluation of stepwise and linear heating rate experiments, by the model of pseudo-components, provided highly satisfactory fit of the DTG curves.

We joined our efforts to previous research aiming at establishing unified devolatilization mechanisms for sets of related experiments under widely varied experimental conditions. By involving isothermal sections in our experimental work, we accumulated more kinetic information about the chemical heterogeneity of the samples, than with the traditional use of single linear heating programs.

Water-washing proved to be an effective pretreatment for the deconvolution of the partial reactions in the kinetic analysis. Resulting activation energies of the water-washed samples were the base of a further evaluation that helped in characterizing the pretreatment effects by quantitative terms. Moreover, this kinetic evaluation methodology allowed to quantitatively characterizing the aforementioned extent of systematic errors from the simultaneous evaluation of experiments coming from different sources, with simulated DTG curves only varying in the position of the partial peaks.

In this way, we provided an approach that emphasizes the similarities between the differently treated samples studied in different apparatus, while expressing the differences in quantitative form, in terms of the kinetic parameters.

This work demonstrated that the assumed reaction kinetics is not only suitable to describe the dynamics of a given sample in a particular experimental case; it is also capable to reveal the actual changes in the samples in a wider range of operational conditions. The kinetic evaluation methodology presented in this thesis can be also useful for the incorporation of the catalytic influence of mineral matter and extractives on the kinetic modeling of pyrolysis and gasification of the whole biomass.

Detail of the heat demand of untreated and pretreated samples is presented. From the information traced by the heat of pyrolysis, the exothermic character of the thistle thermal degradation was revealed. Both pretreatments add endothermic behavior to the process. Our studies revealed the low heat demand of our samples and, thus, they are less affected by heat transfer intrusions during the experiments.

We have performed an in-depth characterization of the thermal behavior of biomass residues with substantial energy and chemical potential, but with minor references in previous works. Thistle, the sample coming from an energy plantation, proved to be an interesting raw material for charcoal production, given the degradation characteristics of the lignin and extractive content, as well as high influence of the inorganic matter present in this biomass. The higher evolution of charring products, compared to those from wood biomass, is also interesting for gasification processes. Apart from these applications, woody residues can be also suitable for processes where the condensable volatile fraction is the main product of interest.

The PCA analysis proved to be a useful statistical technique in the study of related thermogravimetric and mass spectrometry results. The chemometric studies showed, for instance, that the thermal behavior of wood and thistle is still considerably different after the elimination of some of the inorganic ions and extractive compounds, due to the different macromolecular composition of these materials.

Furthermore, the different effect of the extraction on the herbaceous crop than on the wood species was evidenced. While water-washing largely affected the evolution of the pyrolysis products for all the samples, only in the case of thistle extraction had a non-negligible effect on the production the major gas species and other distinctive products of polysaccharides decomposition. This finding represents advancement with respect to the current state of the art around this topic, given the existing lack of conclusive evidence of the intrinsic effects of extraction on the pyrolysis process.

The role of vapor-solid secondary interactions was evidenced by the evolution profiles of the main pyrolysis products. FTIR profiles revealed the higher formation of CO_2 and CO due to the enhancement of char-forming reactions by prolonging the vapor-phase residence times, at the expense of the tarry organic vapor evolution.

This is an interesting result since discussion on the extent of secondary vapor-solid reactions has been traditionally focused on the observation of the final mass, only. Apart from the work of Várhegyi and coworkers in the TG/MS analysis of a small sample of cellulose sealed in a DSC crucible, we know of no other simultaneous observations of the volatile pyrolysis products under conditions that clearly favor secondary vapor-solid interactions.

In the attempt to kinetically describe all the types of experiments considered in this thesis, we added the prediction of some volatile product evolutions to the general kinetic approach, as well as introduced a successive, additional reaction for the description of the secondary char-forming processes. The evolutions of reacted H_2O, CO, and CO_2 were predicted as the sum of fractions of the volatiles released from the simulated pseudocomponents. Further evolution of the two latter products, as a consequence of secondary interactions, was also modeled.

These additional kinetic evaluations were performed in the attempt to provide a kinetic approach that integrates the different chemical phenomena involved in biomass pyrolysis and could be useful for modeling the pyrolysis process as a unit or step in engineering applications. This development can be useful for the selection of the most appropriate configuration and operating conditions of chemical reactors on dependence of the desired composition and yields of the products.

Kinetic models for the description of individual volatile evolutions from pyrolysis are unusually found in the literature. Furthermore, we are unaware of previous approaches coupling the description of secondary interactions with the quantification of individual volatile products.

In short, this thesis aimed at helping in understanding the pyrolytic process as a whole. We fulfilled this objective by the integration of different phenomena making up biomass pyrolysis. The kinetic description for primary decomposition was connected to the evolution pathways of characteristics volatile products. The pyrolytic reactions were then related to the corresponding heat demand of the different processes. Finally, the contribution of the unavoidable secondary interactions between products (vapors and solid) was considered.

The discussion on the applicability of this type of kinetic approaches has been introduced. Other types of material (i.e. a scrap tire sample) appear to thermally decompose according to the approximation by independent partial reactions, too. The successful development of models of whole biomass pyrolysis and gasification is an important goal for the scientific community that still require much effort. The likely success of a pyrolysis model that allows optimizing feed conditions of a gasification or combustion process, in addition to minimize the current drawbacks of these technologies, will be a real boon.

Nomenclature

Although most of the symbols are explained in the place where they appear, this section is a quick reference to the reader for the notation used along this work.

Greek characters

α	= reacted fraction
β	= char formation ratio by secondary interactions
γ	= total volatile formation ratio by secondary interactions
γ_{CO}	= additional CO formation ratio by secondary interactions
γ_{CO_2}	= additional CO_2 formation ratio by secondary interactions
$\rho\delta$	= sample density multiplied by layer thickness (mg.mm^{-2})

Acronyms and abbreviations

A	= preexponential factor (s^{-1})
A_{sec}	= preexponential factor in the secondary vapor-solid interactions (s^{-1})

c	= normalized mass of volatiles formed from a pseudocomponent
$c_{p,bio}$	= specific heat of biomass ($Jg^{-1}K^{-1}$)
$c_{p,char}$	= specific heat of char ($Jg^{-1}K^{-1}$)
$Char$	= solid residue (determined at 550° C and at 900°C)(%)
DTG_{max}	= overall maximum of mass loss rate normalized by the initial sample mass (%/s)
E	= activation energy (kJ/mol)
E_{sec}	= activation energy in the secondary vapor-solid interactions (kJ/mol)
h	= height of a dm^{obs}/dt curve
H_{total}	= total heat of pyrolysis (Jg^{-1})
K_2	= specific secondary reaction rate (s^{-1})
$m_b(t)$	= normalized mass of reactive biomass
$m_{c_1}(t)$	= normalized mass of solid from primary devolatilization
$m_{c_2}(t)$	= normalized mass of carbonaceous char produced by secondary decomposition
$m^{calc}(t)$	= normalized sample mass calculated from a model
$m_{CO}(t)$	= normalized mass of CO produced by secondary reactions
$m_{CO_2}(t)$	= normalized mass of CO_2 produced by secondary reactions
$m_{v_1}(t)$	= normalized mass of total volatiles produced by primary reactions
$m_{v_2}(t)$	= normalized mass of total volatiles produced after secondary decomposition
$m_{v_s}(t)$	= normalized mass of a given volatile calculated by the model of primary decomposition
mf	= moisture free
$m^{obs}(t)$	= experimental sample mass divided by the initial sample mass
M	= number of pseudocomponents
n	= reaction order
N_{exp}	= number of experiments evaluated simultaneously
N	= number of evaluated data on an experimental curve
Q	= heat flow (general) for the representation in the figures (mW, mW/mg)
$Q_{bio,s}$	= calculated heat flow for the heating of biomass (W)
$Q_{char,s}$	= calculated heat flow for the heating of char (W)
Q_{char}	= experimental heat flow from the residual char (W)
Q_{rad}	= heat flow due to heat radiation effects in the DSC instrument (W)
Q_r	= heat flow induced by pyrolysis reaction (W)
Q_{run}	= experimental heat flow from the biomass sample (W)
Q_s	= heat flow to heat the sample without considering any heat of reaction (W)

R = gas constant (8.3143 x 10^{-3} kJ mol^{-1} K^{-1})
S = least squares sum for a series of experiments
t = time (s)
T = temperature (°C, K)
$T_{cellend}$ = offset temperature (° C)
$T_{hcstart}$ = onset temperature (° C)
T_{peak} = temperature of maximum devolatilization (° C)
T_1 = temperature of starting of decomposition (K)
T_2 = temperature of ending of decomposition (K)
VM = Other volatiles different to the four main pyrolysis volatile products (%)
$Width$ = DTG peak width (° C)
W_f = final mass (mg)
W_0 = initial dry mass (mg)
W_t = experimental mass at each monitoring time (mg)
X = conversion of the sample related to dry sample mass (-)
Y_c = char fraction at 550 °C (-)

Subscripts

i = digitized point on an experimental curve
j = pseudocomponent
p = temperature program
s = volatile species

Bibliography

S. S. Alves and J. L. Figueiredo. Pyrolysis kinetics of lignocellulosic materials by multisatge isothermal thermogravimetry. *J. Anal. Appl. Pyrolysis*, 13:123 – 134, 1988.

M. J. Antal and M. Grønli. The art, science, and technology of charcoal production. *Ind. Eng. Chem Res.*, 42:1619 – 1640, 2003.

M. J. Antal and G. Várhegyi. Cellulose pyrolysis kinetics: The current state of knowledge. *Ind. Eng. Chem Res.*, 34:703 – 717, 1995.

M. J. Antal, G. Várhegyi, and E. Jakab. Cellulose pyrolysis kinetics: Revisited. *Ind. Eng. Chem Res.*, 37:1267 – 1275, 1998.

D. B. Anthony and J. B.Howard. Coal devolatilization and hydrogasification. *AIChE J.*, 22:625 – 656, 1976.

A. Antunes, E. Amaral, and M. N. Belgacem. Cynara cardunculus l.: chemical composition and soda-anthraquinone cooking. *Ind. Crops Prod.*, 12:85 – 91, 2000.

E. Aylón, M.S. Callén, J.M. López, A. M. Mastral, R. Murillo, M.V. Navarro, and S. Stelmach. Assessment of tire devolatilization kinetics. *J. Anal. Appl. Pyrolysis*, 74:259 – 264, 2005.

B. V. Babu and A. S. Chaurasia. Modelling for pyrolysis of solid particle: kinetics and heat transfer effects. *Energy Convers. Manage.*, 44:2251 – 2275, 2003.

B.V. Babu and A.S. Chaurasia. Parametric study of thermal and thermodynamic properties. *Energy Convers. Manage.*, 45:53 – 72, 2004.

J. L. Banyasz, J. Lyons-Hart, and K. H. Shafer. Gas evolution and the mechanism of cellulose pyrolysis. *Fuel*, 80:1757 – 1763, 2001.

F. Barontini, V. Cozzani, and L. Petarca. Thermal stability and decomposition products of hexabromocyclododecane. *Ind. Eng. Chem Res.*, 40:3270 – 3280, 2001.

R. Bassilakis, R. M. Carangelo, and M. A. Wójtowicz. Tg-ftir analysis of biomass pyrolysis. *Fuel*, 80:1765 – 1786, 2001.

G. Berndesa, M. Hoogwijkb, and R. van den Broek. The contribution of biomass in the future global energy supply: a review of 17 studies. *Biomass Bioenergy*, 25(1): 1 – 28, July 2003.

C. Berrueco, E. Esperanza, F.J. Mastral, J. Ceamanos, and P. García-Bacaicoa. Pyrolysis of waste tyres in an atmospheric static-bed batch reactor: Analysis of the gases obtained. *J. Anal. Appl. Pyrolysis*, 74:245 – 253, 2005.

E. Biagini, F. Lippi, L. Petarca, and L. Tognotti. Devolatilization rate of biomasses and coal-biomass blends: an experimental investigation. *Fuel*, 81:1041 – 1050, 2002.

R. Bilbao, J. Arauzo, and M. L. Salvador. Kinetics and modeling of gas formation in the thermal decomposition of powdery cellulose and pine sawdust. *Ind. Eng. Chem. Res.*, 34:786 – 793, 1995.

K. W. Boer and J. A. Dufie, editors. *Biomass Pyrolysis: A Review of the Literature. Part 11. Lignocellulose Pyrolysis*, New York, 1985. American Solar Energy Society.

C. Branca, P. Giudicianni, and C. Di Blasi. Gc/ms characterization of liquids generated from low-temperature pyrolysis of wood. *Ind. Eng. Chem. Res.*, 42:3190 – 3202, 2003.

A. V. Bridgwater. Fast pyrolysis of biomass: Technical requirements for commercialisation. In A. V. Bridgwater, editor, *Pyrolysis and Gasification of Biomass and Waste. Proceedings of an Expert Meeting*, pages 33 – 40, Newbury, October 2002. CPL Press.

A. Broido and M. A. Nelson. Char yield on pyrolysis of cellulose. *Combust. Flame*, 24, 1975.

A. Broido and M. Weinstein. Kinetics of solid-phase cellulose pyrolysis. In Wiedemann, editor, *Proceedings of the 3rd International Conference on Thermal Analysis*, pages 285 – 296, Basel, 1971. Birkhauser Verlag.

A. L. Brown, B. R. Hames, J. W. Daily, and D. C. Dayton. Chemical analysis of solids and pyrolytic vapors from. *Energy Fuels*, 17:1022 – 1027, 2003.

E. Chornet and C. Roy. Compensation effect in the thermal decomposition of cellulosic materials. *Thermochim. Acta*, 35:389 – 393, 1980.

J. A. Conesa, R. Font, A. FuIlana, and J. A. Caballero. Kinetic model for the combustion of tyre wastes. *Fuel*, 77:1469 – 1475, 1998.

J. A. Conesa, A. Marcilla, J. A. Caballero, and R. Font. Comments on the validity and utility of the different methods for kinetic analysis of thermogravimetric data. *J. Anal. Appl. Pyrolysis*, 58 - 59:617 – 633, 2000.

W. F. DeGroot, W-P. Pan, M. D. Rahman, and G. N. Richards. First chemical events in the pyrolysis of wood. *J. Anal. Appl. Pyrolysis*, 13:221 – 231, 1988.

W.F. DeGroot and F. Shafizadeh. The influence of exchangeable cations on the carbonization of biomass. *J. Anal. Appl. Pyrolysis*, 6:217 – 232, 1984.

C. Di Blasi. Comparison of semi-global mechanisms for primary pyrolysis of lignocellulosic fuels. *J. Anal. Appl. Pyrolysis*, 47:43 – 64, 1998.

C. Di Blasi and C. Branca. Kinetics of primary product formation from wood pyrolysis. *Ind. Eng. Chem Res.*, 40:5547 – 5556, 2001.

C. Di Blasi, C. Branca, A. Santoro, and R. A. P. Bermudez. Weight loss dynamics of wood chips under fast radiative heating. *J. Anal. Appl. Pyrolysis*, 57:77 – 90, 2001a.

C. Di Blasi, C. Branca, A. Santoro, and E. G. Hernandez. Pyrolytic behavior and products of some wood varieties. *Combust. Flame*, 124:165, 2001b.

C. Di Blasi and M. Lanzetta. Intrinsic kinetics of isothermal xylan degradation in inert atmosphere. *J. Anal. Appl. Pyrolysis*, 40 - 41:287 – 303, 1997.

C. Di Blasi and G. Russo. Modeling of transport phenomena and kinetics of biomass pyrolysis. In A. V. Bridgwater, editor, *Advances in Thermochemical Biomass Conversion*, volume 2, pages 906 – 921, Londres, 1994. Blackie Academic and Professional.

C. Di Blasi, G. Signorelli, C. Di Russo, and G. Rea. Product distribution from pyrolysis of wood and agricultural residues. *Ind. Eng. Chem. Res.*, 38:2216 – 2224, 1999.

R. J. Evans and T. A. Milne. Molecular characterization of the pyrolysis of biomass. 1. fundamentals. *Energy Fuels*, 1(2):123 – 137, 1987.

O. Faix, I. Fortmann, J. Bremer, and D. Meier. Thermal degradation products of wood. a collection of electro-impact (ei) mass spectra of polysaccharide derived products. *Holz Roh Werkst.*, 49:299 – 304, 1991a.

O. Faix, I. Fortmann, J. Bremer, and D. Meier. Thermal degradation products of wood. gas chromatographic separation and mass spectrometric characterization of polysaccharide derived products. *Holz Roh Werkst.*, 49:213 – 219, 1991b.

O. Faix, E. Jakab, F. Till, and T. Szekely. Study on low mass thermal degradation products of milled woods lignins by thermogravimetry-mass spectrometry. *Wood Sci. Technol.*, 22:323 – 334, 1988.

O. Faix, D. Meier, and I. Fortmann. Thermal degradation products of wood. a collection of electro-impact (ei) mass spectra of monomeric lignin derived products. *Holz Roh Werkst.*, 48:351 – 354, 1990a.

O. Faix, D. Meier, and I. Fortmann. Thermal degradation products of wood. gas chromatographic separation and mass spectrometric characterization of monomeric lignin derived products. *Holz Roh Werkst.*, 48:281 – 285, 1990b.

R. Font, A. Marcilla, E. Verdu, and J. Devesa. Thermogravimetric kinetic study of the pyrolysis of almond shells and almond shells impregnated with cocl2. *J. Anal. Appl. Pyrolysis*, 21:249 – 264, 1991.

M. Grønli, M. J. Antal, and G. Várhegyi. A round-robin study of cellulose pyrolysis kinetics by thermogravimetry. *Ind. Eng. Chem Res.*, 38:2238 – 2244, 1999.

M. G. Grønli, G. Várhegyi, and C. Di Blasi. Thermogravimetric analysis and devolatilization kinetics of wood. *Ind. Eng. Chem Res.*, 41:4201 – 4208, 2002.

D. O. Hall and R.P. Overend. *Biomass, regenerable energy.* John Wiley and Sons, Chichester., 1987.

E. Henrich, S. Bürkle, Z.I. Meza-Renken, and S. Rumpel. Combustion and gasification kinetics of pyrolysis chars from waste and biomass. *J. Anal. Appl. Pyrolysis*, 49: 221 – 241, 1999.

M. Hoogwijka, A. Faaij, R. van den Broeka, G. Berndesb, D. Gielenc, and W. Turkenburg. Exploration of the ranges of the global potential of biomass for energy. *Biomass Bioenergy*, 25(2):119 – 133, August 2003.

J. E. Jackson. *A User's Guide to Principal Components.* Wiley Series in Probability and Statistics. J. Wiley and Sons, Hoboken, New Jersey, 2003.

E. Jakab, O. Faix, and F. Till. Thermal decomposition of milled wood lignins studied by Thermogravimetry/Mass spectrometry. *J. Anal. Appl. Pyrolysis*, 40 - 41:171 – 186, 1997.

E. Jakab, O. Faix, F. Till, and T. Székely. Thermogravimetry/Mass spectrometry study of six lignins within the scope of an international round robin test. *J. Anal. Appl. Pyrolysis*, 35:167 – 179, 1995.

M. Kaltschmitt and L. Dinkelbach. Biomass for energy in europe. In M. Kaltschmitt and A. V. Bridgwater, editors, *Biomass Gasification and Pyrolysis. State of the art and future prospects*, pages 7 – 23, Newbury, August 1997. CPL Press.

S. Kersten, X. Wang, W. Prins, and W. Swaaij. Biomass pyrolysis in a fluidized bed reactor. part 1: Literature review and model simulations. *Ind. Eng. Chem. Res.*, 44:8773 – 8785, 2005.

D.L. Klass. *Biomass for renewable energy, fuels, and chemicals.* Academic Press, San Diego, CA., 1998.

C. A. Koufopanos, G. Maschio, and A. Lucchesi. Kinetic modeling of the pyrolysis of biomass and biomass components. *Can. J. Chem. Eng.*, 67:75 – 84, 1989.

C. A. Koufopanos, N. Papayannakos, G. Maschio, and A. Lucchesi. Modelling of the pyrolysis of biomass particles. studies on kinetics, thermal and heat transfer effects. *Can. J. Chem. Eng.*, 69:907 – 915, 1991.

J. C. Lagarias, J. A. Reeds, M. H. Wright, and P. E. Wright. Convergence properties of the nelder-mead simplex method in low dimensions. *SIAM J. Optim.*, 9:112 – 121, 1998.

A. G. Liden, F. Berruti, and D. S. Scott. A kinetic model for the production of liquids from the flash pyrolysis of biomass. *Chem. Eng. Comm.*, 65:207 – 221, 1988.

D. Lienert, E. Anklam, and U. Panne. Gas chromatography-mass spectral analysis of roots of echinacea species and classification by multivariate data analysis. *Phytochem. Anal.*, 9:88 – 98, 1998.

K. Maniatis, G. Guiu, and J. Riesgo. The european commission perspective in biomass and waste thermochemical conversion. In A. V. Bridgwater, editor, *Pyrolysis and Gasification of Biomass and Waste. Proceedings of an Expert Meeting*, pages 1 – 18, Newbury, October 2002. CPL Press.

J. J. Manyà, E. Velo, and L. Puigjaner. Kinetics of biomass pyrolysis: a reformulated three-parallel-reactions model. *Ind. Eng. Chem Res.*, 42:434 – 441, 2003.

J.J. Manyà. *Contribució a l'estudi de la cinètica de la piròlisi primària de materials lignocel·lulòsics per a diferents règims d'escalfament.* PhD thesis, Universitat Politècnica de Catalunya, Av, Diagonal, 647, December 2002.

K. Marsanich, F. Barontini, V. Cozzani, and L. Petarca. Advanced pulse calibration techniques for the quantitative analysis of tg-ftir data. *Therm. Acta*, 390:153 – 168, 2002.

E. Mészáros, E. Jakab, G. Várhegyi, P. Szepesváry, and B. Marosvölgyi. Comparative study of the thermal behavior of wood and bark of young shoots obtained from an energy plantation. *J. Anal. Appl. Pyrolysis*, 72:317 – 328, 2004a.

E. Mészáros, G. Várhegyi, E. Jakab, and B. Marosvölgyi. Thermogravimetric and reaction kinetic analysis of biomass samples from an energy plantation. *Energy Fuels*, 18:497 – 507, 2004b.

R. S. Miller and J. Bellan. A generalized biomass pyrolysis model based on superimposed cellulose, hemicellulose and lignin kinetics. *Combust. Sci. Technol.*, 126:97 – 134, 1997.

W. S-L. Mok, M. J. Antal, P. Szabo, G. Várhegyi, and B. Zelei. Formation of charcoal from biomass in a sealed reactor. *Ind. Eng. Chem Res.*, 31:1162 – 1166, 1992.

R. Narayan and M. J. Antal. Thermal lag, fusion, and the compensation effect during biomass pyrolysis. *Ind. Eng. Chem Res.*, 35:1711 – 1721, 1996.

T. R. Nunn, J. B. Howard, J. P. Longwell, and W. A. Peters. Product compositions and kinetics in the rapid pyrolysis of sweet gum hardwood. *Ind. Eng. Chem. Process Des. Dev.*, 24:836 – 844, 1985.

A. Oasmaa, E. Kuoppala, S. Gust, and Y. Solantausta. Fast pyrolysis of forestry residue. 1. effect of extractives on phase separation of pyrolysis liquids. energy and fuels. *Energy Fuels*, 17:1 – 12, 2003a.

A. Oasmaa, E. Kuoppala, and Y. Solantausta. Fast pyrolysis of forestry residue. 2. physicochemical composition of product liquid. *Energy Fuels*, 17:433 – 443, 2003b.

J. J. M. Orfao, F. J. A. Antunes, and J. L. Figueiredo. Pyrolysis kinetics of lignocellulosic materials -three independent reactions model. *Fuel*, 78:349 – 358, 1999.

W.-P. Pan and G.N. Richards. Influence of metal ions on volatile products of pyrolysis of wood. *J. Anal. Appl. Pyrolysis*, 16:117 – 126, 1989.

A. Pappa, K. Mikedi, N. Tzamtzis, and M. Statheropoulos. Chemometric methods for studying the effects of chemicals on cellulose pyrolysis by thermogravimetry - mass spectrometry. *J. Anal. Appl. Pyrolysis*, 67:221 – 235, 2003.

I. Petersen and J. Werther. Experimental investigation and modeling of gasification of sewage sludge in the circulating fluidized bed. *Chem. Eng. Proc.*, 44:717 – 736, 2005.

J. Piskorz, P. Majerski, D. Radlein, D. S. Scott, and A. V. Bridgwater. Fast pyrolysis of sweet sorghum and sweet sorghum bagasse. *J. Anal. Appl. Pyrolysis*, 46:15 – 29, 1988.

A. D. Pouwels, A. Tom, G.B. Eijkel, and J.J. Boon. Characterisation of beech wood and its holocellulose and xylan fractions by pyrolysis-gas chromatography-mass spectrometry. *J. Anal. Appl. Pyrolysis*, 11:417 – 436, 1987.

D. L. Pyle and C. A. Zaror. Heat transfer and kinetics in the low-temperature pyrolysis of solids. *Chem. Eng. Sci.*, 39:147, 1984.

R. Radmanesh, Y. Courbariaux, J. Chaouki, and C. Guy. A unified lumped approach in kinetic modeling of biomass pyrolysis. *Fuel*, 85:1211 – 1220, 2006.

J. Rath, M.G. Wolfinger, G. Steiner, G. Krammer, F. Barontini, and V. Cozzani. Heat of wood pyrolysis. *Fuel*, 82:81 – 91, 2003.

F. B. Salisbury and C. W. Ross. *Plant Physiology.* Wadsworth Publishing Co., Belmont, CA, 1992.

D. S. Scott, P. Majerski, and J. Piskorz. A second look at fast pyrolysis of biomass - the rti process. *J. Anal. Appl. Pyrolysis*, 51:23 – 37, 1999.

S. Seidelt, M. Müller-Hagedorn, and H. Bockhorn. Description of tire pyrolysis by thermal degradation behaviour of main components. *J. Anal. Appl. Pyrolysis*, 75: 11 – 18, 2006.

F. Shafizadeh. Introduction to pyrolysis of biomass. *J. Anal. Appl. Pyrol.*, 3:283 – 305, 1982.

F. Shafizadeh. Pyrolytic reactions and products of biomass. In L.K. Mudge R.P. Overend, T.A. Milne, editor, *Fundamentals of Thermochemical Biomass Conversion*, pages 183 – 217, London, 1985. Elsevier.

F. Shafizadeh and P. P. S. Chin. Thermal deterioration of wood. *ACS Symp. Ser.*, 43:57, 1977.

F. Shafizadeh and G. D. McGinnis. Chemical composition and thermal analysis of cottonwood. *Carbohyd. Res.*, 16:273 – 277, 1971.

L. F. Shampine and M. W. Reichelt. The matlab ode suite. *SIAM J. Sci. Comput.*, 18:1 – 21, 1997.

E. J. Shin, M. R. Nimlos, and R. J. Evans. Kinetic analysis of the gas-phase pyrolysis of carbohydrates. *Fuel*, 80:1697 – 1709, 2001.

M. Statheropoulos and K. Mikedi. Pca-contvardia: an improvement of the pca-vardia technique for curve resolution in gc-ms and tg-ms analysis. *Anal. Chim. Acta*, 446: 353 – 370, 2001.

M. Stenseng, A. Jensen, and K. Dam-Johansen. Investigation of biomass pyrolysis by thermogravimetric analysis and differential scanning calorimetry. *J. Anal. Appl. Pyrolysis*, 58 - 59:765 – 780, 2001.

P. Szabó, G. Várhegyi, F.Till, and T.Székely. Investigation of hungarian subbituminous coals by thermogravimetry - mass spectrometry. part 1: Evolution of hydrocarbon products. *Thermochim. Acta*, 170:167 – 177, 1990.

T. Székely, G. Várhegyi, F. Till, P. Szabó, and E. Jakab. The effects of heat and mass transport on the results of thermal decomposition studies : Part 1. the three reactions of calcium oxalate monohydrate. *J. Anal. Appl. Pyrolysis*, 11:71 – 81, 1987.

H. Teng, H. C. Lin, and J. A. Ho. Thermogravimetric analysis on global mass loss kinetics of rice hull pyrolysis. *Ind. Eng. Chem Res.*, 36:3974 – 3977, 1997.

H. Teng and Y-C. Wei. Thermogravimetric studies on the kinetics of rice hull pyrolysis and the influence of water treatment. *Ind. Eng. Chem Res.*, 37:3806 – 3811, 1998.

F. Thurner and U. Mann. Kinetic investigation of wood pyrolysis. *Ind. Eng. Chem. Process Des. Dev.*, 20:482 – 488, 1981.

G. Várhegyi, M. J. Antal, E. Jakab, and P. Szabó. Kinetic modeling of biomass pyrolysis. *J. Anal. Appl. Pyrolysis*, 42:73 – 87, 1997.

G. Várhegyi, M. J. Antal, T. Székely, and P. Szabó. Kinetics of the thermal decomposition of cellulose, hemicellulose, and sugar cane bagasse. *Energy Fuels*, 3:329 – 335, 1989a.

G. Várhegyi, M. J. Antal, T. Szekely, F. Till, and E. Jakab. Simultaneous thermogravimetric-mass spectrometric studies of the thermal decomposition of biopolymers. 1. avicel cellulose in the presence and absence of catalysts. *Energy Fuels*, 2:267 – 272, 1988a.

G. Várhegyi, M. J. Antal, T. Székely, F. Till, E. Jakab, and P. Szabó. Simultaneous thermogravimetric-mass spectrometric studies of the thermal decomposition of biopolymers. 2. sugar cane bagasse in the presence and absence of catalysts. *Energy Fuels*, 2:273 – 277, 1988b.

G. Várhegyi, M. G. Grønli, and C. Di Blasi. Effects of sample origin, extraction, and hot-water washing on the devolatilization kinetics of chestnut wood. *Ind. Eng. Chem Res.*, 43:2356 – 2367, 2004.

G. Varhegyi, E. Jakab, and M. J. Antal. Is the broido-shafizadeh model for cellulose pyrolysis true? *Energy Fuels*, 8:1345 – 1352, 1994.

G. Várhegyi, E. Jakab, F. Till, and T. Székely. Thermogravimetric - mass spectrometric characterization of the thermal decomposition of sunflower stem. *Energy Fuels*, 3:755 – 760, 1989b.

G. Várhegyi, P. Szabó, and M. J. Antal. Reaction kinetics of the thermal decomposition of cellulose and hemicellulose in biomass materials. In T. Bridgwater, editor, *Advances in Thermochemical Biomass Conversion*, pages 760–771, London, Vol. 2 1994. Chapman and Hall.

G. Várhegyi, P. Szabó, and M. J. Antal. Kinetics of charcoal devolatilization. *Energy Fuels*, 16:724 – 731, 2002.

G. Várhegyi, P. Szabo, E. Jakab, and F. Till. Least squares criteria for the kinetic evaluation of thermoanalytical experiments. examples from a char reactivity study. *J. Anal. Appl. Pyrolysis*, 57:203 – 222, 2001.

G. Várhegyi, P. Szabó, F. Till, B. Zelei, M. J. Antal, and X. Dai. Tg, tg-ms, and ftir characterization of high-yield biomass charcoals. *Energy Fuels*, 12:969 – 974, 1998.

G. Várhegyi and F. Till. Computer processing of thermogravimetric - mass spectrometric and high pressure thermogravimetric data. part 1. smoothing and differentiation. *Thermochim. Acta*, 329:141 – 145, 1999.

W. Winding and P. G. Kistamaker. Chemical interpretation of differences in pyrolysis/mass spectra of simulated mixtures of biopolymers by factor analysis with graphical rotation. *J. Anal. Appl. Pyrolysis*, 3:199 – 212, 1981.

M. A. Wójtowicz, R. Bassilakisand W. Smith, Y. Chen, and R. M. Carangelo. Modeling the evolution of volatile species during tobacco pyrolysis. *J. Anal. Appl. Pyrolysis*, 66:235 – 261, 2003.

S. Yaman. Pyrolysis of biomass to produce fuels and chemical feedstocks. *Energ. Convers. and Manage.*, 45:651 – 671, 2004.

Appendix

A

Publications

Research work developed in the scope of this thesis has resulted in several publications either articles in scientific journals, articles in conference proceedings and communications in congresses. Besides, there has been the opportunity to participate in different research projects. All this contributions are detailed in this appendix.

A.1 Journal articles

Gómez, C. J., Barontini, F., Cozzani, V., Velo, E., Puigjaner, L., 2006. Slow Pyrolysis of Biomass Materials: Thermal Study by TG-DSC and TG-FTIR (Manuscript in preparation, to be sent to *Fuel*).

Gómez, C. J., Mészáros, E., Jakab, E., Velo, E., Puigjaner, L., 2006. Thermogravimetry/Mass Spectrometry Study of Woody Residues and an Herbaceous Biomass Crop Using PCA Techniques. *Journal of Analytical and Applied Pyrolysis* (Submitted).

Gómez, C. J., Várhegyi, G., Puigjaner, L., 2005. Slow pyrolysis of woody residues and an herbaceous biomass crop. *Industrial and Engineering Chemistry Research* 44, 6650 - 6660.

Gómez, C. J., Manyà, J. J., Velo, E., Puigjaner, L., 2004. Further applications of a revisited summative model for kinetics of biomass pyrolysis. *Industrial and Engineering Chemistry Research* 43, 901 - 906.

A.2 Articles in conference proceedings

Gómez, C. J., Velo, E., Puigjaner, L., 2004. Thermokinetic characterization of biomass pyrolysis by differential scanning calorimetry. In: AIChE Annual Meeting, Austin Texas, (USA), ISBN: 0-8169-0965-2.

Gómez, C. J., Velo, E., Puigjaner, L., 2004. Kinetic study of biomass pyrolysis at moderate and high heating regimes. In: AIChE Annual Meeting, Austin Texas, (USA), ISBN: 0-8169-0965-2.

Gómez, C. J., Manyà, J. J., Velo, E., Puigjaner, L. 2003. Pyrolysis kinetic modelling of biomass feedstocks. Application of a three-independent-reactions model. In: 53rd Canadian Chemical Engineering Conference (6th Conference on Process Integration, Modelling, and Optimization for Energy Saving and Pollution Reduction), (Ed. CSChE), Hamilton (Canada), ISBN: 0-920804-36-5.

Gómez, C. J., Manyà, J. J., Velo, E., Puigjaner, L. 2003. Kinetic modelling of wood chips pyrolysis by means of a three-independent-reactions model. In: 4th European Congress of Chemical Engineering, Granada (Spain), ISBN: 84-88233-35-3.

Gómez, C. J., Manyà, J. J., Velo, E., Puigjaner, L., **2003**. Pirólisis y gasificación como alternativas al tratamiento de biomasa. XII Congreso Colombiano de Ingeniería Química, Bucaramanga, Colombia, pp 64-69, ISSN: 1692-925X.

A.3 Communications in congresses

Gómez, C. J., Mitta, N. R., Velo, E., Puigjaner, L., 2007. Modelling and simulation of a biomass pyrolysis unit within a gasification-based plant. Abstract accepted for the European Symposium on Computer-Aided Process Engineering - 17. Bucharest, Romania.

Mészáros, E., **Gómez, C. J.**, Velo, E., Puigjaner, L., Várhegyi, G., Jakab, E., 2007. Study of artichoke thistle (Cynara cardunculus) by analytical pyrolysis. Abstract submmited to 15th European Biomass Conference and Exhibition - From Research to Market Deployment - Biomass for Energy, Industry and Climate Protection. Berlin, Germany.

Mitta, N. R., **Gómez, C. J.**, Velo, E., Puigjaner, L., 2006. Modeling and simulation of biomass pyrolysis as a first step in a gasification-based system. AIChE Annual Meeting, San Francisco, (USA).

Gómez, C. J., Velo, E., Puigjaner, L., 2006. Thermokinetic Characterization of an Herbaceous Crop Pyrolysis by Differential Scanning Calorimetry. CHISA, 17th International Congress of Chemical and Process Engineering, Prague, Czech Republic.

Mitta, N. R., **Gómez, C. J.**, Velo, E., Puigjaner, L., 2005. Pyrolysis kinetic study of scrap tyres in air and nitrogen atmospheres. 10th Mediterranean Congress of Chemical Engineering, Barcelona.

Gómez, C. J., Mészáros, E., Jakab, E., Velo, E., Puigjaner, L., 2005. Comparative Thermogravimetry/Mass Spectrometry Study of Woody Residues and an

Herbaceous Biomass Crop Using PCA Techniques. AIChE Annual Meeting, Cincinnati (USA).

Manyà, J. J., **Gómez, C. J.**, Velo, E., Puigjaner, L., 2002. Pyrolysis of sugarcane bagasse: kinetic study at high heating rates. 9th Mediterranean Congress of Chemical Engineering, Barcelona.

A.4 Participation in research projects

AGAPUTE, *Advanced gas purification technologies for co-gasification of coal, refinery by-products, biomass and waste, targeted to clean power produced from gas & steam turbine -generator sets and fuel cells*, supported by the *European Community* (RFC-CR-04006), 2004-2007.

Diseño de una planta de gasificación de lodos de EDAR para el tratamiento de 50000 toneladas/año de lodo deshidratado, supported by the *Generalitat de Catalunya* (C-05871), 2005-2006.

REMGAS, *Demostración de un nuevo proceso de tratamiento y valorización energética de residuos de madera*, supported by the *Ministerio de Ciencia y Tecnología de España* (PPQ2000-0300-P4-2), 2002-2003.

Appendix

B

PCA analysis

Principal component analysis (PCA) was employed to help in the evaluation of the large data set of results in several sections of this thesis. The information of this appendix is included so as to give the reader an understanding of the theory and calculations behind the analysis applied in this work. As this technique is a well established method in the field of chemometrics, the reader is referred to appropriate literature for further in-depth discussion. A brief summary of the specific principles applied in this thesis will be given. Fragments of the Matlab code used for the calculations will be also provided.

B.1 The PCA method

Principal component analysis is a multivariate statistical method, commonly used for the analysis, monitoring and diagnosis of process operating performance (Pappa et al., 2003). It has been also extensively used for the resolution of overlapping spectral signals from different analytical techniques (Statheropoulos and Mikedi, 2001; Bassilakis et al., 2001; Evans and Milne, 1987). PCA has been started to be used as an statistical tool for the analysis of thermal characteristics and product evolution pathways in biomass pyrolysis (Mészáros et al., 2004a).

With this technique, large set of observed variables can be replaced with a smaller set of new variables, the principal components, retaining the patterns of the original data. Data is compressed by identifying redundancy between variables and, thus, reducing the number of dimensions (in the matrix of observations and variables) without much loss of information (Jackson, 2003; Lienert et al., 1998). This data reduction makes possible graphical display of the data that not only shows trends but also can provide chemical insight into the transformations.

Being the original data matrix (X_{origin}) of n variables and m observations (corresponding to the objects to be analyzed), the principal components (PCs) are eigenvectors of a variance-covariance matrix. These orthogonal composite of latent variables are linear combinations of the original variables. In this work, we have subtracted

the mean from each of the columns (dimensions) of the matrix X_{origin}. The mean subtracted is the average across each dimension. This produces a data set whose mean is zero. We also divided by the standard deviation. The purpose of this pretreatment is to give equal importance to all the variables. From the formed X matrix, the successive PCA calculations are performed.

```
[m n]=size(X_orig);
media = mean(X_orig);
stand = std(X_orig);
X_n = X_orig - repmat(media,[m 1]);
X = X_n./repmat(stand,[m 1]);
[COEFF, SCORE, LATENT] = princomp(X)
```

The eigenvector with the highest eigenvalue is the first principle component of the data set. In other words, the first principal component is the linear combination of variables that accounts for more of the variance in the data than any other combination of variables. The subsequent principal components are similarly extracted on the basis of the residual variance, after the effect of the previous factors have been removed from the data. The data compression occurs by ignoring the principal components of minimum variance. The original data can be then expressed in terms of these selected perpendicular eigenvectors, which form the so called principal component space.

Results of PCA are given as the loading matrix $COEFF$ (size n x n) and the score matrix $SCORE$ (size m x n). The loadings represent the correlation coefficients between the PCs and the original variables. The scores represent the new coordinates of the observations in the PCs' space (Jackson, 2003). By multiplying $SCORE$ with $COEFF$ the data matrix X is reproduced:

$$X = SCORE.COEFF \tag{B.1}$$

$LATENT$ (size n) is the vector containing the eigenvalues of the covariance matrix of X. From this result, the number of principal components to consider in an analysis is selected. Figure E.1 is an example of the resulting variance accounted by an entire set of principal components. This corresponds to the PCA analysis of the DTG characteristics of experiments coming from different sources in Chapter 3.

```
figure (1)
bar(LATENT/sum(LATENT)*100);
title('Variance');
xlabel('Principal Components');
ylabel('% Variance');
```

The relationships between objects (e.g. samples) are uniquely revealed by their projection (scores) on the PCs, i.e. the score plots. When objects lie close to one another in a score plot (see e.g. Figure 3.10A), they are assumed to behave similarly

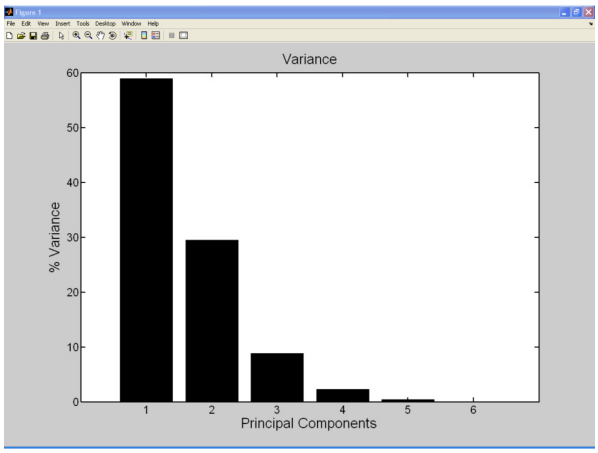

Figure B.1: Example of resulting variances. Principal components in the analysis of the DTG characteristics (Figure 3.5, Chapter 3).

since their positions in the new coordinates are similar, whereas, considerably different objects result in large distances. As a result, the similar objects are arranged into groups or clusters. In this way, the PCA method expresses the data so as to highlight the similarities and differences between different objects to be analyzed.

Listing B.1: Clusters.

```
names2 = [{'NET'},{'PE'},{'SET'},{'TA'},{'Cahn'}];
pcclusters = clusterdata(SCORE(:,1:3),2);
for j =1:length(pcclusters)
    switch pcclusters(j)
        case 1
            color = 'k';
            marker = 'o';
        case 2
            color = 'k';
            marker = '*';
        otherwise
            disp('group out of the range')
        end
            plot3(SCORE(j,1),SCORE(j,2),SCORE(j,3),'Color',...
                color,'Marker',marker,'MarkerSize',15,...
                'LineWidth',1.5); text(SCORE(j,1),...
                SCORE(j,2),SCORE(j,3),names2(j),'FontSize',18);
            hold on
end
```

Listing B.1 corresponds to the Figure 3.6, where the three first principal components were selected and 2 clusters were identified. The *clusterdata* function in Matlab uses the Euclidean distance between pairs of objects, as well as the Single Linkage algorithm (Jackson, 2003) to construct clusters from data $SCORE$.

Another way to represent the clusters is by creating a dendrogram (like Figure 3.5C). It consists of many U-shaped lines connecting objects in a hierarchical tree. The height of each U represents the distance between the two objects being connected. In this work, we applied Euclidean distances and created hierarchical cluster trees using the Single Linkage algorithm.

The loadings (matrix $COEFF$) signify the importance of the original variables for a principal component. Hence, a loading plot (like Figure 3.5B) maps the object space onto the principal components. In this way, one can identify how a given original variable has affected the similarities or differences in a group of objects. The position of a clusters relative to one another on the principal component space, with distances determining the degree of similarity between clusters, can be then connected to the meddling of the variable or group of variables with major importance (loading) for a given principal component.

Appendix

C

Kinetic evaluation

In this appendix we will provide detail of the computational procedures followed in the kinetic evaluations of this thesis. Fragments of the different program codes used for getting kinetic parameters will be given.

C.1 Matlab program for kinetic evaluation

The following code belongs to the main structure of the Matlab program applied to the kinetic evaluation of single experiments. It corresponds to the evaluation of DTG curves assuming three partial reactions and third-order kinetics for the last pseudocomponent. Listing C.1 is a piece of the main program. Listings C.2 and C.3 are files associated to this program. Other evaluations employing Matlab programs followed a similar structure.

Listing C.1: Main program.

```
% Parametric estimation in biomass pyrolysis
% A and E are normalized by the initial parameters
% Evaluation of single experiments. Model of three partial
% reactions. Data from an excel file "experimentalbio.xls"
% Copyright (C) 2003 Claudia Gomez
% <claudia.juliana.gomez@upc.edu>

% 03/08/06 last revision
warning off
global TC
global M
global M0
global erate
global T
global rate
```

```
channel=ddeinit('excel','experimentalbio.xls');
Temp = ddereq(channel, 'r143c1:r244c1');
Masa = ddereq(channel,'r143c4:r244c4');
DTG = ddereq(channel,'r143c5:r244c5');
load beta0muestra;
TC=Temp;
M=Masa;
erateg=DTG;
T=TC+273;
Tj=T;
M0=M(1);
V=M0-M;
Vlast=V(end);
erateg=erateg.*(-1);

%Smoothing-----------------------------
i=1;
k=length (T);
j=1;
a=4;
for j=1:k
    for i=1:k
        SN(i)=erateg(i)*exp(-((T(j)-T(i))^2)/(2*a^2));
        SD(i)=exp(-((T(j)-T(i))^2)/(2*a^2));
    end
    S(j)=sum(SN);
    W(j)=sum(SD);
end
erategs=S./W;
erate=erategs';

%------
% DTG characteristic points
Derate=diff(erate);
Derate=[0;Derate];
[maxe,i]=max(erate);
Tmaxc=TC(i);

% Shoulder ------------------------------

% % Noise elimination j=1;
% for j=1:i if Derate(j)<5e-5;
% Derate(j)=0;
```

```
DDerate=diff(Derate);
DDerate=[0;DDerate];

k=1;
Tmaxhe=[];
m=[];
for k=1:i
    if DDerate(k)<0
        Tmaxhe=[Tmaxhe;TC(k+1)];
        m=[m;k+1];
    end
end
Tmaxhe=Tmaxhe(1);
m=m(1);

q=length(DDerate);
k=1;
Tultimce=[];
o=[];
for k=i:q
    if DDerate(k)>0;
        Tultimce=[Tultimce;TC(k)];
        o=[o;k];
    end
end
Tultimce=Tultimce(1);
o=o(1);

% Parametric estimation
load beta0muestra;
%%------ First pseudocomponent
betah0=beta0muestra(1:2);
betah0(3)=V(m);
Ah=betah0(1);
Eh=betah0(2);
%%------ Second pseudocomponent
betac0=beta0muestra(3:4);
betac0(3)=V(o)-V(m);
Ac=betac0(1);
Ec=betac0(2);
%%------ %Third pseucomponent
betal0=beta0muestra(5:6);
betal0(3)=Vlast;
Al=betal0(1);
El=betal0(2);
```

```
%-------
% Optimization algorithm
beta=[1;1;betah0(3);1;1;betac0(3);1;1;betal0(3)];
options=optimset('Display','iter','Diagnostic','on',...
    'MaxFunEvals',500);
betafinal=fminsearch('EloError',beta,options,...
    Ah,Eh,Ac,Ec,Al,El);
% FMINSEARCH Multidimensional unconstrained...
% nonlinear minimization (Nelder-Mead).

% Calculation of the final curve
% ....

v=[vhe vce vlign];
v1 = v(:,1);
v2 = v(:,2);
v3 = v(:,3);
prod=v1+v2+v3;
sm=M0-(v1+v2+v3);
res=sm-M;
finalfit=100*sqrt(sum(res.^2)/length(T))/M0;

%-------
% fit DTG
srate=sratehe+sratece+sratelign;
res=srate-erate;
% [maxe,v]=max(erate);
finalfitDTG=100*sqrt(sum(res.^2)/length(TC))/maxe;

betafinal(1)=betafinal(1)*Ah;
betafinal(2)=betafinal(2)*Eh;
betafinal(4)=betafinal(4)*Ac;
betafinal(5)=betafinal(5)*Ec;
betafinal(7)=betafinal(7)*Al;
betafinal(8)=betafinal(8)*El;
betafinal=betafinal';
```

Listing C.2: Main file of the optimization algorithm (*Eloerror*).

```
% ODE15S Solve stiff differential equations
% and DAEs, variable order method.
function fit=EloError(EloParameters,Ah,Eh,Ac,Ec,Al,El)
global T
global M
```

```
global M0
global erate

beta = EloParameters;
H = 20; % heating rate
t0=385;
tf=1173;
v0=0;
p1=[beta(1:3)];
p2=[beta(4:6)];
p3=[beta(7:9)];
options=[];
[the,vhe]=ode15s(@firsth,[t0,tf],v0,options,p1,Ah,Eh);
dvhe=diff(vhe);
dvhe=[0;dvhe];
tihe=(1/H)*(the-t0);
dtihe=diff(tihe);
dtihe=[0;dtihe];
sratehe=dvhe./dtihe;
sratehe(1)=0;
sratehe=interp1(the,sratehe,T,'spline');
vhe=interp1(the,vhe,T,'spline');

[tce,vce]=ode15s(@firstc,[t0,tf],v0,options,p2,Ac,Ec);
dvce=diff(vce);
dvce=[0;dvce];
tice=(1/H)*(tce-t0);
dtice=diff(tice);
dtice=[0;dtice];
sratece=dvce./dtice;
sratece(1)=0;
sratece=interp1(tce,sratece,T,'spline');
vce=interp1(tce,vce,T,'spline');

[tlign,vlign]=ode15s(@thirdl,[t0,tf],v0,options,p3,Al,El);
dvlign=diff(vlign);
dvlign=[0;dvlign];
tilign=(1/H0)*(tlign-t0);
dtilign=diff(tilign);
dtilign=[0;dtilign];
sratelign=dvlign./dtilign;
sratelign(1)=0;
sratelign=interp1(tlign,sratelign,T,'spline');
vlign=interp1(tlign,vlign,T,'spline');
v=[vhe vce vlign];
```

```
v1 = v(:,1);
v2 = v(:,2);
v3 = v(:,3);
prod=v1+v2+v3;
sm=M0-prod;
srate=sratehe+sratece+sratelign;
res=srate-erate;
[maxe,v]=max(erate);
fit=100*sqrt(sum(res.^2)/length(T))/maxe;
```

Listing C.3: Kinetic model of the last partial reaction (*thirdl* file).

```
function deriv=thirdl(t,v,p3,Al,El)
% deriv=dV/dT, gives the predicted values...
% of the reaction rate, as a
% function of the parameter vector, BETA,
% and the matrix of data,X.
% T is temperature
% V [=] production of volatile matter accumulated m. f.
% thirdrate : Arrhenius law of third order
% beta: kinetic parameters; b7: A; b8:E; b9:V*
b7 = p3(1);
b8 = p3(2);
b9 = p3(3);
deriv=(60/H)*b7*Al*exp(-b8*El/(8.314*t))*(b9-v)^3/(b9^2);
```

C.2 Fortran, C++ programs

In this section, we are including fragments of the Fortran, C++ programs developed by G. Várhegyi. The use of this programs followed a process so as to get suitable derivatives from the original data, produce input data for the kinetic programs and handle the programs according the given evaluation strategy. Here some examples of the output files.

```
// Obtaining derivatives

UBeech, TA

 Spline DTG: estimated noise  of G =     .17\mug
 Spline DTG: actual deviation of G = .50\mug
 (estimated noise + .33\mug)
 Spline DTG: normalized deviation of G = .500
```

```
      G_s_max:100.0%  ( 5.962 mg) at   25.7°C
      G_s_min: 15.3%  (  .914 mg) at  550.0°C
      Residue: 15.3%  (  .914 mg) at  550.0°C
      DTGmax:   3.536E-01%/s  (  2.108E-02 mg/s) at  375.1°C

#COMMENT
 Tfirst=   25.7  Tlast=  550.0
 Tmin=   25.7           Tmax=  550.4 oC
 Gfirst=  5.962  Glast=   .914
 Gmin=   .914           Gmax=  5.962 mg
 Apparatus_DTGmin=-.00714 Apparatus_DTGmax= .35315 mg/s
     Time is given in MINUTES
     T=50oC was selected to t=0

     T in axis labels: center-points of first order
     polynomials in intervals of 11 points (10.904 s
```

```
// Producing input data for the kinetic programs

#Comment Experiment identifier:
CardoDSC_4_20_50_Rep4_5sec

 Spline DTG: estimated noise  of G = .2\mug
 Spline DTG: actual deviation of G = .50\mug
 (estimated noise + .26\mug)

 01-Dec-04 12:39:50
 From: I=  598.8   t=  26.702', T=  150.0°C
 to: I=  808.7   t=  44.198'T=  500.0°C
 (Tmin=  150.0    Tmax=  500.0 °C)
 Average dT/dt =  20.01°C/min
 Initial sample mass:  3.762 mg
 G DTG MS-intensities are divided by initial sample mass
 T in axis labels: center-points of first order polynomials
 in intervals of  3 points (.167 min)
 Normalizing factor of intensities =.2658
 Ref.inten. m/z  0   Gas flow:.0ml/min
 Minima for BL def.: 1st order polynomials of length 2.333'
 T=50°C was selected to t=0
 DOMAIN: from  150.0 to 500.0°C
```

Appendix C

```
// Handling the kinetic programs.
// Example: simultaneous evaluation of eleven experiments
// coming from different apparatus and repetitions.
// Four partial reactions,
// third order kinetics for the last pseudocomponent.
// Only the preexponential factors were allowed to vary.

Untreated thistle, all devices, some repetitions
Overall relative deviation =  1.80%
Dev=  4.700E-03 (  2.48%)  OBSmax=  0.189      CALCmax=  0.187
norm=  0.189

t0.5[1]:     7.30 min,    T0.5[1]:    256.1°C
t0.5[2]:    10.21 min,    T0.5[2]:    314.1°C
t0.5[3]:    12.22 min,    T0.5[3]:    354.3°C
t0.5[4]:    17.06 min,    T0.5[4]:    451.3°C
(t0.7-t0.3)[1]:     1.29 min,    (T0.7-T0.3)[1]:     25.9°C
(t0.7-t0.3)[2]:     1.25 min,    (T0.7-T0.3)[2]:     25.0°C
(t0.7-t0.3)[3]:     1.02 min,    (T0.7-T0.3)[3]:     20.5°C
(t0.7-t0.3)[4]:     3.54 min,    (T0.7-T0.3)[4]:     70.7°C
t_peak(1):     7.62 min, T_peak(1):    262.3°C,   d alpha(1) /dt=
5.603E-003
t_peak(2):    10.51 min, T_peak(2):    320.2°C,   d alpha(2) /dt=
5.823E-003
t_peak(3):    12.49 min, T_peak(3):    359.7°C,   d alpha(3) /dt=
7.138E-003
t_peak(4):    16.12 min, T_peak(4):    432.5°C,   d alpha(4) /dt=
2.170E-003
peak_width_t(1):     2.73 min,   peak_width_T(1):     54.7°C
peak_width_t(2):     2.63 min,   peak_width_T(2):     52.5°C
peak_width_t(3):     2.13 min,   peak_width_T(3):     42.6°C
peak_width_t(4):     6.36 min,   peak_width_T(4):    127.1°C
#SKIP
Input T(alpha=0.5):  200.00  260.00  320.00  400.00
  t1=     2.000'   tn=    21.950'
  T1=   150.0°C    Tn=   549.0°C
 BL1=   0.00      BLn=   0.00        <dT/dt> =  20.00°C/min
 # of data:  400  400  393  374  393  353  353  417  373  374
 # of data:  375
Parameters:
E [kJ/mol] log10 A   n         m         z         r.ord.amb.

 Date: 26-Apr-06 15:53:49
Number of LSQ evaluations in current optimization:      354
Number of LSQ evaluations overall in optimization:     1485
```

```
 Ellapsed time in current optimization:       1.10 s
 Ellapsed time overall in optimization:       5.20 s
TRACE OF MODIFIED HOOK-JEEVES MINIMIZATION:
Cylce       1, # of fct evals =       351
Directions without gain: 44    Value= 6.59091E-04
sqrt.value= 2.56728E-02
Decrease in rectangular steps= 4.5E-10
Decrease in valley steps= 3.5E-11
<rectang.step/H> =     0.00
valley step / rectang.step =     0.37
Overall number of LSQ evals:      1482
Overall optimization time:         5.2
 # of ODE steps >=  1000  1000  1000  1000  1000  1000  1000
1000  1000  1000
 # of ODE steps >=  1000
  1. ODE solving from  50°C  by  20.000°C/min.  Toler=  1.0E-10
  2. ODE solving from  50°C  by  20.000°C/min.  Toler=  1.0E-10
  3. ODE solving from  50°C  by  20.000°C/min.  Toler=  1.0E-10
  4. ODE solving from  50°C  by  20.000°C/min.  Toler=  1.0E-10
  5. ODE solving from  50°C  by  20.000°C/min.  Toler=  1.0E-10
  6. ODE solving from  58°C  by  20.000°C/min.  Toler=  1.0E-10
  7. ODE solving from  58°C  by  20.000°C/min.  Toler=  1.0E-10
  8. ODE solving from  50°C  by  20.000°C/min.  Toler=  1.0E-10
  9. ODE solving from  50°C  by  20.000°C/min.  Toler=  1.0E-10
 10. ODE solving from  50°C  by  20.000°C/min.  Toler=  1.0E-10
 11. ODE solving from  50°C  by  20.000°C/min.  Toler=  1.0E-10
CONSTANT AND VARIABLE PARAMAMETERS:
Experiment  1: CVCCCC CVCCCC CVCCCC CVCCCC
Experiment  2: CVCCCC CVCCCC CVCCCC CVCCCC
Experiment  3: CVCCCC CVCCCC CVCCCC CVCCCC
Experiment  4: CVCCCC CVCCCC CVCCCC CVCCCC
Experiment  5: CVCCCC CVCCCC CVCCCC CVCCCC
Experiment  6: CVCCCC CVCCCC CVCCCC CVCCCC
Experiment  7: CVCCCC CVCCCC CVCCCC CVCCCC
Experiment  8: CVCCCC CVCCCC CVCCCC CVCCCC
Experiment  9: CVCCCC CVCCCC CVCCCC CVCCCC
Experiment 10: CVCCCC CVCCCC CVCCCC CVCCCC
Experiment 11: CVCCCC CVCCCC CVCCCC CVCCCC
 Identical p.:  T F T T T T T T T T
 Identical C.:  T
Parameter transformation: 2
1st order kinetics:
Integral A exp(-E/RT) dt
 by Gauss-Legendre quadrature of 12 points
```

Appendix C

```
INDEPENDENT PARALLEL REACTIONS, GENERAL T(t):
dalpha/dt = SUM cj Aj exp(-Ej/RT) f(alphaj)
f(alphaj) = (alphaj+z)^mj (1-alphaj)^nj
dalpha/dt = SUM cj Aj exp(-Ej/RT)
T(t): input
Transf 0: (E, log A, m, n, z)
Transf 1:      log A => ln k(T_0.5_inp)
Transf 2:      log A => ln k(T_0.5_inp)/int.f(x)
Dimensions: kJ/mol, 1/s and °C
ODE solving: Runge-Kutta with adaptive stepsize
```

Appendix

D

Treatment of intensity signals

In order to perform the PCA analysis on the MS intensities, as well as quantify yields of characteristic products from pyrolysis, the MS intensity signals required some mathematical treatment. Detail of these calculations will be presented in this appendix.

D.1 Analysis of MS intensity profiles

D.1.1 Calculation of integrals for PCA analysis

In a first analysis of the MS curves, we required the integrated intensities of the most significant mass spectrometric fragment ions to introduce to the PCA analysis. We subtracted baselines from the MS data so as to correct the curves by their baseline shift during the experiments. In order to get reliable comparisons between the different types of samples and pretreatments, common baseline types were tried to use for a given m/z ion. A proper baseline correction was differently applied for the wood and for the thistle samples in those cases when background signals were highly enclosed (like the m/z 18 intensity).

Two different baseline types were used: a straight line from end to end in a currently defined domain, and, an optimal straight line. For the optimal base line correction, the minima in the first third and in the last third of smoothed curves is obtained. A simple linear interpolation is made between the two minima. Then, such parts of the curves where negative values arise due to the base line correction are tried to avoid. An algorithm tries iteratively several times to get the minima on the corrected baseline and use these points[1].

Corrected MS signals were integrated into temperature domains of interest. All numerical integrations in this thesis were calculated by the Gauss-Legendre quadrature method of 12 points. Given the wider range of decomposition of thistle biomass

[1] Várhegyi, G., personal communication.

compared to the wood samples, somewhat different temperature ranges between types of biomasses were used for the processes in Table 5.2. Table D.1 shows specific temperature domains and resulting integrals (inte.). The appropriate selection of baseline corrections led to the slightly different temperature domains between untreated and pretreated samples in some cases.

For the other m/z ions considered in the PCA analysis (Table 5.1), proper temperature domains were selected individually, within the range of entire decomposition. All these ion intensities were corrected by optimal straight lines. Tables D.2 and D.3 shows the resulting integrated intensities with their corresponding temperature domains.

D.1.2 Calculation of volatile compositions

An additional consideration was taking into account in order to get the volatile composition from the MS integrated intensities. The volatile formation in the 50 - 200 °C temperature range corresponds to the release of adsorbed water, only. Thus, the amount of water evolved in this process should correspond to the global mass loss at the same temperature range. Accordingly, we tried to use the baseline corrections that provided the closest water amounts to the corresponding mass loss values. In some cases, a given baseline type was different to the corresponding one used for the PCA calculations. We obtained the volatile compositions in Table 5.3 dividing the resulting integrals by corresponding calibration factors. All the values related to these calculations are presented in Tables D.4 and D.5.

Table D.1: Processes in the integration of MS profiles of the main evolved products from pyrolysis

	ion, m/z											
	2		**18 adsortive**		**18 reactive**		**28 below 600**[a]		**28 above 600**		**44**	
	T range (°C)	**inte.**[b]	**T range (°C)**	**inte.**[b]	**T range (°C)**	**inte.**[b]	**T range (°C)**	**inte.**[b]	**T range (°C)**	**inte.**[b]	**T range (°C)**	**inte.**[b]
UT[c]	490-900	65192	50-180	30513	200-410	163583	220-560	26000	600-900	16690	200-750	65887
WT	520-900	58419	50-180	30370	200-420	166623	220-560	30005	600-900	16416	200-740	64178
ET	520-900	74165	50-200	26731	200-410	174839	220-560	33685	600-900	15316	200-750	69673
WET	520-900	77263	50-200	32653	200-420	178640	220-560	30927	620-900	17121	200-720	69414
UP[d]	590-900	25753	50-180	4260	230-410	44521	250-600	38216	700-900	3865	200-720	35881
WP	620-900	22457	50-180	1572	230-410	24255	250-600	35757	700-900	1173	200-750	33312
EP	590-900	25924	50-180	1743	230-410	42841	250-600	38444	700-900	3394	200-720	36784
WEP	630-900	23193	50-180	2804	230-410	23695	250-600	34557	700-900	2342	200-720	31884
UB	620-900	19142	50-180	1407	230-410	37033	250-600	40460	700-900	1125	200-750	37924
WB	620-900	14252	50-180	687.3	230-420	31439	250-600	38824	700-900	2712	200-720	30920
EB	620-900	18199	50-180	1546	230-410	28868	250-600	40659	700-900	1402	200-720	38853
WEB	620-900	17490	50-180	1951	230-410	20833	250-600	37806	700-900	1314	200-720	32918

[a] A straight line from end to end in a given domain was used as the baseline correction for this process.
[b] Arbitrary units.
[c] All the untreated and pretreated thistle MS intensities were corrected by the optimal base line, except the m/z 28 below 600 process.
[d] All the untreated and pretreated wood MS intensities were corrected by the straight line from end to end in the given domains.

Appendix D

Table D.2: Integrated intensities of other characteristic evolved products from pyrolysis. Thistle

	UT		**WT**		**ET**		**WET**	
m/z	**range (°C)**	**integ.**[a]	**range (°C)**	**integ.**[a]	**range (°C)**	**integ.**[a]	**range (°C)**	**integ.**[a]
15	'220-700'	15241	'220-750'	16045	'200-750'	15588	'220-750'	16604
16	'200-700'	14776	'230-700'	14089	'230-700'	14015	'230-700'	15351
29	'190-560'	11537	'200-600'	14973	'200-560'	13253	'220-600'	14221
30	'200-560'	4920	'220-560'	6953	'210-560'	5543	'210-600'	6446
31	'200-460'	5196	'200-460'	6592	'200-460'	7475	'210-480'	6543
41	'250-570'	2597	'250-620'	2408	'230-620'	2958	'200-640'	2757
43	'200-530'	5867	'240-560'	6645	'230-570'	6571	'240-560'	7040
45	'220-580'	1123	'170-600'	1226	'200-500'	1232	'230-500'	1052
55	'240-560'	753.2	'230-570'	901	'230-580'	843	'240-560'	915
57	'230-560'	549	'240-580'	505	'180-610'	705	'220-530'	494
58	'210-540'	676.6	'250-580'	717	'210-530'	610	'220-520'	674
60	'230-600'	564.6	'220-620'	693	'240-470'	675	'230-600'	730
84	'240-520'	138.5	'200-520'	165	'240-500'	175	'200-580'	162

[a]Arbitrary units.

Table D.3: Integrated intensities of other characteristic evolved products from pyrolysis. Wood

	UP		**WP**		**EP**		**WEP**	
m/z	**range (°C)**	**integ.**[a]	**range (°C)**	**integ.**[a]	**range (°C)**	**integ.**[a]	**range (°C)**	**integ.**[a]
15	'250-750'	17853	'250-750'	17231	'250-750'	17270	'220-750'	17075
16	'270-750'	13930	'230-750'	12295	'183-750'	13870	'280-750'	12685
29	'200-530'	20056	'200-560'	23478	'220-530'	20645	'220-530'	22839
30	'210-530'	9854	'220-530'	11974	'210-530'	9839	'220-530'	11859
31	'220-480'	10328	'230-480'	10843	'230-480'	10655	'230-480'	11119
41	'230-640'	2166	'230-590'	1925	'183-600'	2100	'260-620'	1898
43	'230-540'	7326	'230-530'	8049	'230-530'	7352	'230-550'	8117
45	'200-580'	1270	'260-590'	1399	'240-550'	1480	'230-590'	1490
55	'210-620'	1172	'250-620'	1103	'250-480'	1103	'230-570'	1037
57	'210-560'	570	'250-540'	603	'250-540'	603	'180-530'	553
58	'220-520'	909	'270-530'	934	'220-560'	979	'250-530'	1028
60	'240-480'	776	'240-570'	1003	'240-530'	846	'240-530'	887
84	'250-470'	221	'220-500'	196	'250-520'	232	'250-500'	224
	UB		**WB**		**EB**		**WEB**	
m/z	**range (°C)**	**integ.**[a]	**range (°C)**	**integ.**[a]	**range (°C)**	**integ.**[a]	**range (°C)**	**integ.**[a]
15	'200-750'	17285	'250-750'	17748	'250-750'	17582	'250-750'	17299
16	'270-750'	11362	'280-750'	11952	'230-750'	11719	'200-750'	10830
29	'220-530'	22280	'220-530'	23396	'230-520'	22579	'220-530'	24249
30	'200-530'	10188	'220-530'	12507	'220-530'	10536	'230-530'	12026
31	'230-470'	12226	'230-480'	11856	'230-470'	12596	'230-470'	12550
41	'260-640'	2175	'210-620'	1937	'250-530'	1892	'220-570'	2109
43	'220-530'	8775	'250-550'	8094	'250-530'	8824	'250-530'	9156
45	'250-600'	1869	'230-550'	1614	'260-550'	1894	'230-570'	1846
55	'250-540'	1423	'230-570'	1099	'210-560'	1417	'250-580'	1198
57	'260-530'	749	'220-610'	590	'230-500'	711	'220-650'	710
58	'220-560'	1022	'220-540'	957	'270-520'	923	'220-560'	1042
60	'220-530'	1176	'220-550'	1121	'230-600'	1172	'220-550'	1102
84	'220-500'	302	'230-450'	221	'240-520'	313	'260-500'	264

[a]Arbitrary units.

Table D.4: Processes in the calculation of volatile composition. Thistle

	m/z	CF (calibration factor)	range (°C)	integ.[a b]	% (integ./CF)	range (°C)	integ.[a b]	% (integ./CF)	total (%)
UT	**2**	150000	500 - 900	64878	0.43				0.43
	18	11270	50 - 200	34175	3.03	200 - 410	93095	8.26	11.29
	28	8766	220 - 600	29115	3.32	600 - 900	16690	1.90	5.23
	44	5457	200 - 550	60292	11.05				11.05
WT	**2**	150000	500 - 900	58217	0.39				0.39
	18	11270	50 - 180	12932	1.15	200 - 420	91117	8.08	9.23
	28	8766	220 - 570	32747	3.74	600 - 900	16416	1.87	5.61
	44	5457	200 - 550	48709	8.93				8.93
ET	**2**	150000	500 - 900	74165	0.49				0.49
	18	11270	50 - 170	11531	1.02	210 - 410	127144	11.28	12.30
	28	8766	220 - 560	36685	4.18	600 - 900	15316	1.75	5.93
	44	5457	200 - 550	54357	9.96				9.96
WET	**2**	150000	520 - 900	77263	0.52				0.52
	18	11270	50 - 185	13012	1.15	200 - 420	118080	10.48	11.63
	28	8766	250 - 570	34182	3.90	620 - 900	17121	1.95	5.85
	44	5457	200 - 550	53400	9.79				9.79

[a]Differences compared to values in Table D.1 are due to different baseline corrections applied or slightly different temperature ranges.
[b]Arbitrary units.

Table D.5: Processes in the calculation of volatile composition. Wood

	m/z	range (º C)	integ.[a]	%[b]	range (º C)	integ.[a]	%[b]	total (%)
UP	**2**	600 - 900	37558	0.25				0.25
	18	50 - 150	4023	0.36	200 - 420	136047	12.07	12.43
	28	250 - 570	41146	4.69	650 - 900	4941	0.56	5.26
	44	220 - 780	35358	6.48				6.48
WP	**2**	610 - 900	36771	0.25				0.25
	18	50 - 130	1554	0.14	220 - 410	112284	9.96	10.10
	28	250 - 650	40536	4.62	650 - 900	2584	0.29	4.92
	44	230 - 690	27561	5.05				5.05
EP	**2**	600 - 900	38926	0.26				0.26
	18	50 - 160	1688	0.15	230 - 400	136463	12.11	12.26
	28	260 - 580	43254	4.93	660 - 900	3384	0.39	5.32
	44	200 - 700	35220	6.45				6.45
WEP	**2**	610 - 900	36108	0.24				0.24
	18	50 - 150	2514	0.22	230 - 410	114262	10.14	10.36
	28	250 - 640	41415	4.72	680 - 900	2148	0.25	4.97
	44	200 - 720	30925	5.67				5.67
UB	**2**	620 - 900	34145	0.23				0.23
	18	50 - 130	1804	0.16	200 - 420	130698	11.60	11.76
	28	240 - 700	46044	5.25	710 - 900	3779	0.43	5.68
	44	190 - 680	35892	6.58				6.58
WB	**2**	630 - 900	26012	0.17				0.17
	18	50 - 120	618.4	0.05	210 - 420	102546	9.10	9.15
	28	240 - 700	42491	4.85	710 - 900	2996	0.34	5.19
	44	200 - 730	31313	5.74				5.74
EB	**2**	600 - 900	34660	0.23				0.23
	18	60 - 160	868.8	0.08	220 - 410	128536	11.41	11.48
	28	260 - 690	47258	5.39	700 - 900	3948	0.45	5.84
	44	190 - 700	37771	6.92				6.92
WEB	**2**	630 - 900	29811	0.20				0.20
	18	60 - 190	6837	0.61	210 - 420	115776	10.27	10.88
	28	240 - 670	43011	4.91	720 - 900	902.5	0.10	5.01
	44	190 - 700	31851	5.84				5.84

[a]Differences compared to values in Table D.1 are due to different baseline corrections applied or slightly different temperature ranges.

[b]Integrals divided by corresponding calibration factors in Table D.4.

Appendix

E

The pyrolysis Aspen Custom model

We introduced all the meaningful results of this thesis in a pyrolysis model, employing Aspen Custom Modeler as the simulation tool. In this appendix, we will provide some detail of the program developed.

E.1 Model structure

Aspen Custom Modeler (ACM) is a process modeling language, specially suited to model complex phenomena and many different type of processes for which a custom-built model is required[1]. Time differential equations are directly entered for use in dynamic models. The program internally handles equation-based solution techniques and numerical methods to solve the equations.

We are enclosing part of the code that makes the basic structure of this program. In a text editor, parameters, variables, equations, ports (statements to define the values passed between models or units) and tasks (sequence of actions that take place during a dynamic simulation) are stated. Figure E.2 shows typical outputs of the Aspen model.

```
Version "12.1-0";
Libraries "Modeler.acml", "SystemLibrary.acml";
Port Material
// <variable name> as <variable type>
// (<default value>, description:"<description>");
m as Flow_mass;

End
Model pyrolysis
```

[1] Aspentech. Aspen Custom Modeler, 20 September 2006, <*http://www.aspentech.com*>.

Appendix E

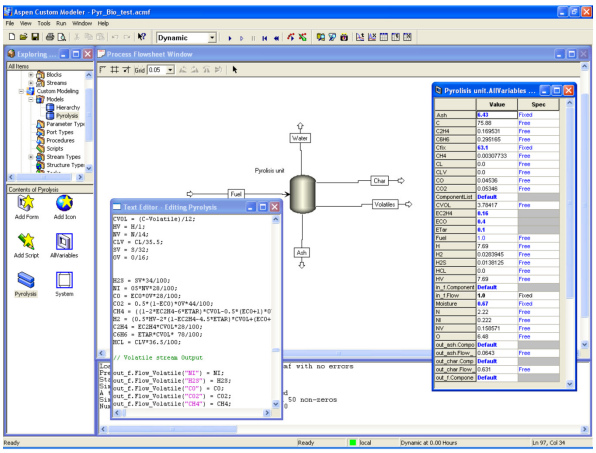

Figure E.1: General appearance of an Aspen Modeler program.

```
//Untreated Beech values
 //Alpha     as realvariable;
  T as Temperature_abs;
  R as realparameter(8.314e-3);

// Kinetic parameters are introduced from 'listofparameters.dat

 mt as realvariable;
 vt as realvariable;
 vol as realvariable;
 DTG as realvariable;

 biomass as INPUT Material;
 char as OUTPUT Material;
 volatiles as OUTPUT Material;
 water as OUTPUT Material;
 carbondioxide as OUTPUT Material;
 carbonmonoxide as OUTPUT Material;
 hydrogen as OUTPUT Material;
 othervolatiles as OUTPUT Material;

// %%%% Section primary decomposition

   $Alpha = A1*exp(-E1/(R*(T)))*(1-Alpha1);
   $Alphan = A4*exp(-E4/(R*(T)))*(1-Alphan)^3;
```

```
   DTG = c1*(A1*exp(-E1/(R*(T)))*(1-Alpha1)) + ...
    c2*(A2*exp(-E2/(R*(T)))*(1-Alpha2 ))...
    + c3*(A3*exp(-E3/(R*(T)))*(1-Alpha3)) + ...
    c4*(A4*exp(-E4/(R*(T)))*(1-Alpha4)^3);
// DTG of every compound is calculated individually
// by similar equations

   $mt = -DTG;
   $mtindep = -DTGindep;
   $mtH2O = -DTGH2O;
   $mtCO2 = -DTGCO2;
   $mtCO = -DTGCO;
   $mtH2 = -DTGH2;

   vtH2O = (1-mtH2O)*100;
   vtCO2 = (1-mtCO2)*100;
   vtCO = (1-mtCO)*100;
   vtH2 = (1-mtH2)*100;
   $vol = DTG;
   vtothervolatiles = 100-mt*100-vtH2O-vtCO2-vtCO-vtH2;

   volatiles.m = vol*biomass.m;
   water.m = vtH2O*biomass.m/100;
   carbondioxide.m = vtCO2*biomass.m/100;
   carbonmonoxide.m = vtCO*biomass.m/100;
   hydrogen.m = vtH2*biomass.m/100;
   othervolatiles.m = volatiles.m - water.m - carbonmonoxide.m -...
    carbondioxide.m - hydrogen.m;
   char.m = biomass.m - volatiles.m;


// %%%% Section secondary decomposition

   $vol1 = DTG - Asec*exp(-Esec/(R*(T)))*vol1;
   char1 = mt;
   $vol2 = (c1+c2+c3+c4-csec)*Asec*exp(-Esec/(R*(T)))*vol1;
   $char2 = csec*Asec*exp(-Esec/(R*(T)))*vol1;
   mtsec = char1 + char2;
   voltsec =100*(1-mtsec);
   DTGsec = DTG - csec*Asec*exp(-Esec/(R*(T)))*vol1;

 DTGCOsec = DTGCO + cCOsec*Asec*exp(-Esec/(R*(T)))*vol1;
 DTGCO2sec = DTGCO2+cCO2sec*Asec*exp(-Esec/(R*(T)))*vol1;
   $vtCO2sec = 100*DTGCO2sec;
```

Appendix E

```
␣␣␣$vtCOsec␣=␣100*DTGCOsec;
␣␣␣vtothervolatilessec␣=␣100-mtsec*100-vtCO2sec-vtCOsec;

//SYSTEM_SECTION␣-␣WARNING:␣DO_NOT␣EDIT

FLOWSHEET
␣␣B1␣as␣pyrolysis;

CONSTRAINTS
␣␣//␣Flowsheet␣variables␣and␣equations...
END

Task␣Temperature␣RUNS_AT␣0

//T␣as␣realvariable;
//␣For␣event␣driven␣tasks,␣<Trigger>␣can␣be␣one␣of:
//␣␣␣Runs␣At␣<time>␣␣␣␣␣␣␣␣␣␣␣␣␣␣e.g.␣Runs␣At␣2.5␣or
//␣␣␣Runs␣When␣<condition>␣␣␣␣␣␣␣e.g.␣Runs␣When␣b1.y␣>=␣0.6␣or
//␣␣␣Runs␣Once␣When␣<condtition>␣e.g.␣Runs␣Once␣When␣b1.y␣>=␣0.6
␣RAMP␣(B1.T,␣1173.15,␣2625);
//␣SRamp(<variable>,␣<final␣value>,␣<duration>,␣<type>);
//␣Wait␣For␣<condition>␣e.g.␣when␣b1.y␣<␣0.6;
//␣(Use␣Wait␣For␣to␣stop␣the␣task␣firing␣again␣once
//␣trigger␣condition␣has␣been␣met)
//␣Note␣that␣all␣variable␣values␣must␣be␣in␣base␣units␣(usually␣Metric


End


Options
␣␣AbsPerturb:␣1.e-0010;
␣␣AbsTearTol:␣1.e-0010;
␣␣AbsTol:␣1.e-0010;

␣␣␣␣␣
```

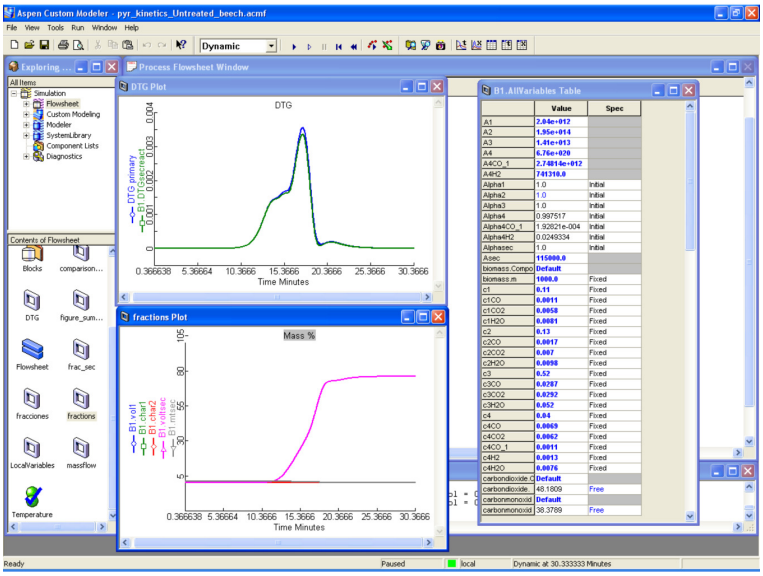

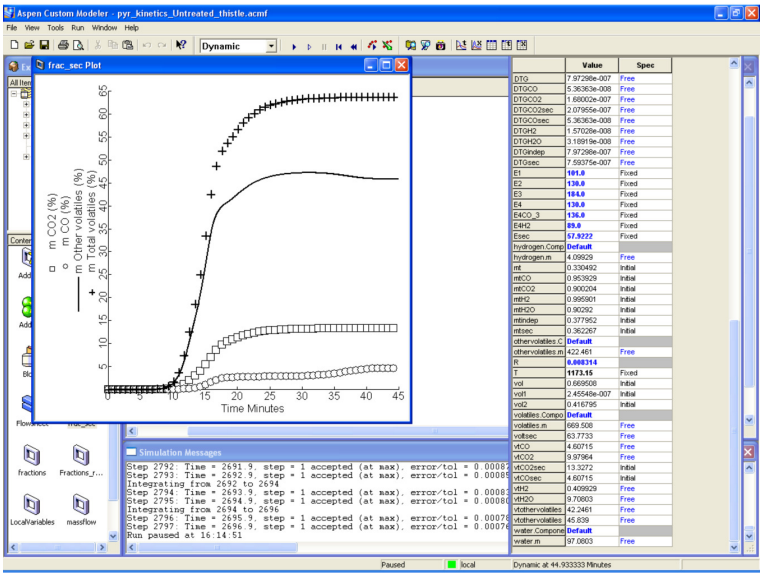

Figure E.2: Example of the type of results obtained from the pyrolysis Aspen model.

List of Figures

List of Tables